



Total Control

*Advanced integrated supervisory and wind turbine control
for optimal operation of large Wind Power Plants*

Optimization of WPP set-points Deliverable D2.3

Delivery date: 12.04.2021
Lead beneficiary: DTU
Dissemination level: Public



This project has received funding
from the European Union's Horizon
2020 Research and Innovation
Programme under grant agreement
No. 727680

Author(s) information (alphabetical):		
Name	Organisation	Email
Anand Natarajan	DTU	anat@dtu.dk
Andreas Knauer	EQUINOR	andkn@equinor.com
Ervin Bossanyi	DNV	ervin.bossanyi@dnvgl.com
Gunner Chr. Larsen	DTU	gula@dtu.dk
Ishaan Sood	KUN	ishaan.sood@kuleuven.be
Matthieu Irondele	EQUINOR	
Nikolay Dimitrov	DTU	nkdi@dtu.dk
Renzo Ruisi	DNV	Renzo.Ruisi@dnv.com

Document information

Version	Date	Description		
		Prepared by	Reviewed by	Approved by
1.0	12.04.2021	Anand Natarajan	Gunner Chr. Larsen	Malene Pogager

TABLE OF CONTENTS

Table of Contents	3
1. Executive Summary	5
2. Introduction	6
3. Description of Low Fidelity Wake Approaches.....	8
3.1 DTU (FUGA).....	8
3.2 KUL (Gaussian Wake).....	12
3.3 DNV (LongSim).....	13
4. Optimal performance using low fidelity wake models	32
4.1 DTU	32
4.2 KUL.....	42
4.3 DNV	48
4.4 Comparison of results with different low fidelity wake models.....	74
5. Setpoint optimization with the dynamic wake meandering approach (DTU)	77
5.1 fatigue vs. power production	77
5.2 De-Rating strategies and surrogate model implementation	78
5.3 Comparison of results with low fidelity approach	81
5.4 Uncertainties in the set-point optimization process	84
5.5 Conclusions from the set-point optimization using DWM.....	86
6. Ancillary services (DNV).....	87
6.1 Curtailment.....	87
6.2 Delta control	93
7. Application of multidimensional set point control to the DTU 10 MW turbine in the reference wind farm (Equinor).....	94
7.1 The DTU 10 MW turbine	94
7.2 Induction control.....	95
7.3 Setpoint modification based on power reduction	96
7.3.1 Single operational point analysis.....	99
7.3.2 Wind speed range tests	101
7.3.3 Wind speed range and turbine distance range simulations	104
7.4 Setpoint modifications based on thrust clipping.....	106
7.4.1 Wind speed range tests for thrust reduction	110
7.4.2 Wind speed range and turbine distance range simulations	112
7.5 Setpoint tests with thrust reductions with improved C_p/C_t ratio.	114

7.5.1 Single point investigation for Cp/Ct optimised thrust reduction..... 114

7.5.2 Wind speed range tests 116

7.5.3 Wind speed range and turbine distance range simulations117

7.6 Summary 118

8. Conclusions..... 121

9. Bibliography 122

1. EXECUTIVE SUMMARY

This report quantifies the benefit to wind farm production and fatigue damage reduction to major wind turbine structures through the use of selective wind turbine de-rating and yaw control strategies. These wind farm supervisory control strategies are modelled in diverse software that possess various wake models of different fidelity. We compare the results on the power production and loads reduction in the Lillgrund wind farm using 3- low fidelity wake model approaches (FUGA, Gaussian Wake and LONGSIM) and one medium fidelity wake model approach (Dynamic Wake Meandering (DWM)). It should be noted that the term fidelity refers more to computational speed than with the accuracy, that is low fidelity models are computationally fast.

The Lillgrund wind farm comprises of Siemens 2.3 MW wind turbines and the farm is tightly packed with 48 turbines spaced over a small area. The de-rating of wind turbines is implemented selectively keeping several objectives such as maximizing power or maintaining a certain power level, while minimizing loads. The yaw control is implemented to maximize power production separately uncoupled to de-rating. The DWM model is also tested on a larger 10 MW wind turbine with a single wake from a neighbouring turbine, so that the quantification of the effects of selective turbine de-rating at larger scales and with limited number of turbines can be understood.

2. INTRODUCTION

The current approach to wind farm control is based on individual regulation of each turbine and supervisory control for operator actions. Supervisory control allows an operator to switch off or derate the complete wind farm or individual turbines. This approach neglects interconnections between the turbines. The most direct interconnection is the wake interaction between turbines coupled to the wind direction. Each turbine changes the wind inflow and in this way influences turbines down wind. This can lead to severely increased loads on turbines that are down wind from the predominant wind direction. By considering the wake effect interconnections coupled to the demand from the grid, maintenance needs, the fatigue damage of the turbines, the wind farm open loop control can produce selected tailored de-rating that can maximize energy capture or minimize loads or both.

Wake losses in offshore wind parks are typical in the range from 10 to 15% depending on the park design and wind climate. Turbines are typically operated individually to generate a maximum of energy, disregarding the wake development and the impact on downwind turbines in the park. This leads often to an uneven power and load distribution in a wind park. The wake losses depend on turbine operational parameters and wind conditions. Particularly, the atmospheric stability has an influence on the wake decay, amplifying convective motion and turbulent mixing. Atmospheric conditions are fixed boundary conditions for an offshore wind park, but there are approaches for the application of technical flow control in an offshore park. A modification of the operational behaviour of the turbines can be applied to change park flow patterns to increase power production and to mitigate loads.

One control method is to deflect the wake by yaw of the turbines relative to each other. Through the yaw operation a turbine can move the wake away from a downstream turbine to increase power production and reduce loads. However, yaw operation might increase loads for the operating turbine and large yaw angles should be avoided. Wake deflection by yaw has been investigated in numerical and experimental approaches, see (Jimenez, 2009) (Schottler, 2017) (Vollmer, 2016). The method is part of the 'wake adapt' package available for SGS turbines. Another method to increase or distribute the power production more even is induction control. The upwind turbines are operated with reduced power generation to enhance downwind power production as carried out by (Bossanyi, 2018) (Munters, 2018) (J.A. Vitulli, 2021).

A brief overview of each of the software used to quantify the impact of selected wind turbine de-rating or yaw steering is made in the subsequent sections and also introduced here. DNV GL's wind farm simulation code LongSim is an engineering code designed to simulate the dynamic behaviour of wind turbines and their wakes within a realistic wind field. It includes engineering simplifications in terms of the flow modelling and wind turbine aeroelastic behaviour, so as to achieve high computational speed to allow repeated control design iterations and long simulations to be carried out easily, with minimal computing power. A fast boundary layer model, the Three Layer Model Model (TLM) has been previously developed at KU Leuven to study windfarm operation in a variety of atmospheric conditions (Allaerts, D. and Meyers, J, 2015). Wind turbine forces in the TLM are obtained through a Gaussian Wake Model (GWM), which accounts for wake overlap between different turbines of the windfarm. FUGA is a linear CFD RANS model, where the governing Navier

Stokes equations are linearized and conveniently formulated in a mixed spectral domain, which facilitates extremely fast solutions as based on a "system" of look-up tables, where some are general and some are WT specific. These tables are used to determine the velocity field behind a single solitary WT. Due to the linearity of the model, multiple wakes from many turbines can be constructed from the wake dictated velocity perturbation of a single turbine. These are constructed from Fourier components by a fast Fourier integral transform. Dynamic wake meandering is model is a time domain solution that is initialized with the flow just behind the wind turbine that is shedding the wake. The model is composed of three parts,

- 1) a wake deficit formulated in the meandering frame of reference;
- 2) a stochastic model of the downstream wake meandering process;
- 3) a model of the self-induced wake turbulence described in the meandering frame of reference.

The results of these wind farm control studies can be readily implemented in practise since all the control mechanisms are supervisory and do not require a feedback mechanism or added instrumentation. Some of the look-up tables thus generated to de-rate selected turbines herein will be implemented in the Lillgrund wind farm in the next steps to validate the conclusions presented herein. The next sections describes the models and the conclusions reached based on each model used.

3. DESCRIPTION OF LOW FIDELITY WAKE APPROACHES

3.1 DTU (FUGA)

DTU has developed a platform for optimal open-loop scheduling of wind farm control. The resulting wind farm control schedules are conditioned on wind direction and mean wind speed. The model of the wake affected flow field inside the wind farm is based on the linearized Reynolds Averages Navier Stokes (RANS) CFD code Fuga (Ott, S., Berg, J. and Nielsen, M), which is an extremely fast CFD solver - popular speaking one million times faster than a conventional non-linear CDF (RANS) solver. It is therefore very well suited as a 'working horse' for optimized wind farm control scheduling, where the wind farm flow usually needs to be re-computed thousands of times before a converged solution of the optimal wind farm control schedule is found.

Being a RANS code, stationary flows are considered, which support production estimates of the wind farm wind turbines (WTs), but not dynamic loading (e.g. fatigue loading) of these. Thus, the metric for the developed optimizer is wind farm production. The design variables are rotor tip speed ratio, collective pitch and WT yaw error for each and every WT within a given wind farm. Thus, the facilitated active wake control includes both WT de-rating and wake deflection caused by provoked WT error settings.

In Fuga, the WTs are formulated as actuator discs (ADs). The original formulation of Fuga did not support the modelling of yawed WTs, Therefore, for the purpose of supporting simulation of active wake control in the form of wake deflection, Fuga has been generalized to account for such situations (Ott, S., Laan, P. van der and Larsen, G.C.).

Platform basic elements

In addition to the Fuga CFD solver, the optimization platform consists of a detailed aerodynamic model of the WT rotor, a fast and accurate surrogate of the detailed aerodynamic model and an optimization platform.

The *CFD solver* simulate the atmospheric boundary layer (ABL) with the wind farm WTs embedded. Ambient mean wind shear and turbulence characteristics are specified in terms of a terrain roughness height conditioned on wind direction, which implicitly dictates the ambient turbulence conditions via the turbulence closure of the CFD model. The WTs are modeled as ADs with characteristics defined as based on the aerodynamic model. Note, that for yawed WTs the ADs representing the rotor forcing embedded in the flow field have a force component in the mean flow direction as well a force component in the lateral direction.

The linearized Navier-Stokes equations are conveniently formulated in a *mixed spectral* domain, which facilitates extremely fast solutions as based on a "system" of *look-up tables*, where some are general and others are WT specific. These tables are used to determine the velocity field behind a single solitary WT. Due to the linearity of the model, multiple wakes from many turbines can be constructed from the wake dictated velocity perturbation of a single turbine. These are in turn constructed from Fourier components by a fast Fourier integral transform.

The wake interactions within the wind farm flow field are determined using a parabolic type of solution scheme, in which the wind field conditions at each WT location inside the wind farm will

depend on wakes emitted from only upstream WTs. For a given ambient wind direction, the wind turbine locations are therefore first sorted according to their upwind distance. Next, the local wake affected wind speed, the thrust coefficient(s) and the power production are evaluated starting with the undisturbed upwind turbines locations and progressively evaluated at WT locations in the downwind direction. Finally, when the thrust of all turbines are known for the specified ambient wind conditions, we can evaluate the combined wake affected wind farm flow field at any position by linear superposition of wake ‘perturbations’. This process is handled by PyWake (Pedersen, M.M., van der Laan, P., Friis-Møller, M., Rinker, J. et.al.), which is an open source python framework for calculating AEP including wake effects.

The *aerodynamic model* is based on a detailed aerodynamic description of the rotor and its operational conditions (i.e. tip speed ratio, collective pitch setting and provoked WT yaw errors) and model rotor aerodynamic forces - defining the ADs for the Fuga flow modeling - as well as rotor power used as input to the optimizer. We use the aerodynamic code HAWC2Aero (Larsen, T. J. (2008)) for this purpose. The aerodynamic model in this code is based on a variant of the conventional blade element momentum (BEM) code (Madsen, H. Aa., Mikkelsen, R., Sørensen, N.N. et.al.), meaning that detailed aerodynamic description of the rotor is needed - i.e. blade twist and blade profiles with their respective aerodynamic coefficients. Consistent with the static undeformable ADs used in Fuga, HAWCAero is not including static deformation of WT components.

Although the Fuga solver allows for non-uniform ADs, we have for the present purpose for simplicity chosen *uniformly loaded* ADs. These are in turn characterized by their individual power- and thrust coefficients - i.e. $C_p(U|\alpha, \lambda, \vartheta_y)$ and $C_t(U|\alpha, \lambda, \vartheta_y)$, respectively - conditioned on the WT operational conditions. The operational conditions are in turn characterized by mean hub height wind speed, U , collective pitch setting, α , tip speed ratio, λ , and the WT yaw error ϑ_y . Accounting for the influence from wind shear, tower shadow, WT yaw error and WT tilt, the tip speed ratio may be defined as

$$\lambda \equiv \frac{1}{2\pi} \int_0^{2\pi} \frac{R\Omega}{U(R, \varphi)} d\varphi \quad (1)$$

where $U(R, \varphi)$ is the mean inflow wind speed seen by the tip of the blade (defined by rotor radius R) at azimuthal position φ , and Ω is rotor rotational speed. However, for the present purpose we use the traditional simplistic definition

$$\lambda \equiv \frac{R\Omega}{U} \quad (2)$$

which is expected to be close to the value defined by eq. (1), and which in the end is equally good as a state parameter for the intended optimization.

The dimensionless WT power- and thrust coefficients are defined by respectively

$$C_p(U|\alpha, \lambda, \theta_y) \equiv \frac{P_{WT}(U|\alpha, \lambda, \theta_y)}{\frac{1}{2}\rho AU^3} \quad (3)$$

and

$$\mathbf{C}_t(U|\alpha, \lambda, \theta_y) \equiv \frac{\mathbf{T}_{WT}(U|\alpha, \lambda, \theta_y)}{\frac{1}{2}\rho AU^2} \quad (4)$$

in which ρ is the air density, A is the rotor area, P_{WT} denotes WT power production, and \mathbf{T}_{WT} is the rotor thrust force perpendicular to the rotor plane. Both P_{WT} and \mathbf{T}_{WT} result from the aerodynamic model. The power coefficient, C_p , is a *scalar*, whereas the thrust coefficient, \mathbf{C}_t , is a *vector* specifying normalized magnitude as well as direction of the rotor thrust force.

We assume that only the inflow perpendicular to the rotor plane contribute to power production and rotor loading. Referring to a two dimensional Cartesian frame of reference, with axes directed along the mean wind direction and the lateral flow direction, we resolve \mathbf{C}_t as follows

$$\mathbf{C}_t(U|\alpha, \lambda, \theta_y) \equiv (C_{t\rightarrow}(U|\alpha, \lambda, \theta_y), C_{t\uparrow}(U|\alpha, \lambda, \theta_y)) \quad (5)$$

in which $C_{t\rightarrow}(U|\alpha, \lambda, \theta_y)$ denotes the component in the mean wind direction, and $C_{t\uparrow}(U|\alpha, \lambda, \theta_y)$ is the component in the lateral direction. Using eqs. (4) and (5) the rotor thrust force may be expressed as

$$\begin{aligned} \mathbf{T}_{WT}(U|\alpha, \lambda, \theta_y) &= 2AU^2 (C_{t\rightarrow}(U|\alpha, \lambda, \theta_y), C_{t\uparrow}(U|\alpha, \lambda, \theta_y)) \\ &= 2A(U \cos \theta_y)^2 (\cos \theta_y C_t(U \cos \theta_y|\alpha, \lambda, 0), \sin \theta_y C_t(U \cos \theta_y|\alpha, \lambda, 0)) \end{aligned} \quad (6)$$

From eq. (6) we finally obtain

$$\begin{aligned} C_{t\rightarrow}(U|\alpha, \lambda, \theta_y) &= (\cos \theta_y)^3 C_t(U \cos \theta_y|\alpha, \lambda, 0) \\ C_{t\uparrow}(U|\alpha, \lambda, \theta_y) &= \sin \theta_y (\cos \theta_y)^2 C_t(U \cos \theta_y|\alpha, \lambda, 0) \end{aligned} \quad (7)$$

Thus, the two components of the thrust coefficient vector can, in a simple way, be expressed in terms of the conventional thrust coefficient for a non-yawed WT (i.e. $\vartheta_y = 0$). This is a considerable simplification, because the thrust coefficient hyper surface is then spanned by only two of the three dimensions of the state vector space representing the operational condition of the WT.

In analogy with the above considerations, we find the following reduced expression for the power coefficient

$$C_p(U|\alpha, \lambda, \theta_y) = (\cos \theta_y)^3 C_p(U \cos \theta_y|\alpha, \lambda, 0) \quad (8)$$

Accounting for both rotor tilt (ϑ_t) and rotor coning (ϑ_c), the rotor may be expressed as

$$A = \pi(R \cos \theta_c \cos \theta_t)^2 \quad (9)$$

In order to facilitate fast simulations supporting the iterative optimization approach, a fast and accurate surrogate model is used as a proxy for the detailed aerodynamic model described above. First, the steady state performance values of respectively $C_p(U|\alpha, \lambda, 0)$ and $C_t(U|\alpha, \lambda, 0)$ are calculated for every combination of tip speed ratio, pitch angle and mean wind speed from a suitable user-defined grid of selected sample points. Next, multi-dimensional polynomial

representations of respectively $C_p(U|\alpha, \lambda, \theta)$ and $C_t(U|\alpha, \lambda, \theta)$ are fitted to the computed grid values, whereby continuous C^1 -surfaces are obtained for the surrogates, and finally these are used together with the eq.(7 - 9) to map the thrust- and power characteristics of *arbitrary* yawed WTs. As the surrogates are to be used in combination with gradient-based optimization algorithms, it is important that the partial derivatives of the constructed continuous multi-dimensional surfaces are continuous. In the present work a spline-interpolation was applied.

With the described input and using the wind farm production as the objective function, the optimization platform compute optimal wind farm control schedules, conditioned on the ambient inflow conditions; i.e. mean wind speed and mean wind direction. Selected WT specific constraints like upper and lower limits on the pitch setting, the tip speed ratio and the yaw error setting can be imposed.

Without a wind farm controller functionality, each individual WT will operate at *maximum* C_p below rated wind speed. The goal for the present optimized wind farm control approach is to find the *optimal balance* between individual WT de-ratings and/or yaw settings, which result in maximum wind farm power production. The optimal WT settings will clearly depend on the wind farm topology and thereby in turn on the mean inflow wind direction, ϑ . It will, moreover, depend on the mean wind speed as long as one or more WTs operates below rated wind speed. Consequently, the optimal wind farm operation is formulated as a set control schedules, conditioned on the wind farm mean inflow wind speed and the wind farm mean inflow wind direction.

The objective function is thus accordingly defined as

$$P(U, \theta) = \sum_{i=1}^N P_i(\lambda_i, \alpha_i, \theta_{y,i} | U, \theta) \quad (10)$$

where N denotes the number of WTs in the wind farm, and lower indices, i , refer to WT no. i . The optimization problem to be solved is defined in terms of the objective function (10) accompanied by a set of constraints given by

$$\begin{aligned} \lambda_{min}(U) &\leq \lambda \leq \lambda_{max}(U) \\ \alpha_{p,min} &\leq \alpha_p \leq \alpha_{p,max} \\ \theta_{y,min} &\leq \theta_y \leq \theta_{y,max} \end{aligned} \quad (11)$$

The relevant values for the Siemens SWT-2.3-93 WT used in the case study in section 4.1 are: $\lambda_{min}(U) = 36\text{ms}^{-1}/U$; $\lambda_{max}(U) = 75.15\text{ms}^{-1}/U$; $\alpha_{p,min} = -2^\circ$; $\alpha_{p,max} = 90^\circ$; $\vartheta_{y,min} = -30^\circ$; and $\vartheta_{y,max} = 30^\circ$.

The workflow in the developed optimization platform is illustrated in Figure 3.1. The optimization "module" is based on a re-developed version of TOPFARM (Réthoré, P.-E., Fuglsang, P., Larsen, G. C., Buhl, T. et.al.)**Error! Reference source not found.** A genetic optimization algorithm (GA) is used for first pass of the solution supplemented by a gradient based method (SLSQP) for final refinement.

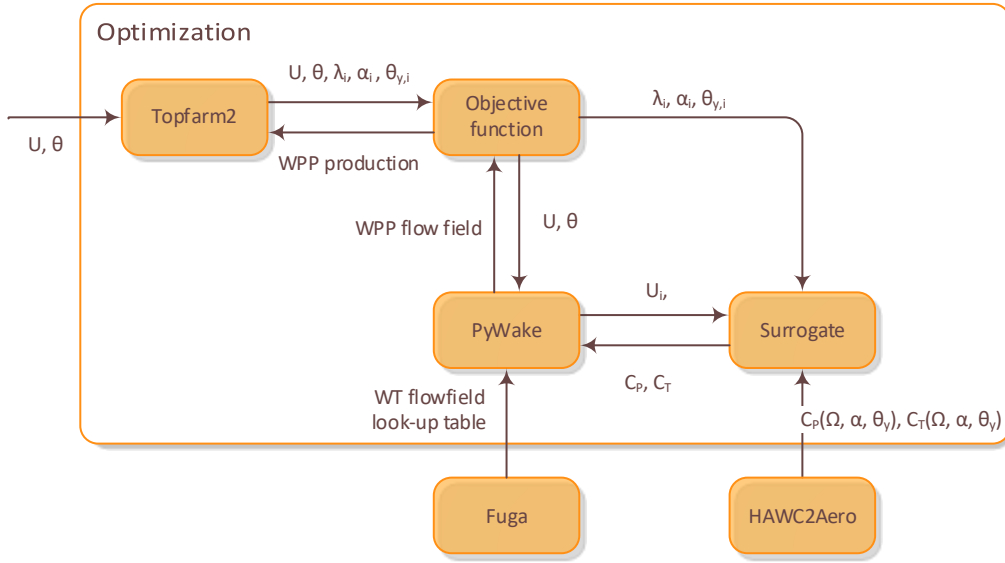


Figure 3.1. Platform workflow.

3.2 KUL (GAUSSIAN WAKE)

In recent years, Large Eddy Simulations (LES) have proven to be a valuable asset to test wake misalignment control strategies under different atmospheric conditions. However, the high computational cost associated with these simulations makes studying a large number of wake misalignment combinations expensive. A fast boundary layer model, the Three Layer Model Model (TLM) has been previously developed at KU Leuven to study windfarm operation in a variety of atmospheric conditions (Allaerts and Meyers, 2019). Wind turbine forces in the TLM are obtained through a Gaussian Wake Model (GWM), which accounts for wake overlap between different turbines of the windfarm. Windfarm simulation results from the TLM have been recently compared against LES datasets from the TotalControl Windfarm database and shown to be in good agreement (Sood et al., 2020).

The GWM is further extended to include individual turbine yawing capabilities to provide a platform for rapid evaluation of yaw misalignment strategies under varying inflow conditions (Bastankhah and Porté-Agel, 2016). The wake deficit behind a yawed turbine is given by,

$$W(x, y, z) = \left(1 - \sqrt{1 - \frac{C_T \cos \gamma}{8 \zeta^2}} \right) \exp \left[-\frac{1}{2 \zeta^2} \left(\frac{z^2}{D^2} + \frac{(y - \delta)^2}{D^2} \right) \right]$$

Where, γ is the turbines yaw angle, C_T is the wind turbine thrust set point coefficient and D is the turbine diameter. ζ is a wake spreading parameter which depends upon the incoming turbulence intensity TI , the wake deflection δ , and the downstream positions x , y and z . Further details of the model and its parameters can be found in the reference.

Individual wind turbine wakes in the farm are recursively superimposed by following the new wake merging methodology by (Lanzilao and Meyers). The inflow velocity at a point on a wind turbine in the farm is given by

$$U_k(x) = (U_{k-1}(x) \cdot e_{\perp,k})(1 - W_k(x))e_{\perp,k} + (U_{k-1}(x) \cdot e_{\parallel,k})$$

k is the wind turbine index going from 1 to N_t , while the unit vectors $e_{\perp,k} = (\cos\theta_k, \sin\theta_k)$ and $e_{\parallel,k} = (-\sin\theta_k, \cos\theta_k)$ account for the incoming wind direction θ at turbine k . The total inflow velocity of the turbine k for the computation of its power is computed by averaging the velocity across the disc. To this end, we use the quadrature rule with $N_q = 16$ points, spread over the rotor disk. The quadrature-point coordinates are denoted by $x_{k,q}$ and are chosen following the rule proposed by Holoborodko with uniform weighting factor of $w_q = 1/N_q$ (H. P, 2011). Hence, the disk average turbine inflow velocity can be determined by

$$U_k = \sum_{q=1}^{N_q} w_q S(x_{k,q})$$

Where, $S(x) = \|U(x)\|_2$.

3.3 DNV (LONGSIM)

The LongSim model has been developed internally by DNV GL, for the purpose of exploring the possibilities of wind farm control, and testing and evaluating wind farm control algorithms in a realistic dynamic environment. The model is designed for low computational cost so that different control options can be investigated rapidly. Although starting with relatively low-fidelity empirical models, the intention is to allow more sophisticated models to be implemented easily as and when this becomes appropriate. This table gives an outline specification:

Computational cost	Time-domain simulations to run in approximately real time on a typical laptop for a wind farm of ~100 turbines
Steady-state optimisations	Automated to generate optimal control settings
Turbine aerodynamics	Either power and thrust curves, or power and thrust coefficients as functions of tip speed ratio, pitch angle and yaw misalignment
Turbine dynamics	Rotor speed, pitch & yaw DOFs are available
Turbine control	Dynamics of generator torque, blade pitch, and yaw control can be simulated if required
Turbine loads	Surrogate model based on high-fidelity <i>Bladed</i> simulations
Timestep	Typically ~ 1 second
Input wind data	Met mast 10-minute averages (typically) or similar
Simulation length	Hours to years

Wind field	Low frequencies correlated across farm, evolving as it advects
Wake profile	Various models available, including Ainslie and EPFL/Bastankah
Wake turbulence	Options include Quarton-Ainslie and Crespo-Hernandez
Wake meandering	Driven by low-frequency turbulence in wind field
Wake advection	Driven by low-frequency wind field with wake deficit modification
Wake deflection	Options include Jiménez and EPFL/Bastankah
Wake superposition	Various options including dominant wake and sum of deficits with corrections available for large wind farm effects and streamtube expansion
Wind farm control	Configurable, with built-in options for axial induction control and/or wake steering, and wind condition estimation including consensus options.

A detailed description was previously provided in TotalControl deliverable D1.9, although there have since been many detailed improvements, and some of the newer wake modelling options have been introduced since that time. The wake model used in this report was the Ainslie-based deficit model with Obukhov length -200m (slightly unstable), using the EPFL model for lateral deflection due to yaw. A new surrogate loads model has been introduced, as described in the next subsection, which has been used in this report, allow the effect of wind farm control on turbine fatigue loads to be evaluated.

SURROGATE LOADS MODEL IN LONGSIM

The surrogate model for turbine loading has been developed primarily for predicting turbine fatigue loads in wind farms, taking detailed wake effects into account. The model can be used both for steady-state setpoint optimisation against a merit function which includes both power and turbine loads, and for dynamic time-domain simulations, for example to evaluate the effects of wind farm control on turbine loading.

For this, fatigue loads need to be evaluated much more rapidly than is possible with full aeroelastic turbine simulations. Surrogate models based on large numbers of pre-computed simulations can be used, as in Dimitrov et al (2018). A simple example (Bossanyi, 2018) uses a fatigue loads database (FLD) generated with the aeroelastic code Bladed, containing damage equivalent loads (DELs) for a wide variety of wind conditions, from which the DELs for a particular condition are simply interpolated. The wind conditions may include wind speed, turbulence intensity, wind shear, etc., as separate dimensions of a multi-dimensional look-up table of DELs. For wind farm control, a separate dimension needs to be added for any wind farm control setpoints, e.g. thrust reduction and/or yaw misalignment setpoints. Wake effects on the loads are modelled only by increased turbulence intensity, due to the wake-added turbulence. To take into account important effects such as partial wake immersion, wake meandering, and wake superposition would add too many further dimensions to the database, making it quite impractical.

Therefore, a new model has been developed which allows the loads to be synthesised from information contained a much smaller set of aeroelastic simulations. This is done by assuming that each load is made up of stochastic and deterministic components which can be predicted separately and summed together. The method involves combining the deterministic effects of wake profiles, shear, yaw misalignment, rotor tilt etc. with the stochastic effects of rotationally sampled turbulence coupled with structural dynamics. The effects are calculated separately from models fitted to appropriate targeted sets of Bladed runs, and then combined. The step of combining the load components derived from different effects is clearly an approximation, but this has been tested by comparing the outcomes against individual Bladed simulations for specific sets of conditions which Bladed is able to deal with, such as a steady single wake.

The following subsections describe how the stochastic part of the load is modelled, how the various deterministic parts are modelled, the calculation of the mean or DC component which has to be added on, and how the different load contributions are combined. Finally, an example validation is provided to show how the predicted loads compare against a detailed Bladed aeroelastic simulation. The examples in this section are all based on a generic 2MW wind turbine model, but the model parameters have been fitted to the Lillgrund turbine for use in subsequent chapters of this report.

STOCHASTIC EFFECTS

The stochastic part of the load is deemed to be caused by wind turbulence, including rotational sampling of turbulence by the rotor blades, in the absence of all the deterministic effects which are described below. The stochastic effects are characterised by running Bladed simulations with turbulent wind but without effects giving rise to deterministic effects, i.e. using axial flow, no gravity, tower shadow or imbalances, and no wakes, wind shear or yaw misalignment. Ten-minute simulations have been used to adequately capture the range of turbulent frequencies, and structural dynamic effects are included since these are mainly excited by the turbulence.

To characterise the stochastic load, a transfer function is calculated from the hub longitudinal wind speed to each of the loads of interest. This is done for each of a number of wind speeds and thrust reduction setpoints (see [Optimal thrust reduction settings](#) below). Interpolation of the transfer functions between wind speeds could be problematic, especially if the rotor speed changes with wind speed leading a shift in the spectral peaks at multiples of the rotational frequency. Therefore, the transfer functions were calculated for closely-spaced wind speeds, so that for any intermediate wind speed, the transfer function for the nearest mean ambient wind speed can be used. In LongSim, the transfer functions are applied to the wind speed spectrum to generate loading spectra, which are then converted to zero-mean time-domain loads using inverse Fast Fourier Transformation (FFT). The resulting loads are scaled by the (time-varying) ratio of the actual standard deviation of incident wind speed at each turbine (including wake-generated turbulence) to the ambient standard deviation. Thus, the loads will automatically increase when the turbine is experiencing a high level of wake-induced turbulence. This works because the transfer function does not depend appreciably on the turbulence intensity. This assumption appears to hold well, although it relies on linearity and so may not work for very high levels of turbulence. As an example, Figure 3.2 shows that the transfers functions from wind speed to yaw moment at the hub for

turbulence levels of 10% and 20% are almost identical. To obtain a smooth transfer function, the magnitude has been filtered using a variable-order median filtering technique.

DETERMINISTIC EFFECTS

In addition to the stochastic loading described above, deterministic load contributions arise from other, non-turbulent, variations of the wind field across the rotor. This includes effects resulting from mean wind shear, yaw misalignment, upflow, rotor tilt, tower shadow, partial wake immersion, wind veer, and so forth. Other asymmetries also cause deterministic effects, such as gravity, and rotor mass and aerodynamic imbalances. All these features are taken into account in the model, with the exception of wind veer and rotor imbalances. However, the method could easily be extended to include these features if desired.

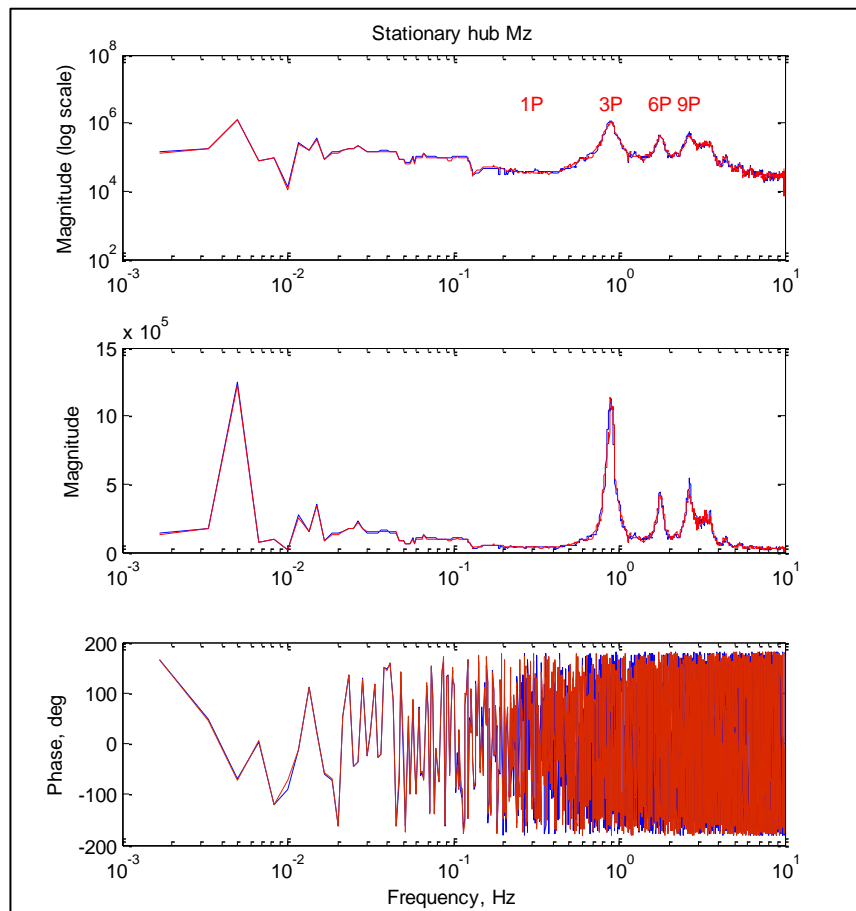


Figure 3.2: Example transfer functions at 9 m/s: 10% TI (blue), 20% TI (red)

The deterministic loading effects are predicted by running a set of short Bladed simulations in a steady, non-turbulent wind flow, each with just one of the deterministic effects included, so that the load variations are solely due to that effect. Then, for each of those effects, an empirical model is fitted to predict the azimuthal variation in loading which occurs as a result of that effect. These azimuthal variations are characterised by the amplitude and phase (with respect to rotor azimuth) of the cyclic load variations which can be seen in the steady wind simulation results. These amplitudes and phases are calculated by the 'Fourier harmonics' post-processing calculation in

Bladed, and converted to equivalent y and z components, and empirical models are fitted to predict these components as a function of the parameters defining each modelled feature. For example, wind shear is usually characterised by a single parameter, such as the shear exponent, and yaw is characterised by the yaw misalignment angle, whereas a Gaussian wake profile is characterised by the wake width, centreline deficit, and the horizontal and vertical displacements of the wake centreline from the rotor centre. Gravity and tilt being constant, only a single simulation is required for each wind speed and thrust setpoint, so no fitting is needed. Depending on the specific load, the azimuthal variation may have components at different multiples of the rotor rotation frequency: the oP component provides a mean offset, and loads in the non-rotating frame can also be expected to have components at multiples of the blade passing frequency, i.e. 3P, 6P etc. for a 3-bladed turbine. The 'Fourier harmonics' calculation generates the amplitudes and phases for all the different harmonics. So far, only the dominant oP and 3P components have been used, but the method could easily be extended to include less important 6P and higher harmonics if this proves important (perhaps for large, highly flexible turbines).

A few typical examples are presented to illustrate the model fitting, for which a least-squares method was used. For wind shear, characterised by the shear exponent α , each component of any load harmonic was modelled simply by a polynomial on α , which gave an excellent fit in most cases. A third-order polynomial was used to fit six different exponents. For the most important components, the oP Stationary hub My and Mz (nod and yaw moments), the fitting errors were tiny, mostly less than 0.01%, with the largest error being 0.2% for Mz. For the various 3P components, the errors were mostly less than 1%. Of the 270 errors, only five exceeded 2%, with the two largest being 3.7% and 5.5%, all in the case of the hub Mx (torque) load. A couple of example fits with 1.9% and 3.7% error is shown in Fig. 3.3.

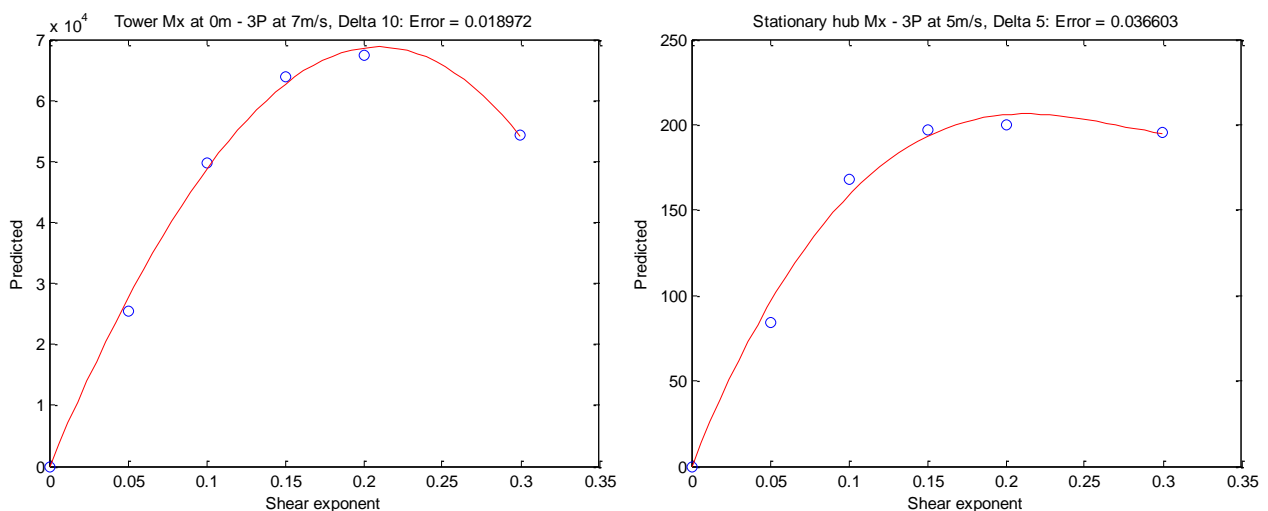


Figure 3.3: Example model fits for wind shear

Variations with yaw misalignment were not quite so smooth, so fourth-order polynomials were fitted to seven yaw misalignments, with positive and negative yaw misalignments treated separately. The errors were generally larger than for the shear model. The fit was generally quite good for the hub My and Mz (nod and yaw) moments, both oP and 3P components, with errors usually very small, and always less than 3% except in one case at 17m/s with the maximum thrust

reduction setting. For the other 3P components, the errors were almost always less than 5%. A couple of example fits with error of 2.8% and 5.3% are shown in Fig. 3.4.

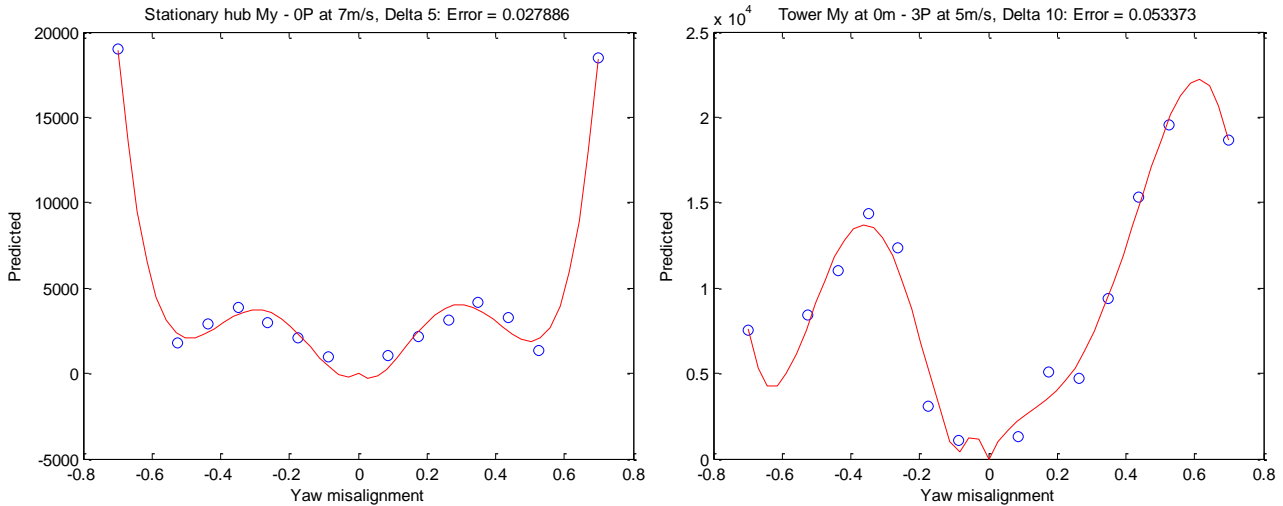


Figure 3.4: Example model fits for yaw misalignment (shown in radians, actually from -40° to $+40^\circ$)

For wakes, the situation is more complicated because wake width, centreline deficit, and the horizontal and vertical displacements of the wake centreline all affect the azimuthal variation of load. Since the wake effect is modelled in the absence of other asymmetries, only three parameters are needed: width ω , centreline deficit δ , and the magnitude of the centreline displacement, y . The phase of each harmonic is then predicted relative to the direction of the displacement, and once the displacement angle is known the phase is corrected accordingly. Thus, a three-parameter empirical model is required. For generality and better numerical scaling, δ is expressed as a fraction, and ω and y are normalised by the rotor diameter D . Furthermore, a new parameter ζ has been defined to represent approximately the change in velocity deficit across the rotor diameter:

$$\zeta = \exp\left(-0.5\left(\frac{y+R}{\omega}\right)^2\right) - \exp\left(-0.5\left(\frac{y-R}{\omega}\right)^2\right)$$

This was found to be a useful explanatory variable. For the oP hub M_y and M_z (nod and yaw) moments, a polynomial in $\delta\zeta$ was fitted:

$$A = \sum_{i=1}^n p_{iz}(\delta\zeta)^i$$

with A being the amplitude of the harmonic component, and a good fit was obtained with order $n = 8$. For the 3P loads, separate polynomials in ζ and δ were found to work better:

$$A = \sum_{i=1}^{n_\zeta} p_{iz}(\zeta)^i \cdot \sum_{i=1}^{n_\delta} p_{iz}(\delta)^i$$

for both the Y and Z components, using $n_\zeta = 6$ and $n_\delta = 2$. The errors are generally larger than for the shear and yaw models. The fit is again better for the hub My and Mz (nod and yaw) moments, with errors usually in the range 3 – 7% for both oP and 3P components, with a maximum of 8.2%. Hub Fx (thrust force) is similar with only one case above 7%, but hub Mx (torque) is not so well predicted, with errors typically in the range 10 – 20%. The other loads come somewhere in between. Two example fits, with errors of 3% and 8%, are shown in Fig. 3.5.

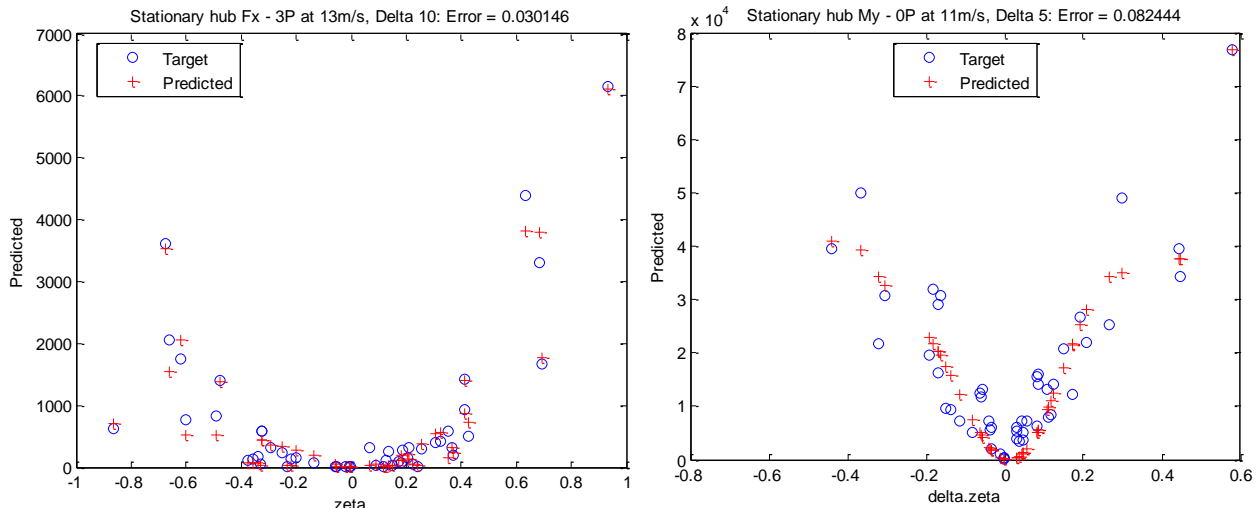


Figure 3.5: Example model fits for wake loads

The *Bladed* runs so far described have had gravity and tower shadow disabled, and wind flow parallel to the rotor axis. Further simulations have been run with gravity and tower shadow enabled, and zero upflow (so that the wind direction is misaligned from the rotor axis by the tilt angle). These three effects add a further deterministic contribution to the loads, but as these effects are not expected to change, their combined effect can be calculated with a single additional simulation at each wind speed and thrust setting – no additional parameters are involved. Imbalance effects have been ignored, but if desired they could simply be included along with the other deterministic effects described in this section.

The deterministic simulations should also include structural dynamics, as some response must be driven by the deterministic forcing. The separation of structural dynamic response between stochastic and deterministic simulations could become an issue in situations where a large resonant response occurs due to the coincidence of a lightly-damped resonant frequency with a harmonic of the rotational frequency, but this would indicate a poor turbine design.

MEAN OR DC LOADS

The modelled 3P deterministic load components and the stochastic loads all have zero mean. For the asymmetric loads like nod and yaw moments, the mean or oP component, which is entirely the result of the deterministic effects is obtained as explained above. For other loads, the mean values must be obtained in a different way. The mean or DC values of thrust and torque are already calculated anyway in the LongSim code, starting from steady-state aerodynamics, and the mean or DC value of other loads can be obtained by multiplying the torque or the thrust by an appropriate

correction factor or DC gain which can be obtained very simply, as a function of wind speed, from the results of one *Bladed* steady operational loads calculation per thrust setpoint.

COMBINING LOAD COMPONENTS IN LONGSIM

The *LongSim* wind field has statistical properties, such as turbulence spectra, which are defined for each period of (usually) 10 minutes. During each period, higher frequency wind variations are generated stochastically from these spectral properties. For this model, the wind speed spectrum is also used together with the stochastic transfer functions to generate zero-mean stochastic load time histories for each period, for every turbine. Then at each simulation time step during the period, this stochastic time history is scaled by the standard deviation of the wind incident in the turbine at that moment, including the effect of any wake turbulence. The rotor average wind speed, combined with the turbine operational state (rotor speed, pitch and yaw) also defines the rotor torque and thrust at each time step. These are multiplied by the appropriate DC gains to generate the DC load values at that time step for the symmetric loads, while the DC values for the asymmetric loads come from the oP deterministic effects of shear, yaw, wakes, gravity etc. The DC values are added to the stochastic values at each time step. However, the low-frequency stochastic variations will also come through in the DC values, leading to some double-counting; to avoid this, the stochastic variations for all variables which have a DC contribution are high-pass filtered. A first-order filter at 0.05 Hz was found to work well (the Hub M_y and M_z , which do not have a DC component, also need a filter to remove spurious very low frequencies, for which 0.01 Hz was used). Finally, the 3P deterministic load values at that time step are calculated from the amplitude A and phase φ of each deterministic load and the rotor azimuth, θ , as $A\cos(3\theta - \varphi)$. This could of course be extended to other harmonics if deemed significant.

So far, the loads are those in the non-rotating reference frame. Rotational transformations can then be used to calculate loads in the rotating frame. For the rotating hub loads, this would be a straightforward conversion using the sine and cosine of the azimuth angle. For the blade root loads (M_{bri} , $i = 1$ to N_B , the number of blades) the Coleman transformation is used to combine the non-rotating hub loads M_y (M_{hy}) and M_z (M_{hz}) together with the sum of the blade root out of plane moments (ΣM_{br}):

$$M_{bri} = (2/N_B) \left(M_{hy} \cos\left(\theta + \frac{2\pi(i-1)}{N_B}\right) + M_{hz} \sin\left(\theta + \frac{2\pi(i-1)}{N_B}\right) + \Sigma M_{br}/N_B \right)$$

where M_{hy} , M_{hz} and ΣM_{br} are total loads including their deterministic, stochastic and DC contributions.

COMBINING LOAD COMPONENTS IN LONGSIM

In future it is hoped to be able to validate the loads model by comparing simulation results against measured loads from wind farms including Lillgrund. Meanwhile some validation of the principles of the model and verification of its implementation has been achieved by comparing LongSim results against Bladed results for some particular situations which Bladed is able to simulate. Bladed can simulate the effect of a defined Gaussian wake deficit profile on a turbine (as was used for the steady wake effect simulations described above), so a two-turbine test case was set up in LongSim, with the second turbine partially waked by the first, and also having a yaw misalignment,

in a steady sheared windflow with no wake meandering. This exercises all the main features of the model, but in a situation which Bladed can reproduce. The setup is shown in Fig. 3.6. The turbulent wind speed time history at the downstream turbine was recorded along with the turbulence intensity and the wake deficit, width and centreline position. The wind speed history was used to generate a Bladed turbulence file, and a simulation was run for the waked turbine using the appropriate wake characteristics and turbulence. The loads generated by Bladed were compared to the LongSim results, in terms of time histories, spectra, damage equivalent loads (DELs) at different Wöhler exponents ('S-N slope'), and rainflow cycle distributions. The results are not expected to match exactly, of course, because the dynamic loads are generated by the particular stochastic wind variations across the rotor seen in the Bladed simulation, whereas in LongSim these effects are embodied in a generalised model through the transfer functions. Therefore the time histories, especially of loads whose oP components are purely stochastic, like the nod and yaw moments, will not match, but the spectra should match fairly well. The DELs should also match, except that they actually depend quite a lot on the random number seed used in the Bladed simulations to generate the spatial turbulence. The Bladed simulation was repeated with two different seeds to illustrate the differences introduced, but a thorough validation would need the DELs averaged over a larger number of seeds, or to use longer simulations so that the results are less seed-dependent. Nevertheless, the agreement obtained is very good, as illustrated by the examples in Fig 3.7Figure 3. to Fig 3.10

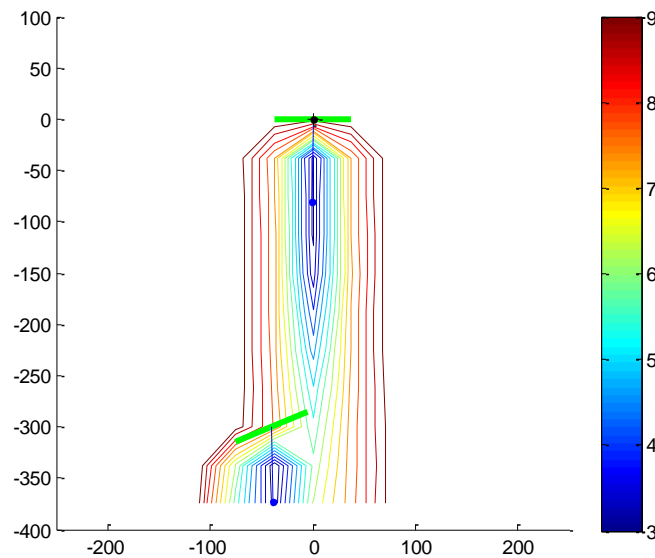


Figure 3.6: Test case for LongSim vs Bladed comparison

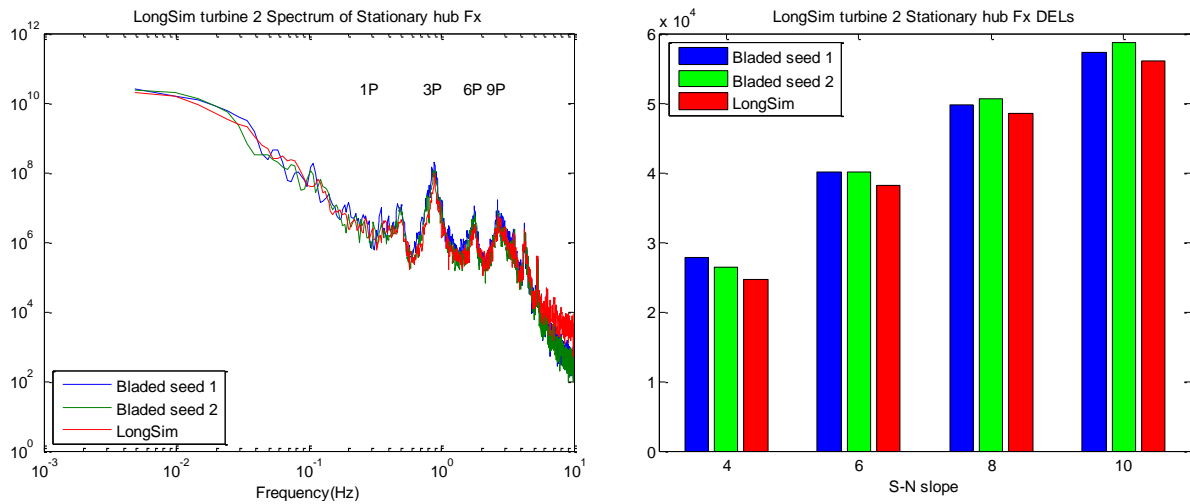


Figure 3.7: Hub thrust comparison: Spectra (left) and DELs (right)

Figure 3.7 shows the hub thrust force F_x . The spectra match extremely well, and for the DELs the small differences are comparable to the effect of different random number seeds. Figure 3.8 shows comparison for the hub M_z (yaw) moment. Here the random number seed has a big effect, affecting also the lower frequencies, but the LongSim result is very comparable. The yaw and nod moments also contribute to blade root out of plane bending, but the DELs are more strongly dominated by the rotational frequency (1P), so the seed differences are smaller, and again the LongSim result matches very well.

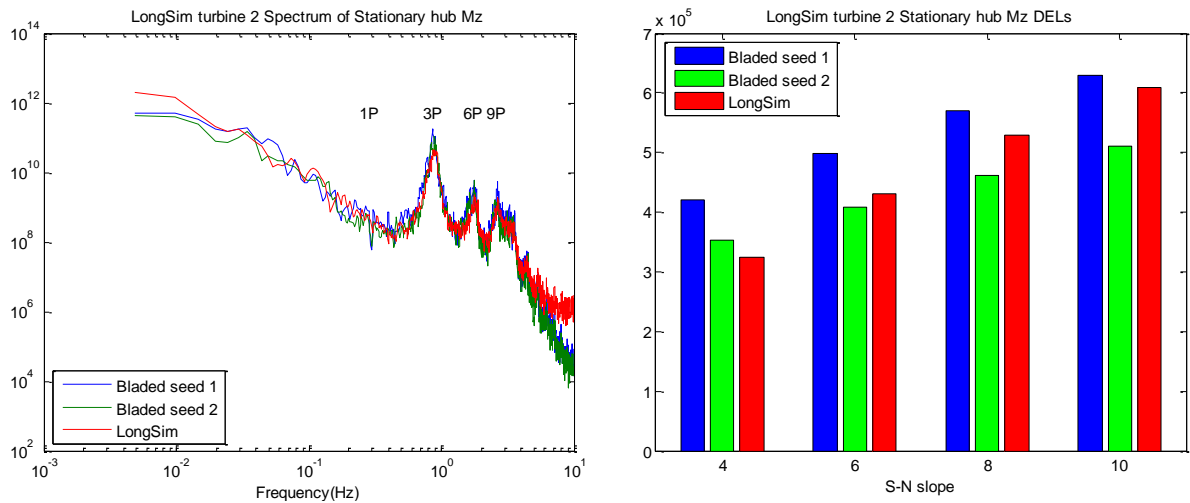


Figure 3.8: Hub yaw moment comparison: Spectra (left) and DELs (right)

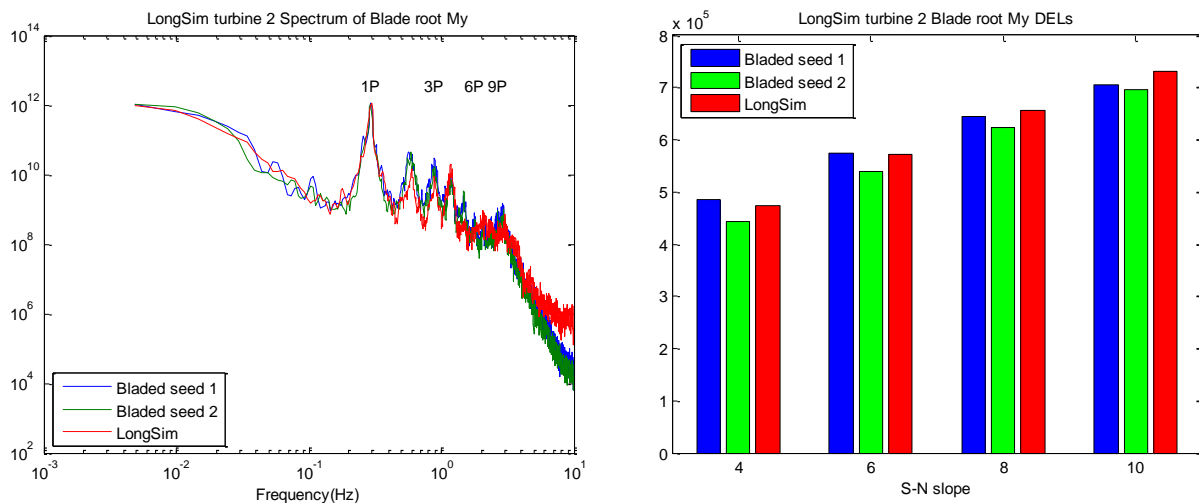


Figure 3.9: Blade root out of plane bending moment comparison: Spectra (left) and DELs (right)

Validation of wake models vs Lillgrund SCADA data

For the analyses carried out as part of TotalControl's deliverable D1.9, only one month worth of data was available at the time of submission, whereas almost eight-months-worth of data was later made available by TotalControl's partners. The data provided and used for wake models comparisons were:

- 10 seconds averaged SCADA data, available from 1st march 2012 to 2nd December 2012,
- 2.5, 5 and 10 minutes averaged SCADA data, available from 1st March 2012 to 31st October 2012,
- Details about four different modes of operation for nine turbines at the site: A05, A06, A07, B07, B08, C07, D07, D08, E07.

Preliminary investigations allowed to confirm the 10-minutes averaged data agreed well with the 10-seconds averaged data.

As it was highlighted in Deliverable D1.9, discrepancies in the Power, RPM or Pitch curves used were found in the shorter period of SCADA data available at that time, along with other issues such as erroneous nacelle direction offset and discrepancies in the indicated wind speeds and the correspondents active-power-derived wind speeds. Therefore, the first step of this analysis has focused on in-depth analysis of the dataset.

Curtailment modes. Four operational modes were provided by the project partners as part of the documentation: operational mode labelled "A" represents standard operations, whereas modes labelled "B", "C" and "D" are curtailed power modes

- 1) Four operational modes were provided by Siemens as part of the documentation: operational mode labelled "A" represents standard operations, whereas modes labelled "B", "C" and "D" are curtailed power modes.
- 2) Further investigations on the provided SCADA dataset allowed to clarify that six different modes of operation were actually flagged. Internal conversation with the turbine

manufacturer allowed to confirm that the operational mode labelled "0" corresponds to the standard mode of operation, whereas modes labelled "1", "2", "3" and "4" are curtailed operational modes. It is noted that mode "0" and mode "1" have a very similar power curve and pitch curve, but differ by the rotational speed curve. Another mode, labelled "5", is also present in the data but it can be disregarded since being used as an experimental curve, as confirmed by the manufacturer.

- 3) Data from the nine curtailed turbines were filtered for non-waked directions and for each operational mode. This allowed to compare the SCADA data points and the provided power, RPM and pitch curves, and allowed to confirm the curtailment modes are operating as prescribed.

Data from all the non-curtailed wind turbines were filtered for non-waked directions and compared to the provided operational curves. This allowed to confirm that all turbines followed the power curve and the pitch curve as prescribed in the standard operational mode. However, this also allowed to confirm that all the turbines follow the RPM curve labelled as mode "1", with the exception of turbines Co8, Ao1, Ao2, Ao3 and Ao4.

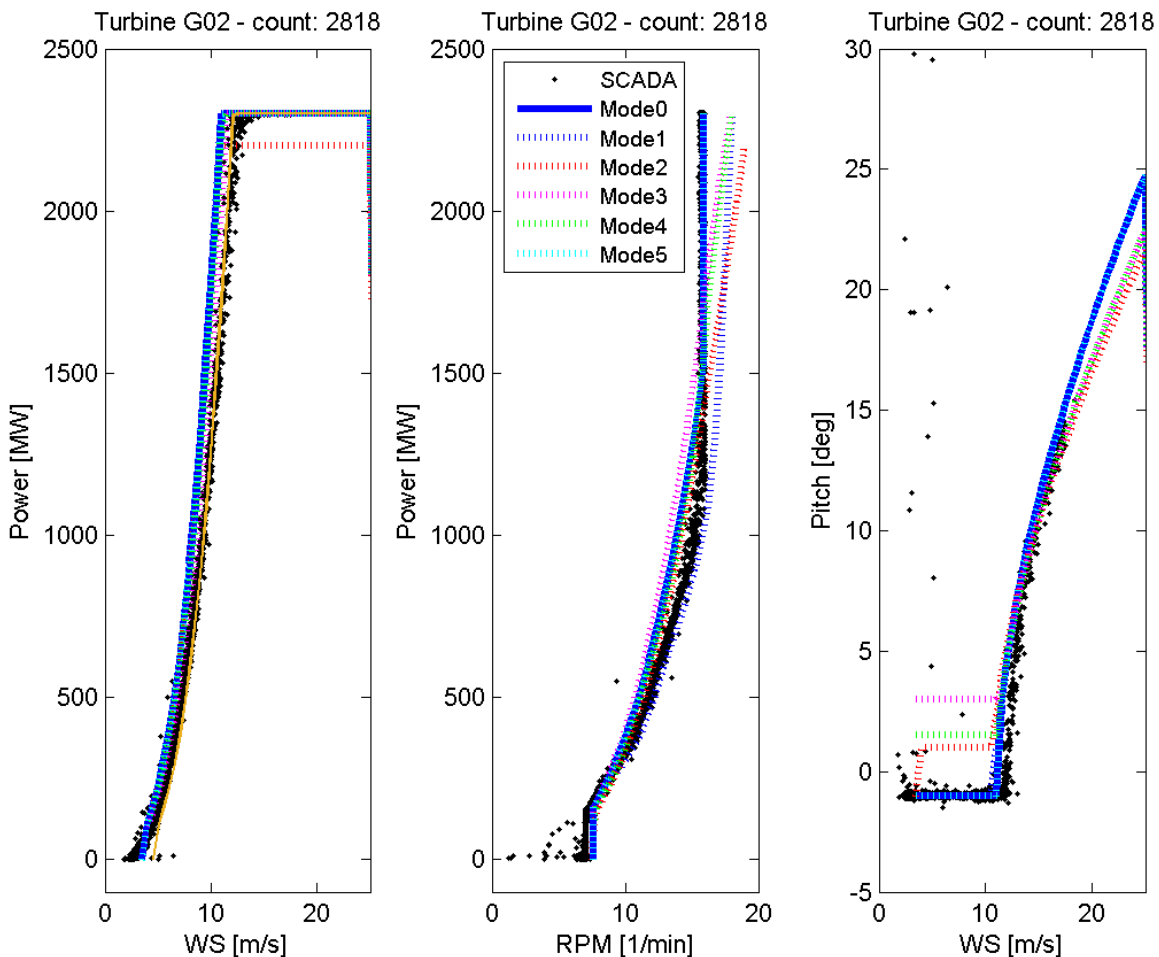


Figure 3.10: Comparison between SCADA data (power, rotor rotational speed and pitch angle) at Lillgrund turbine G02 with provided operational modes.

Directional offset. Extensive checks have been performed to correct erroneous directional offsets between the uncalibrated wind direction signal in the turbines' SCADA signals and the true wind direction.

- 1) Initially, directional signals from non-waked turbines for two different wind direction ranges, respectively centred at 42° and 300° , were filtered and compared within themselves into a correlation matrix. These comparisons allowed to highlight the turbines with an evident shift in wind direction. The biggest inconsistencies were found for turbines Co1 and G05.
- 2) As discussed in the next subsection, no meteorological on-site measurements were available, therefore data from the New European Wind Atlas (NEWA) dataset was downloaded for the area surrounding the site. The average wind directional from the corrected (as described in the point above) wind direction signals was compared to the NEWA's data, giving good results.
- 3) Once some confidence was gained on the wind direction signals from the two clusters of turbines non-waked for the 42° and 300° directional ranges, the wind direction offset was estimated for the waked turbines too. By using the power troughs in the waked sectors when comparing sets of aligned turbines, and by minimising the root-mean-square error between the binned power data and modelled results of the wake effects, the directional offsets could be obtained for all turbines. It is also noted that due to the scattering present in the data and the uncertainties related to the use of the NEWA dataset as a global reference for wind direction, the resolution of the obtained wind direction offsets was set to 5° .

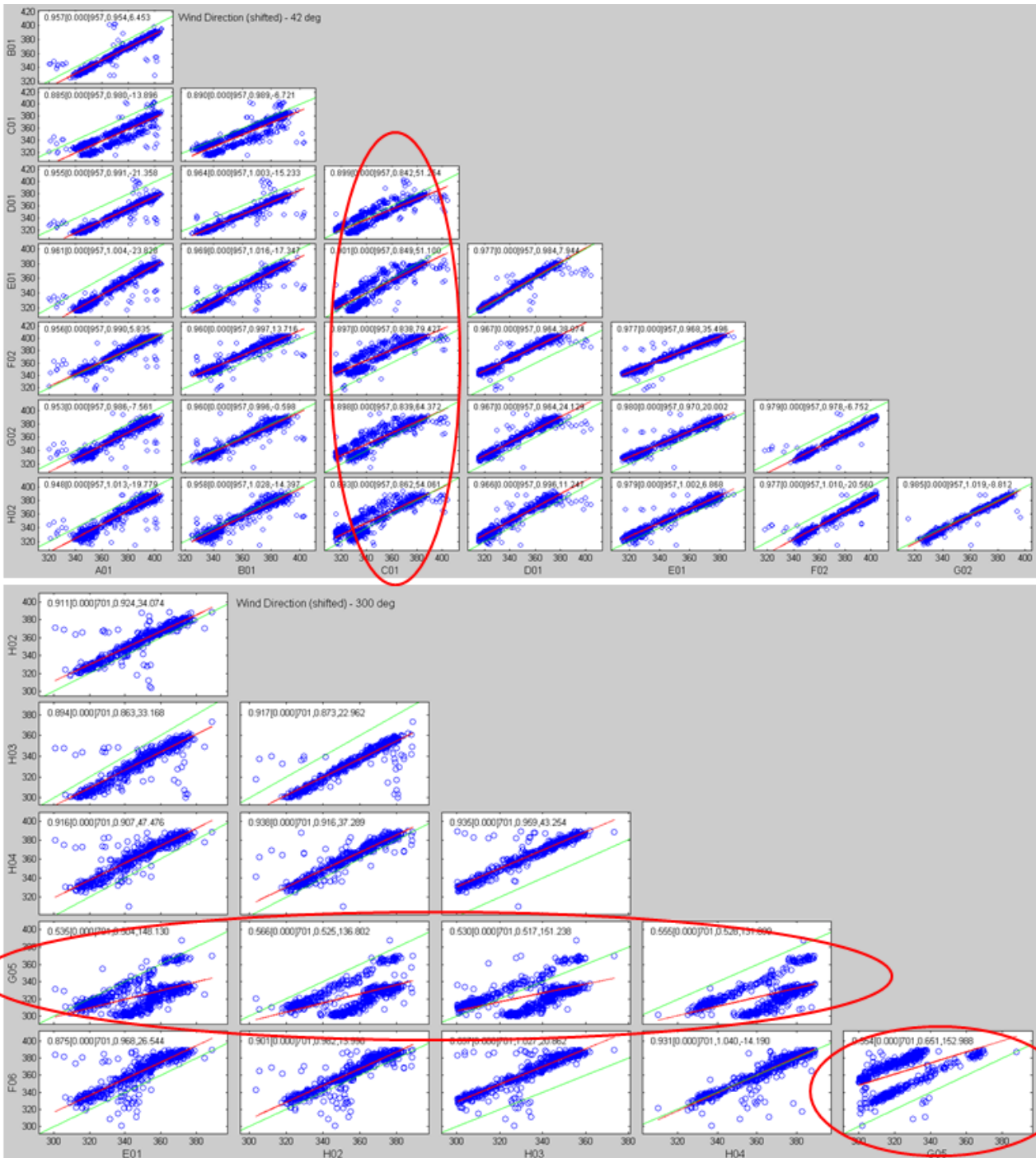


Figure 3.11 correlation matrix between turbines of the north edge of the lillgrund wind farm (above) and the west edge of the lillgrund wind farm (below). THE PLOTS CIRCELD IN RED SHOW THE LARGEST DISCREPANCIES IN WIND DIRECTION.

Moreover, DTU independently estimated the wind direction offsets with a similar methodology and provided a set of offsets that was very similar (but with higher precision than 5°) to the set obtained by DNV. The latter set of corrections was eventually used.

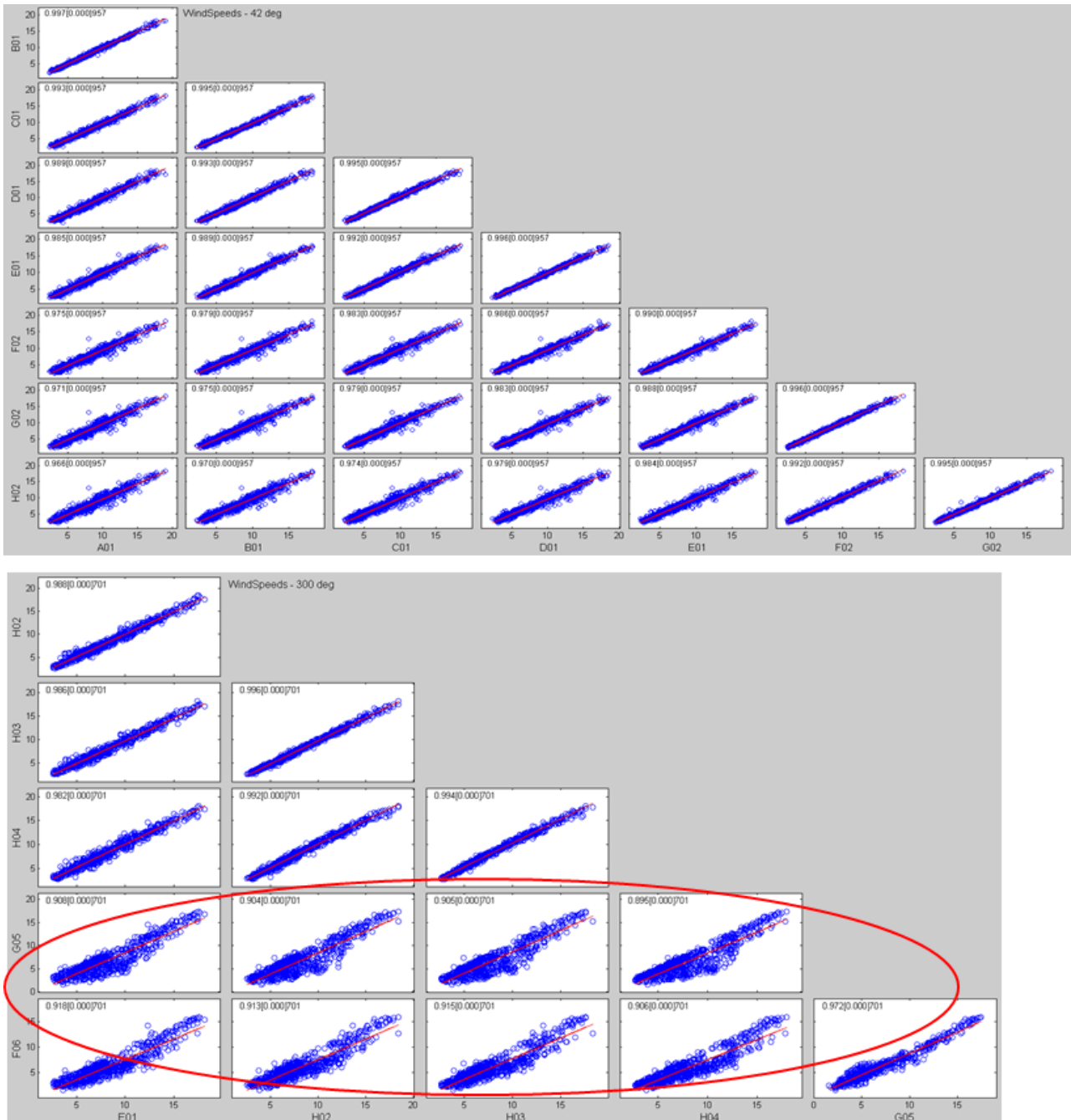


Figure 3.12: correlation matrix between turbines of the north edge of the lillgrund wind farm (above) and the west edge of the lillgrund wind farm (below). THE PLOTS CIRCELD IN RED SHOW THE LARGEST DISCREPANCIES IN WIND SPEED.

Wind speed offset

Comparing measured power curves at each non-waked turbines and the warranted power curves, a wind speed offset was estimated for each of these turbines that minimized the root-mean-square errors. These wind speed offsets, the median of which is -0.6m/s, is probably due to a mix of calibration errors and local site effects. More complex effects, such as coastal gradients and effects induced by blockage effects, were not considered for simplicity.

Meteorological data

The newly provided dataset contains turbine’s SCADA data including typical SCADA signals. It is worth reminding that no direct site measurements were available from masts or LiDAR’s, therefore the atmospheric stability information about the site were obtained using DTU’s software AMOK, using data from the nearby Drogden Fyr lighthouse, available only between 26th May 2008 and 22nd August 2011 and kindly provided by DTU.

For the purpose of this investigation, since no other on-site measurement was available, reanalysis data from the New European Wind Atlas (NEWA) database (freely available at the website <https://map.neweuropeanwindatlas.eu/>) was used.

This data is available from 1st January 2009 to 30th December 2018 and includes modelled values of wind speed, wind direction, turbulent kinetic energy, Obukhov lengths, and other standard atmospheric parameters.

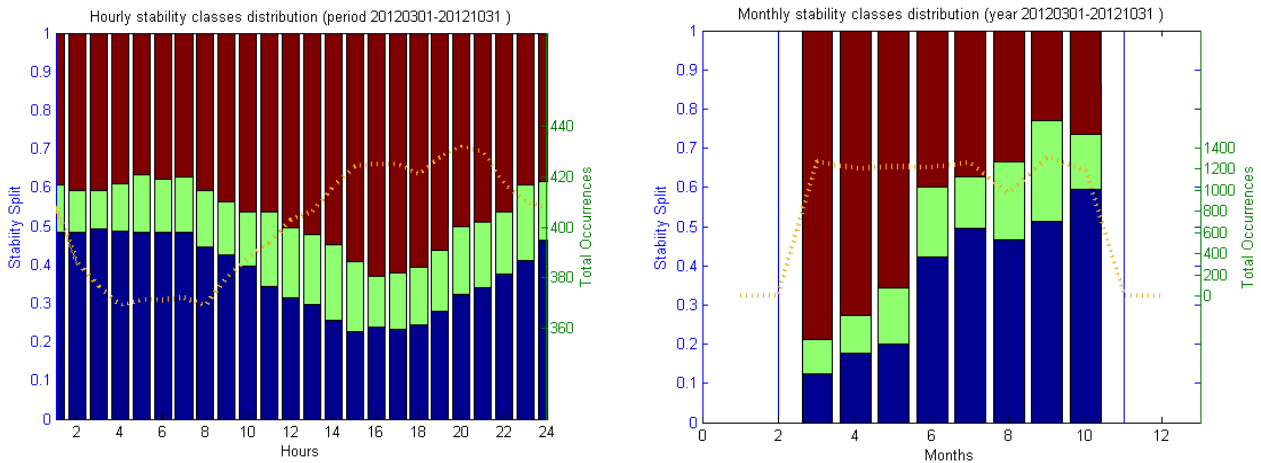


Figure 3.13 Occurrence of unstable, neutral and stable atmospheric conditions, based on hourly data from the newa database, between 2012-03-01 and 2012-10-31. Occurrence is shown binned both for hours of the day (left) and for each month (right). The orange dotted line represents the amount of data points for each bar. Colour Legend is the same as the one in the next Figure.

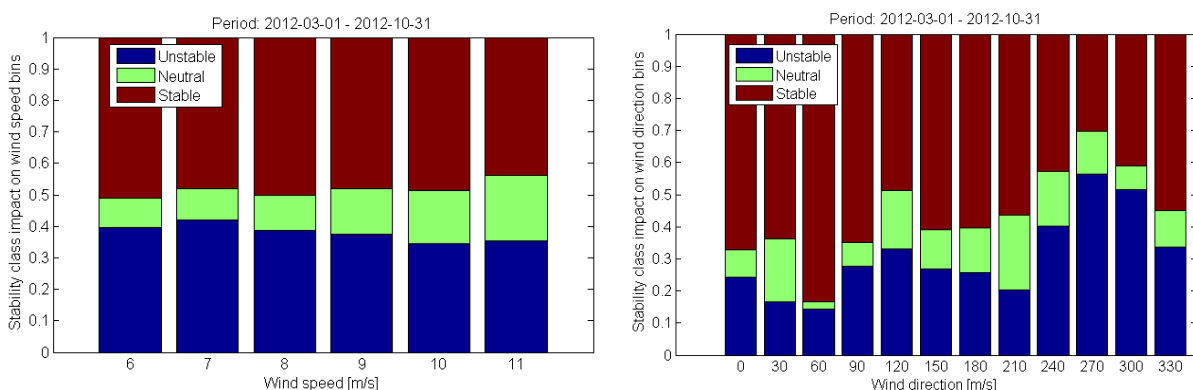


Figure 3.14: Occurrence of unstable, neutral and stable atmospheric conditions, based on hourly data from the newa database, between 2012-03-01 and 2012-10-31. Occurrence is shown binned for both wind speeds (left) and wind Directions (right).

As it can be seen in Figure 3.13 and 3.14, the site is strongly characterised by unstable and stable conditions, which can be defined by the Obukhov lengths provided by the NEWA database. The unstable, neutral and stable conditions have a mean Obukhov lengths of approximately -200, 650 and 100, respectively.

Ambient turbulent intensity at the site

Due to the lack of meteorological measurements on-site, it was not possible to get a reliable measurement of the ambient turbulence intensity. An attempt of obtaining an estimate of turbulence intensity both from the 10 seconds averaged and the values averaged for a different amount of minutes (from 1 to 10 minutes) was carried out, also using the NEWA database's turbulent kinetic energy data as a proxy. These tests did not lead to a definitive conclusion on how to obtain a reliable time-series of ambient turbulent intensity, although they identified the ratio between the standard deviation to mean value of active power from the SCADA data (taken at the unawaked turbines from the different wind directions) as the most credible estimate of the ambient turbulent intensity at the site.

Wake modelling

Several wake models were tested against the provided SCADA data. The wake model deemed most suitable to model the site production is an Ainslie model, modified to account for atmospheric stability. More details on such model can be found in Ruisi and Bossanyi (2019). The wake model used for the Lillgrund site uses a sum of deficit method (i.e. derived from conservation of momentum) for wake superposition and a Quarton-Ainslie model to obtain wake-added turbulence.

A first comparison was carried out using the turbine production data recorded during a series of toggle tests carried out at the site. The toggle test experiment was carried out from mid-February to September 2012, focusing on operating turbine Do8 in operational mode labelled "D", and operating turbine Do7 in mode "A" when the toggle test was off, and in mode "C" when the toggle test was on. The test was focused only on a 30° wind sector centred at 222°.

The data has been filtered for wind direction and making sure all the turbines were operational, and excluding spurious active power records. After filtering, the total number of 10-minute averaged data points remaining are 965 for the toggle-on subset and 670 for the toggle-off subset. Figure 3.15 shows how the measured and modelled powers (calculated as the sum of powers produced by turbines Do8, Do7 and Do6, and normalising this sum by Co8) agree especially for wind directions greater than 220°: this is probably influenced by the reduced number of datapoints present for wind directions lower than 220°. Apart from the good agreement between the wake model and the binned SCADA data, it can be seen how the toggle-on and toggle-off curves are not discernible, as also was pointed out as the outcome of these tests in 2012.

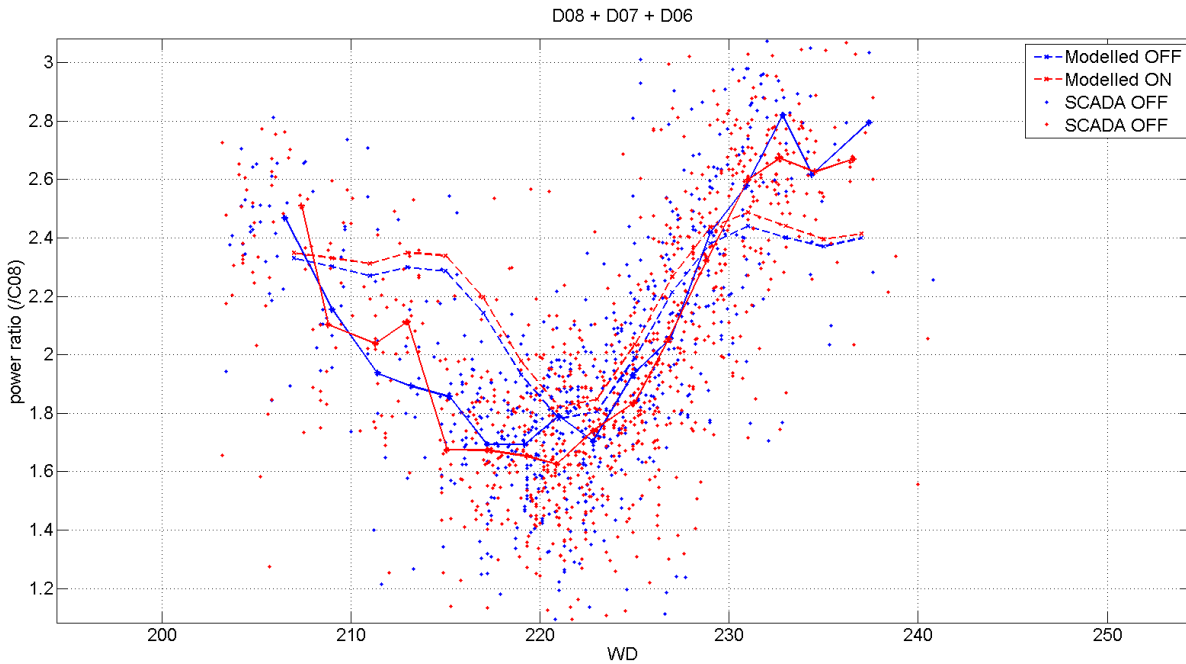


Figure 3.15: Sum of active power of turbines Do8, Do7 and Do6 compared for both toggle-on and toggle-off experiments. The power is normalised by the active power of turbine Co8.

In figure 3.16 the power ratio between turbines Do6 and Co6 is shown. It can be seen how the wake model is in reasonable agreement with the binned experimental data, and how the effect of the change in operational mode has a discernible effect on turbine Do6 (as compared to Co6, which is not affected by any change of operational mode), the third in the testing row of turbine.

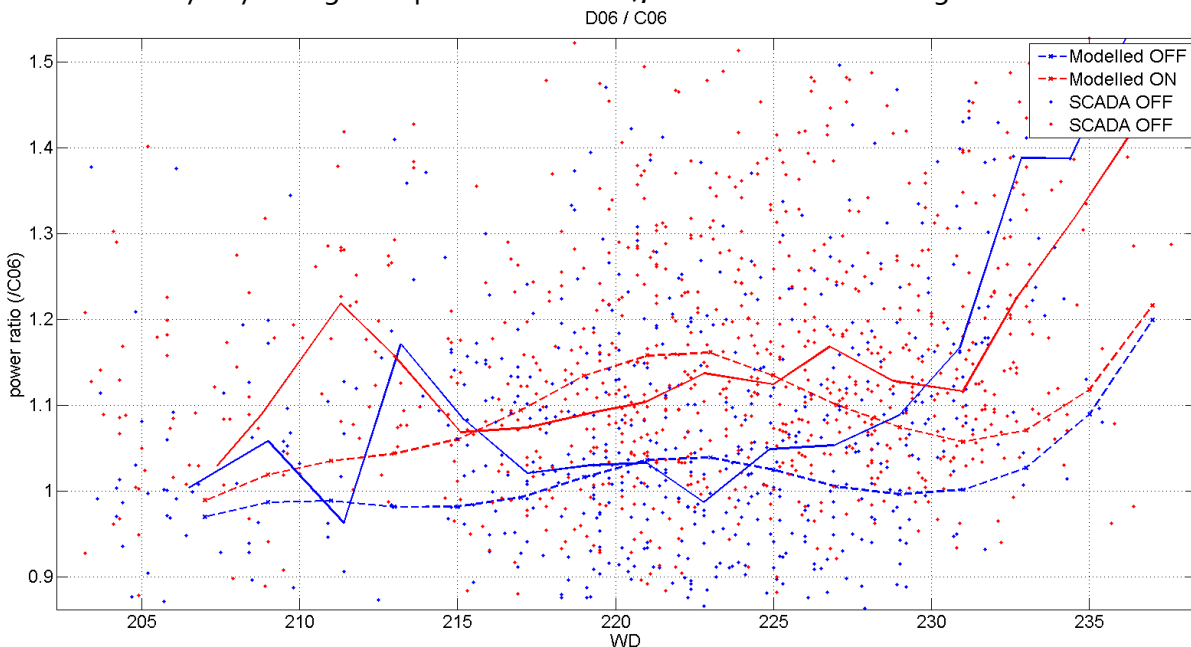


Figure 3.16: Active power of turbine Do6 normalised by the active power of turbine Co6, compared for both toggle-on and toggle-off experiments.

Encouraged by these preliminary results, three different wake models were compared to the whole available dataset. The so-called EPFL model (as defined in Bastankhah and Porté-Agel, 2016) was compared to two different flavours of the stability-modified eddy viscosity model described in Ruisi

and Bossanyi (2019). One of them included a modification of the wake superposition methodology entailing a streamtube expansion for closely aligned turbines. The modified eddy-viscosity models are run three times using three different Obukhov lengths (each representative for unstable, neutral and stable conditions), and then weighted averaged together based on the occurrence of such stability conditions.

Table 3.1 compares of the three models against the mean of power production by using metrics such as mean bias error (MBE), calculated between the total measured and predicted power, and the root-mean-square error (RMSE) calculated taking into account each turbine's measured and predicted power. It is evident from these numbers that the stability-modified eddy-viscosity model, using the sum-of-deficit method for wake superposition and the Quarton-Ainslie model for added wake turbulence, outperforms the other models and it is therefore going to be used in this work.

Table 3.1: Comparisons between error metrics given by different wake models, compared to scada active power data. the two values for each cell represent the comparison for a binned wind speed of 6 m/s and 8 m/s, respectively.

Wake Model	Mean Bias Error (MBE), total production [%]	Root-mean-square Error (RMSE) [-]
1) EPFL	2.4 to 9.2	23.6 to 76.2
2) Stability-modified Ainslie Model + Gunn + Quarton-Ainslie	4.0 to 13.8	23.4 to 79.4
3) Stability-modified Ainslie Model + sum-of-deficit + Quarton-Ainslie	-3.1 to 6.1	18.8 to 51.9

In Figure 3.17 the pattern of production of the whole wind farm is shown in comparison with the three models mentioned above. The measured data has been filtered as follows: wind speed 7 ± 0.5 m/s, wind direction $222^\circ \pm 15^\circ$, active power greater than zero.

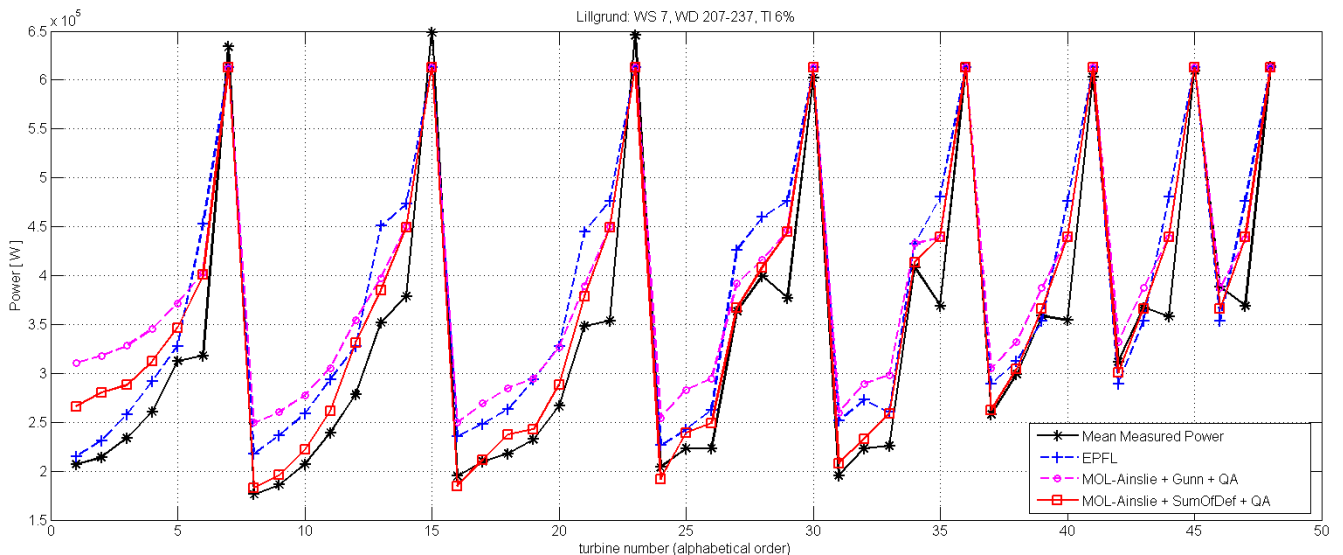


Figure 3.17: pattern of production filtered for 7m/s wind speed bin and wind directions ranging from 207° to 237°. Comparison with three wake models.

4. OPTIMAL PERFORMANCE USING LOW FIDELITY WAKE MODELS

4.1 DTU

We have used the Lillgrund wind farm as show case to demonstrate the capability of the DTU open loop platform for optimal wind farm control described in section 3.1.

The relative efficiency of different types of active wake control is an ongoing discussion within the wind energy community (Bossanyi, E. 2018), and the results of applying the DTU open-loop optimization platform to the Lillgrund wind farm in the this section will add to this discussion on a rational basis. As described in detail in section 3.1, inclusion of all essential interactions between the wind farm WTs are assured.

Three different sets of optimized control schemes for the Lillgrund offshore wind farm are derived - each conditioned on ambient mean wind direction and wind speed: 1) Optimal WPP control schedules as based on WT de-rating; 2) Optimal WPP control schedules as based on WT wake re-direction (facilitated by yawing the wind farm WTs by purpose); and 3) Optimal WPP control schedules as based on integrated WT de-rating and yawing. For each set of control schedules, the aggregated increase of the annual energy production compared to the base case (no wind farm supervisory control) is evaluated using the site sector Weibull distributions combined with the site wind direction probability density function.

The Lillgrund wind farm

The Lillgrund wind farm consists of 48 Siemens SWT-2.3-93 WT's with a layout as shown in Figure 4.1. The layout of the Lillgrund wind farm is characterized by very small WT inter spacing's – i.e. down to 3.3 rotor diameters – and consequently with pronounced wake effects, which makes this wind farm ideally suited for wind farm control. Close WT spacing favours de-rating compared to yaw dictated wake re-direction, because the latter type of active wake control needs some distance to develop significantly. Thus, a priory a pronounced effect of active wake control in the form of WT de-rating is deemed promising. However, for wind directions 'skew' to WT rows, yaw re-direction might be an efficient approach to harvest gains in wind farm power production even for close spacing. Thus, combining both types of active wake control might be the optimal strategy.

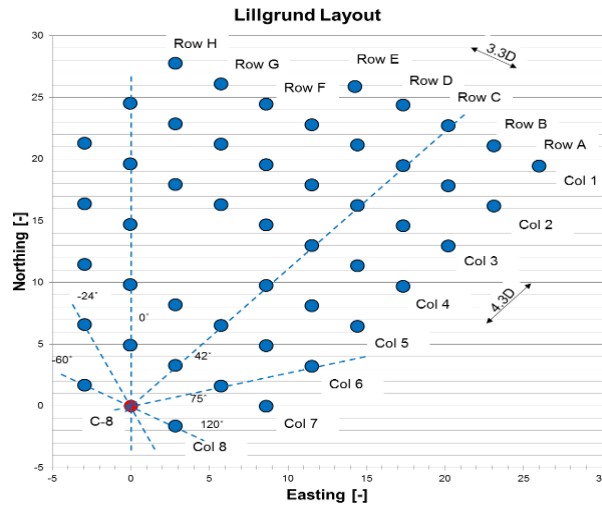


Figure 4-1: Map of lillgrund wind farm

The AEP for the wind farm is computed using the optimized control schedules and compared to the AEP resulting from the traditional “greedy” WT control strategy using site wind characteristics. The complete wind rose is resolved in 30° sectors, and for each of these the sector probability as well as the mean wind speed Weibull parameters (i.e. shape and strength parameter) are given and shown in Table 4.1

Table 4.1: Lillgrund site wind characteristics.

Wind Section (centered)	Wd (%)	Scale (A)	Shape (k)
0 deg	5.4	8.2	1.83
30 deg	4.2	7.6	2.1
60 deg	5.4	8.3	2.29
90 deg	6.6	9.0	2.69
120 deg	8.3	9.8	3.0
150 deg	8.3	9.4	3.16
180 deg	7.6	9.2	2.43
210 deg	10.6	10.1	2.53
240 deg	13.6	10.8	2.81
270 deg	15.4	10.6	2.66
300 deg	9.6	9.4	2.42
330 deg	5.0	9.7	1.92

The average yearly wind farm energy production (AEP) is computed for the investigated control strategies conditioned on mean wind speed (1m/s resolution) and mean wind direction (1° resolution), respectively, and subsequently convoluted with mean wind speed distributions and the mean wind direction distribution to obtain the AEP estimate, which in turn is compared with the base case (no wind farm supervisory control). Note, the high azimuthal resolution of the inflow direction. This is needed as a moderate change in inflow wind direction results in non neglectable changes in the down stream wake flow patterns and thus the optimal wind farm control schedule (cf. Figures 4.5 and 4.6).

Optimal de-rating

Examples of a resulting control schedules – conditioned on a mean wind farm inflow speed of 9m/s and for various mean inflow wind directions – are given in Figures 4.2–4.15. For each WT in the wind farm, the resulting de-rating percentage is indicated by the WT de-rating colour code. The wind farm flow field characteristics are illustrated by the blue wind speed colour code. As seen, optimal de-ratings are, as expected, more pronounced for the upstream WTs affecting the downstream WTs the most, whereas downstream WT's deep into the wind farm are either not affected or only affected to a minor extend.

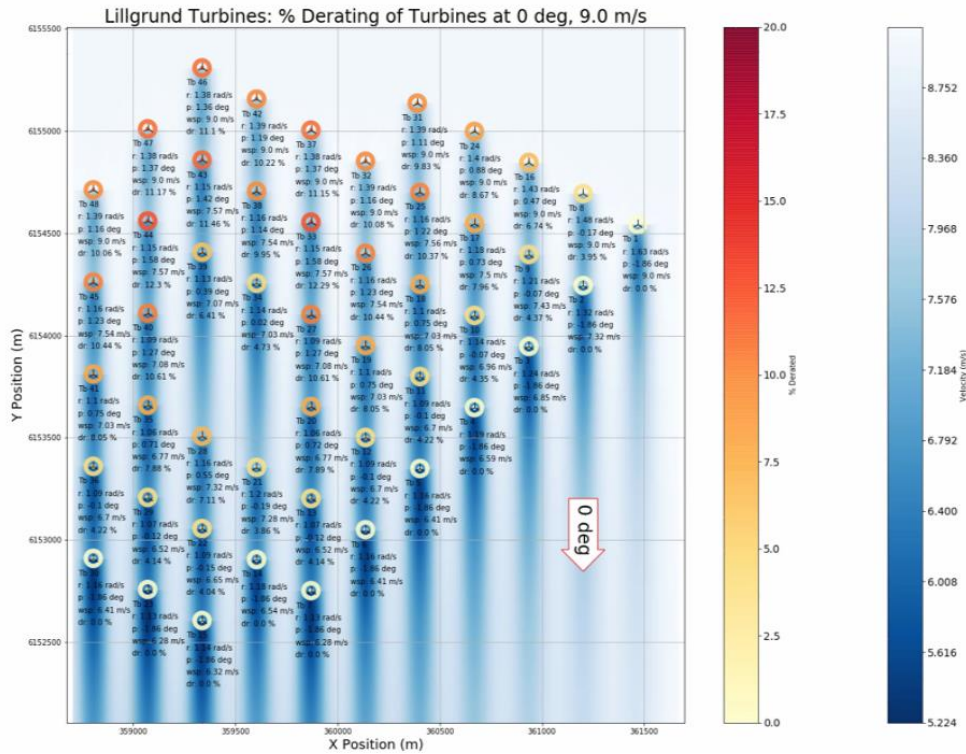


Figure 4-2: Optimal WT de-ratings associated with mean wind speed gm/s and wind direction 0° (northerly winds).

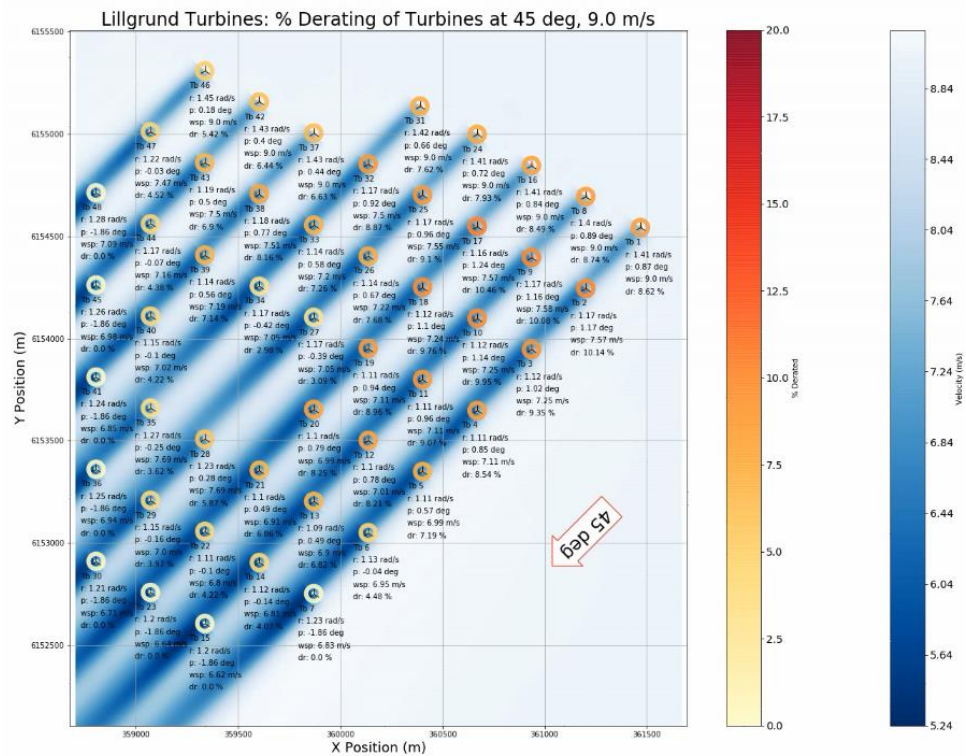


Figure 4-3: Optimal WT de-ratings associated with mean wind speed gm/s and wind direction 45°.

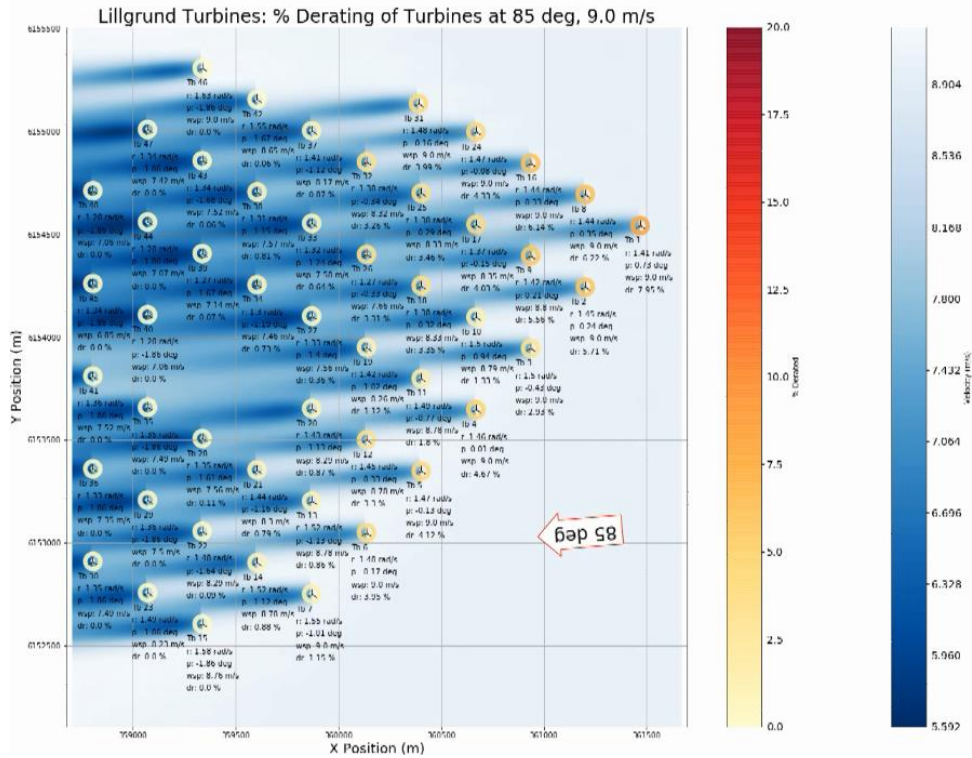


Figure 4-4: Optimal WT de-ratings associated with mean wind speed 9m/s and wind direction 85°.

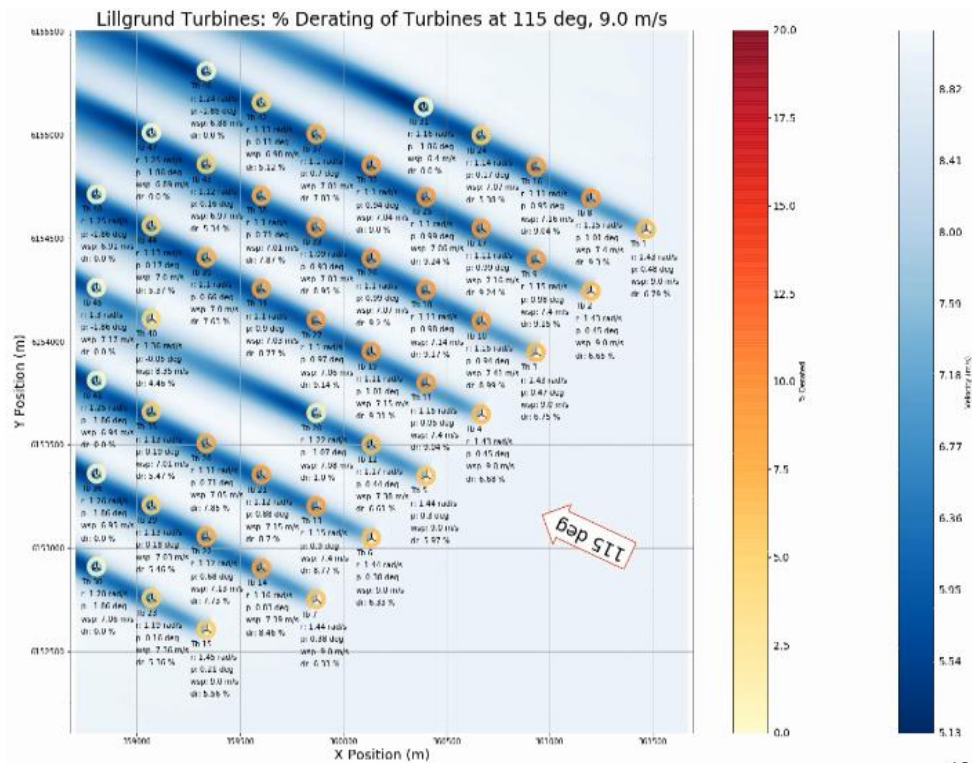


Figure 4-5: Optimal WT de-ratings associated with mean wind speed 9m/s and wind direction 115°.

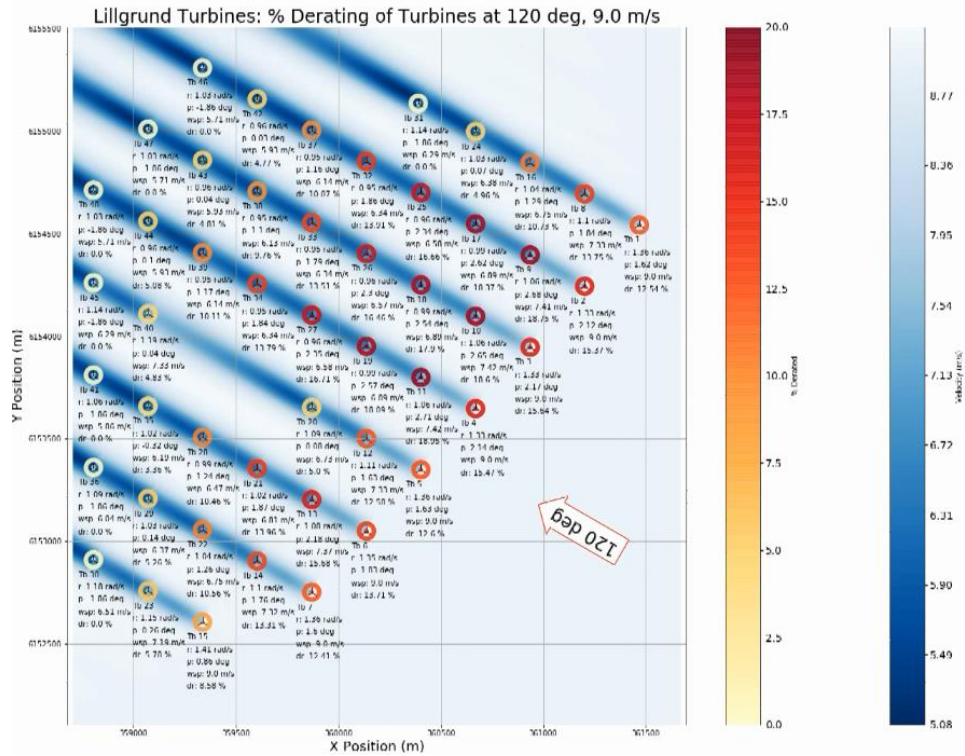


Figure 4-6: Optimal WT de-ratings associated with mean wind speed gm/s and wind direction 120°.

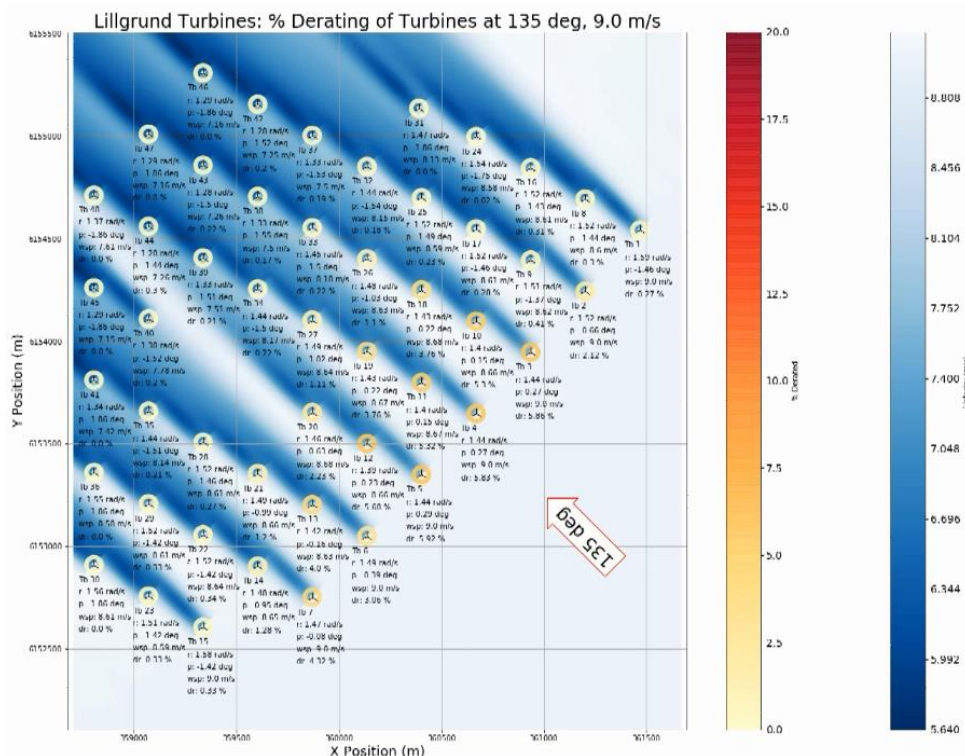


Figure 4-7: Optimal WT de-ratings associated with mean wind speed gm/s and wind direction 135°.

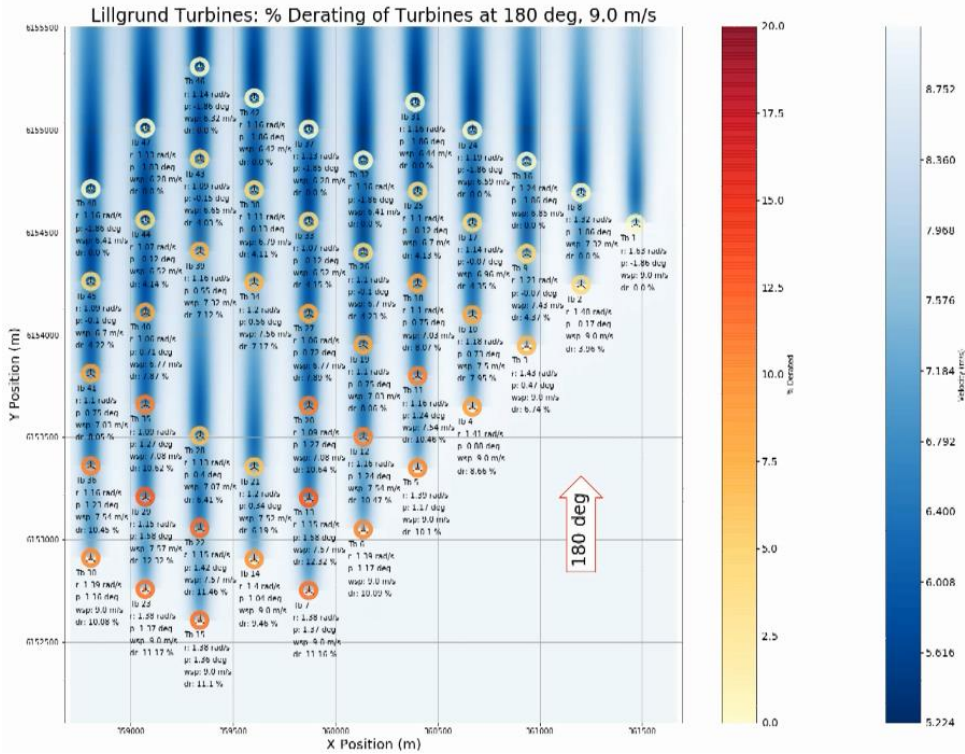


Figure 4-8: Optimal WT de-ratings associated with mean wind speed 9m/s and wind direction 180°.

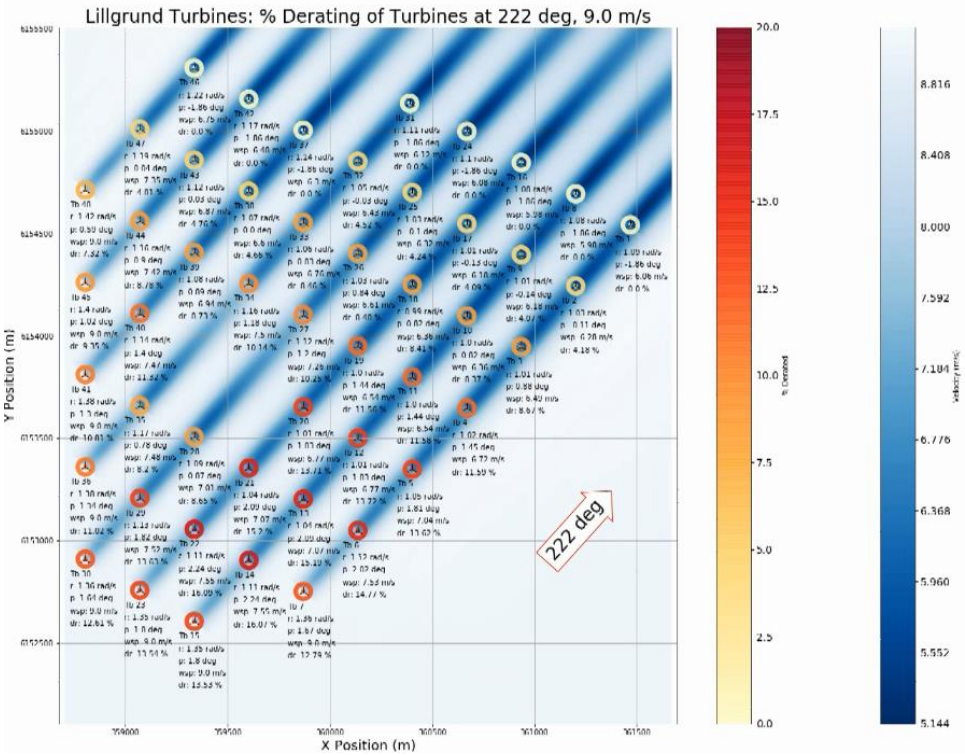


Figure 4-9: Optimal WT de-ratings associated with mean wind speed 9m/s and wind direction 222°.

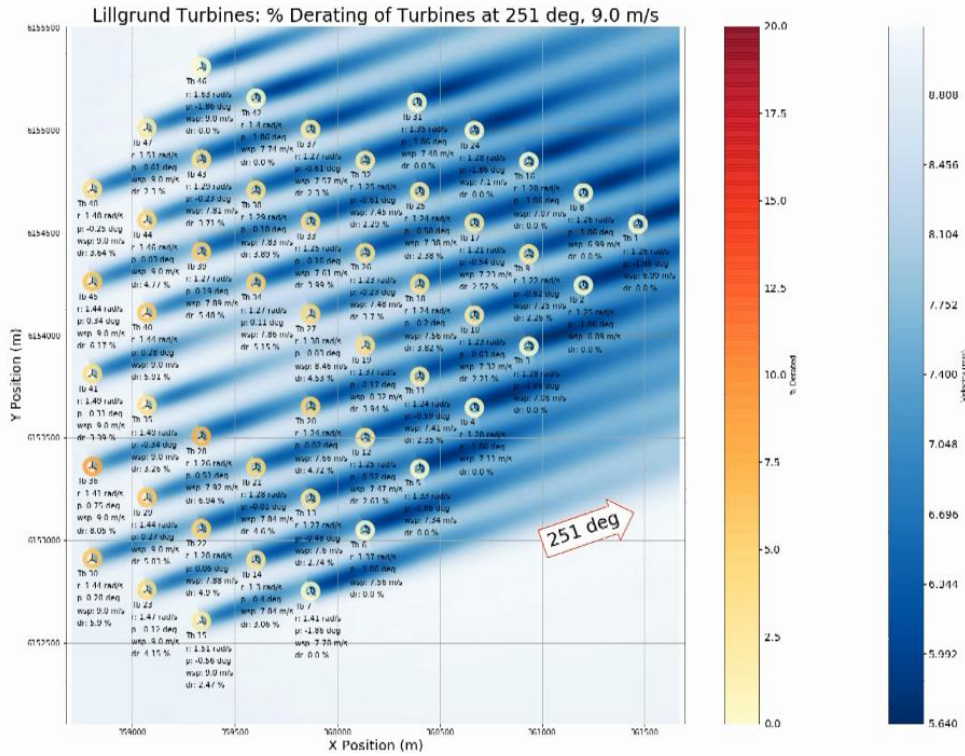


Figure 4-10. Optimal WT de-ratings associated with mean wind speed 9m/s and wind direction 251°.

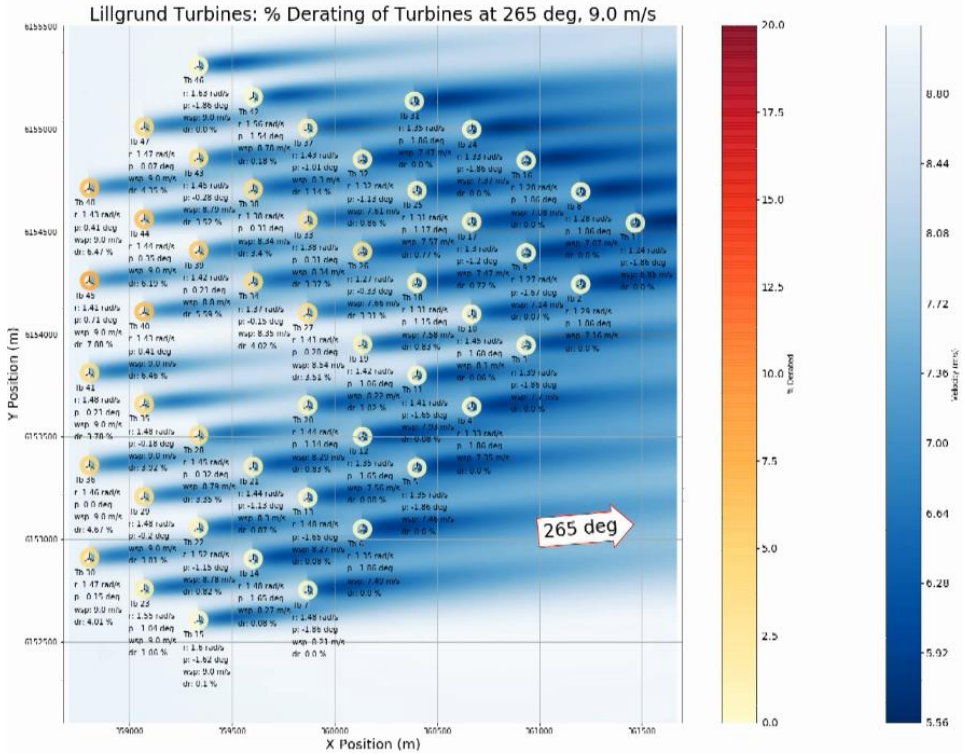


Figure 4-11: Optimal WT de-ratings associated with mean wind speed 9m/s and wind direction 265°.

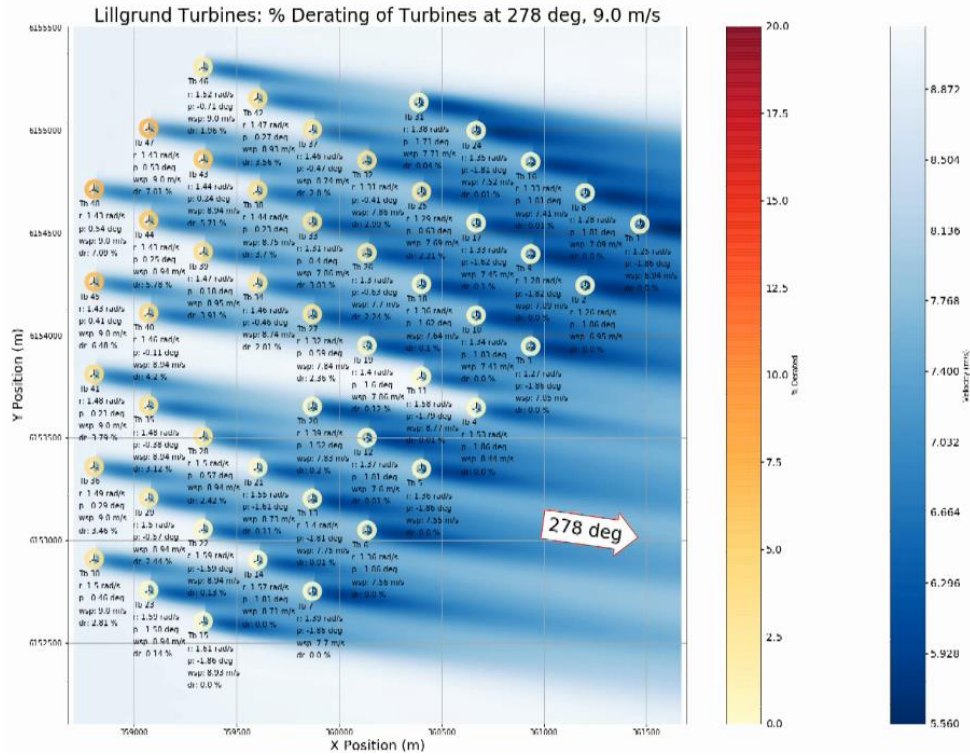


Figure 4-12: Optimal WT de-ratings associated with mean wind speed 9m/s and wind direction 278°.

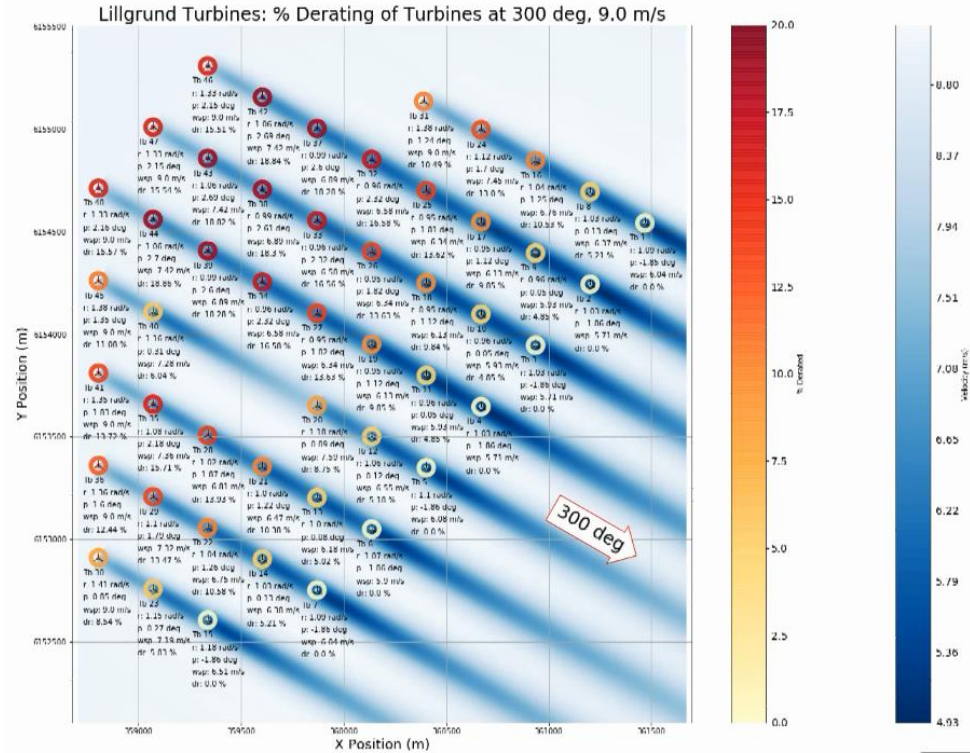


Figure 4-13: Optimal WT de-ratings associated with mean wind speed 9m/s and wind direction 300°.

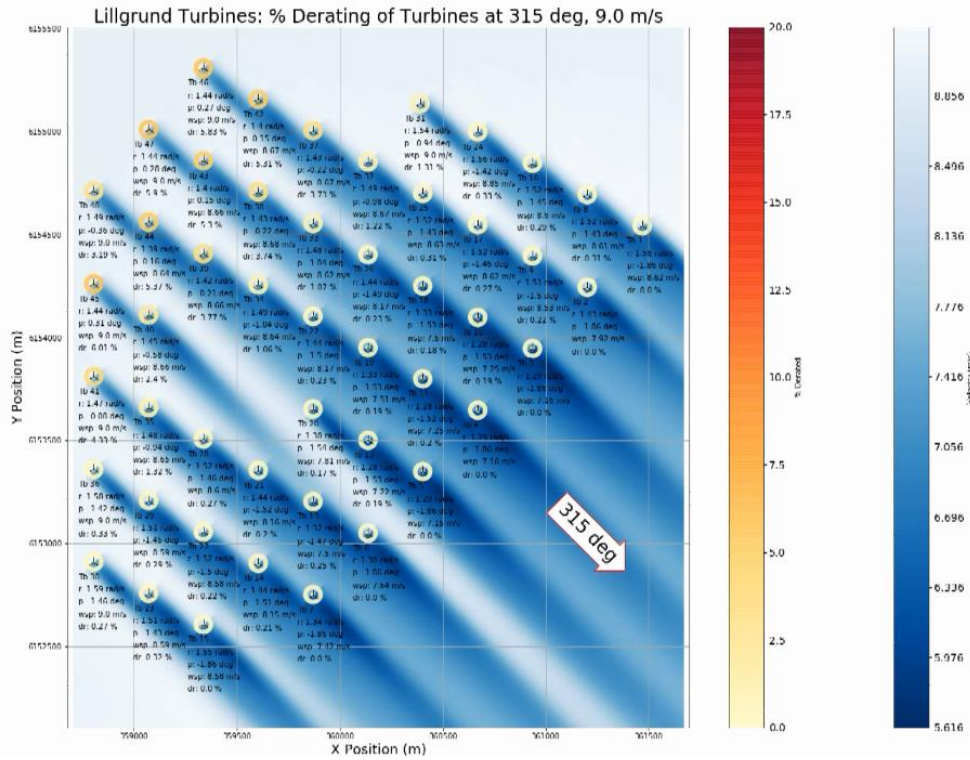


Figure 4-14: Optimal WT de-ratings associated with mean wind speed gm/s and wind direction 315°.

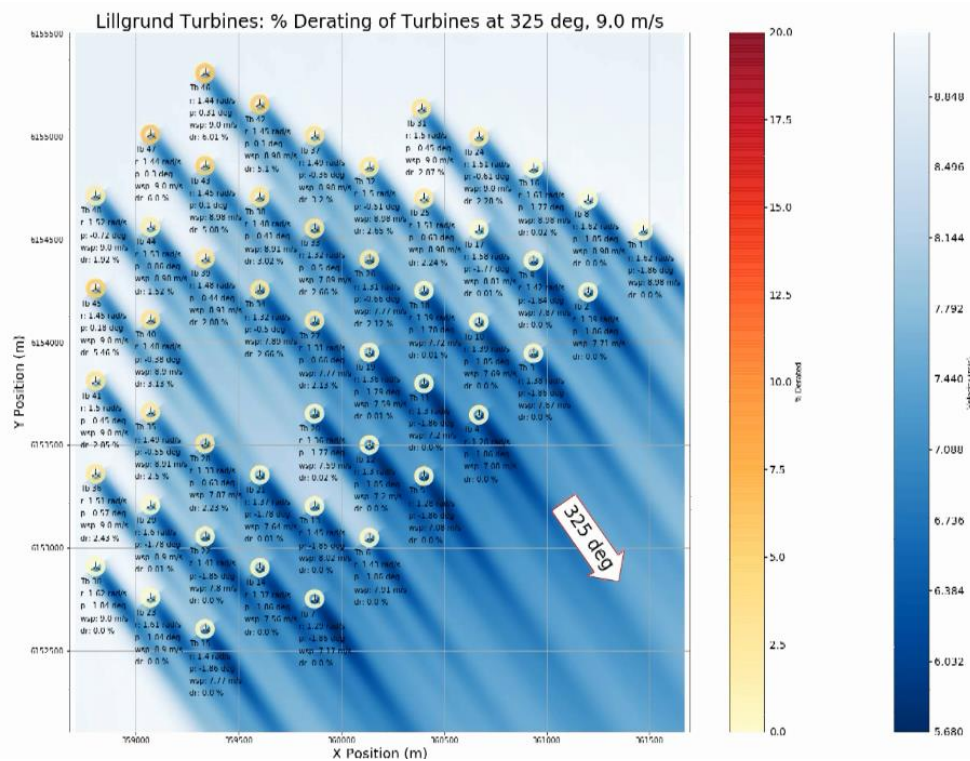


Figure 4-15: Optimal WT de-ratings associated with mean wind speed gm/s and wind direction 325°.

The aggregated AEP results are shown in Figure 4-16. The left plot of this figure shows the AEP gains *conditioned on the inflow mean wind direction* and with reference to the mean wind speed regime [4m/s;25m/s]. The gain is obviously highly dependent on the inflow direction, with the largest potential gains obtain in cases with massive wake effects as expected. The right plot of Figure 4-16 shows the AEP gain *conditioned on mean wind speed*. As expected the largest gains are obtained in the WPP mean inflow wind speed regime, where all WT's are operated below rated wind speed. With increasing wind farm inflow wind speed, more and more WPs are successively operating above rated wind speed, thus gradually reducing the possible AEP gain.

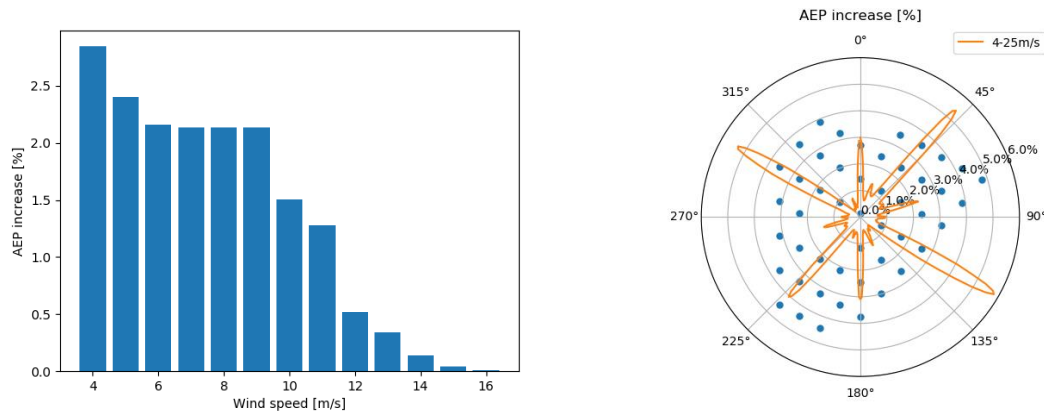


Figure 4-16: AEP gain obtained using optimized de-rating control schedules (Vitulli, J. A., Larsen, G. C., Pedersen, M. M. et.al.)

In total the WPP AEP gain referring to all wind speeds (i.e. 4-25m/s) is approximately 1.0%. If one were only to consider wind speeds between 4m/s to 11m/s, where increased production is possible applying optimized settings, then this gain rises to 1.5%.

4.2 KUL

The updated GWM model with yawing extension defined in Section 3.2 serves as a basis for developing an optimization framework to determine yaw setpoints across a windfarm for different operating conditions with the goal of power maximization.

$$\min P(\gamma) = -1 * \sum_{k=1}^{N_t} \frac{1}{2} \rho C_p(\gamma_k) A_k U_k^3(\gamma_l, \gamma_{l+1}, \dots, \gamma_{N_t}), \quad s. t. \quad -\frac{\pi}{6} < \gamma < \frac{\pi}{6}$$

C_p is the wind turbine power coefficient and the yaw angles are constrained to be within $\pm\pi/6$, as previous studies have shown that the fatigue loads beyond these yaw angles tend to be prohibitive for turbine lifetime. The optimization problem is solved using the 'SLSQP' solver of the scipy.optimize python package. Basinhopping, a multi-start approach is utilized to ensure global optimality.

Reference windfarm cases operating under normal operation are required to demonstrate the benefits of wake steering control. To this end, we make use of two different windfarm setups. For

the first, we utilize the publicly available TotalControl reference windfarm database which comprises of numerical measurements using high fidelity LES spanning different atmospheric conditions and wind directions for the TotalControl reference windfarm (Anderson, S.J., Meyers, J., Sood, I. and Troldborg, N). The TotalControl Reference Wind Power Plant (TC RWP) is a virtual setup which comprises of 32 DTU 10 MW turbines, separated by 5D spacing in the vertical and horizontal directions. Only the cases from the reference database which have significant wake overlap between upstream and downstream turbines are considered for yaw optimization. The layout of the TC RWP is presented in Figure 4-17.

The second windfarm under consideration for performance optimization through wake steering is the real world Lillgrund windfarm situated off the coast of Sweden. The windfarm comprises of 48 Siemens 2.3 MW turbines in a tightly spaced layout, which leads to significant efficiency losses due to wake effects. A comparison of the layout of the TC RWP and the Lillgrund windfarm is shown in . The reference cases used for the Lillgrund windfarm to determine the effect of wake steering are chosen from another TotalControl deliverable, D 1.2.1, in which data from a measurement campaign conducted at Lillgrund was used for validating KU Leuven's LES code, SP-Wind. All the selected cases have been summarized in Table . PDK refers the Pressure Driven Boundary Layer (PDBL) and CNk₂ and CNk₄ refers to the Conventionally Neutral Boundary Layer (CNBL) inflows from the publicly available TotalControl inflow database (Anderson, S.J., Meyers, J., Sood, I. and Troldborg, N). The inflows PDK₁, PDK₂ and , PDK₃ are flowfields obtained by transforming the PDK inflow, achieved by changing the surface roughness and friction velocity to match the inflow conditions at the Lillgrund windfarm during the measurement campaign.

Table 4.2 GWM Power optimization cases

Case No.	Inflow	Windfarm	Wind direction (degrees)	Hub ht wind speed (m/s)
1	PDK	TC RWP	0	9.4
2	CNk ₂	TC RWP	300	11
3	CNk ₂	TC RWP	330	11
4	CNk ₄	TC RWP	300	11.3
5	CNk ₄	TC RWP	0	11.3
6	PDK ₁	Lillgrund	119	8
7	PDK ₂	Lillgrund	243	8.5
8	PDK ₃	Lillgrund	110	4.5

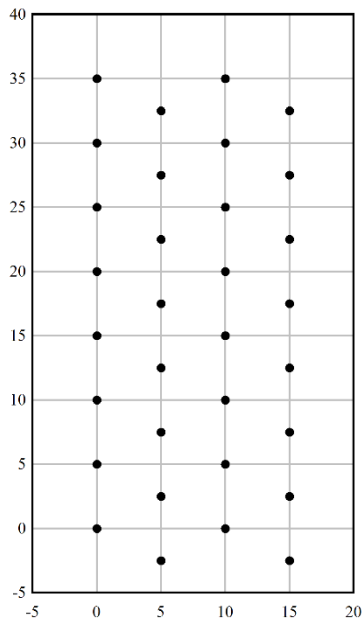


Figure 4-17 Layout of the TC RWP. Axes have units of s/D , with a rotor diameter $D = 178.3$ m.

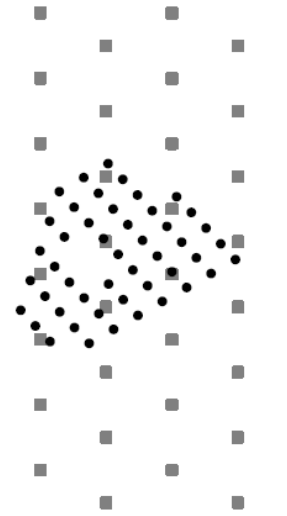


Figure 4-18 Scale comparison of the TC RWP (gray) and the Lillgrund WP (black). LILLGRUND TURBINES HAVE A ROTOR DIAMETER OF $D = 93$ M.

For each of the cases outlined in Table 4.2, the GWM defined in section 3.2 is utilized to determine the optimal yawing setpoints across the windfarm for the purpose of power maximization. The free stream wind velocity and turbulence intensity, which are input parameters required for the GWM, are obtained from the respective flow profile from the reference LES database. The yaw set points are then used to run simulations in a LES high fidelity environment for validating the power gains using the code SP-Wind ((J. P. Goit and J. Meyers), (D. Allaerts and J. Meyers), (W. Munters and J. Meyers)). Spatial discretization in SP-Wind is performed by combining pseudo-spectral schemes with fourth-order energy-conservative finite differences. The equations are marched in time using a fully explicit fourth-order Runge-Kutta scheme, and grid partitioning is achieved through a scalable pencil decomposition approach. Subgrid-scale stresses are modeled with a standard Smagorinsky model with wall damping. Wind turbines are modeled by an actuator sector model, coupled with a nonlinear flexible multi-body dynamics model (A. Vitsas and J. Meyers). Turbulent inflow conditions for wind-farm simulations are generated in separate precursor simulations (W. Munters, C. Meneveau, and J. Meyers). A streamwise slab of the velocity and temperature field is stored to disk when running the precursor, and is later introduced in the wind-farm domain by means of body forces in a so-called fringe region. Similar to the reference database, the simulations are divided into 2 parts. First, a spin-up period of 15 min is initiated for the settling of start-up transients, followed by 60 minutes of data collection. The LES time step is set to 0.5s, while the structural solver operates at a higher frequency of 100 Hz. The general domain parameters for the LES simulations are outlined in Table 4.3.

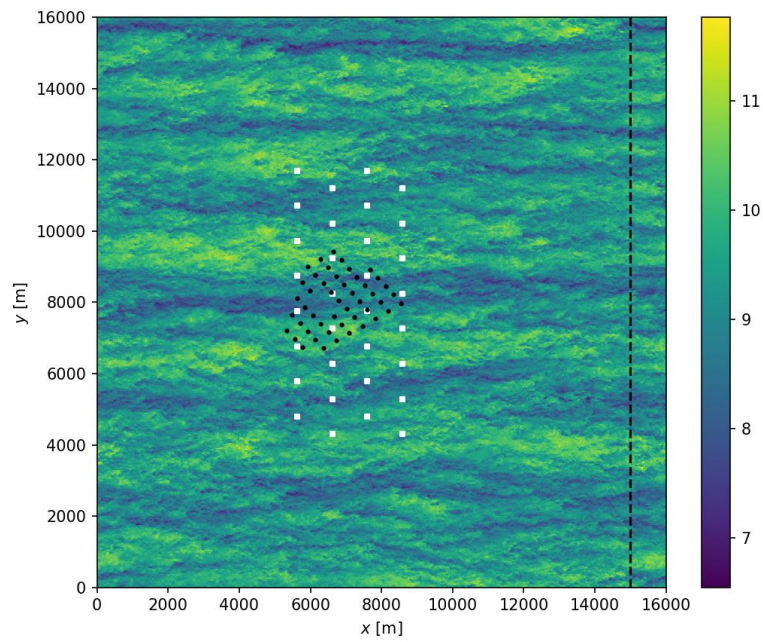


Figure 4-19 Planview of Lillgrund (black) and TotalControl Reference windfarm layout (white) in simulation domain. The black dashed line indicates the extent of the slab from which inflow data is extracted from the precursor simulation (without turbines). The background is colored with a typical instantaneous streamwise velocity field at turbine hub height in a precursor simulation without turbines.

Table 4.3 Simulation parameters for SP-Wind

	Variable	Values
Domain size	$L_x \times L_y \times L_z$	$16 \times 16 \times 1.5 \text{ km}^3$
Grid	$N_x \times N_y \times N_z$	$1200 \times 1200 \times 225$
Resolution	$\Delta_x \times \Delta_y \times \Delta_z$	$13.33 \times 13.33 \times 6.66 \text{ m}^3$
Spinup time	T_{spin}	15 min
Simulation time	T	60 min
Time steps	$\Delta t_{LES}, \Delta t_{struct}$	0.5 s, 0.01 s

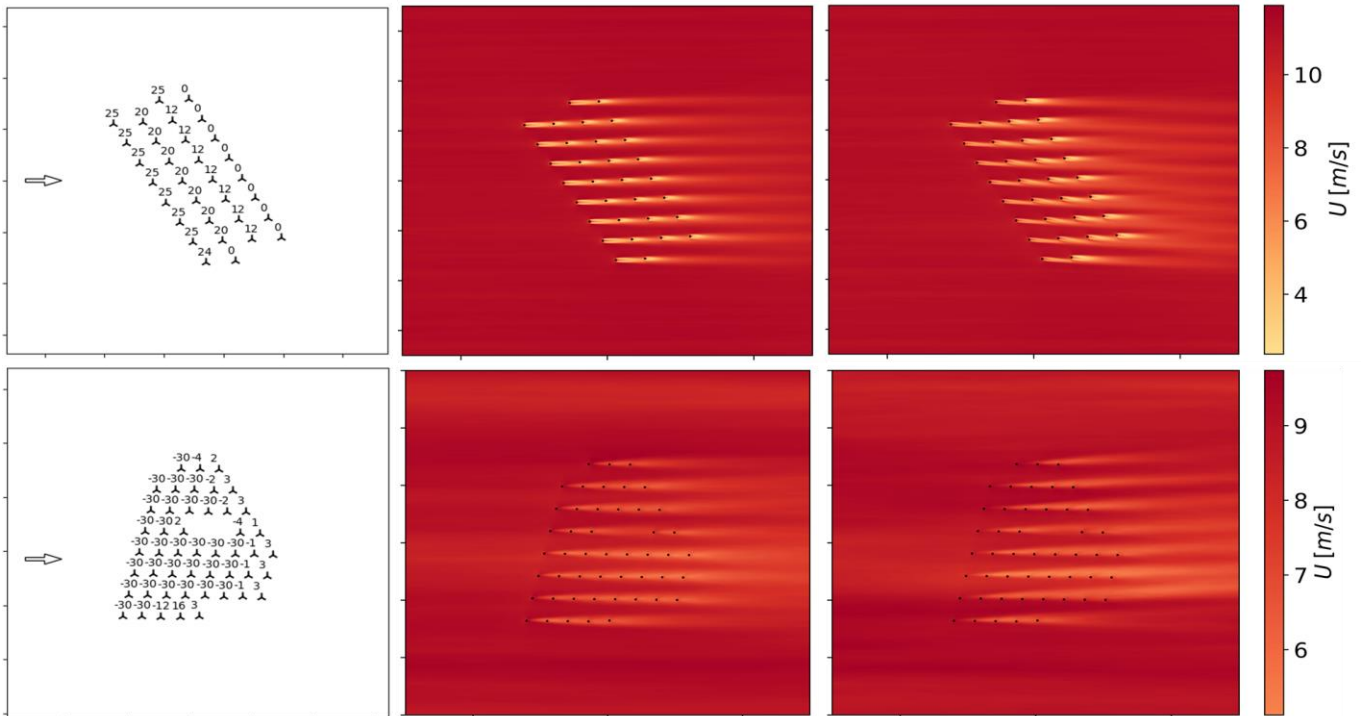


Figure 4-20 FIGURE SHOWING OPTIMAL YAWING SETPOINTS OBTAINED FROM GWM (LEFT). SP-WIND VALIDATION RESULTS COMPARING TIME AVERAGED FLOW FIELD FOR YAWED FLOW (RIGHT) AGAINST REFERENCE DATABASE (MIDDLE). TOP ROW CORRESPONDS TO CASE 2 , BOTTOM ROW CORRESPONDS TO CASE 7

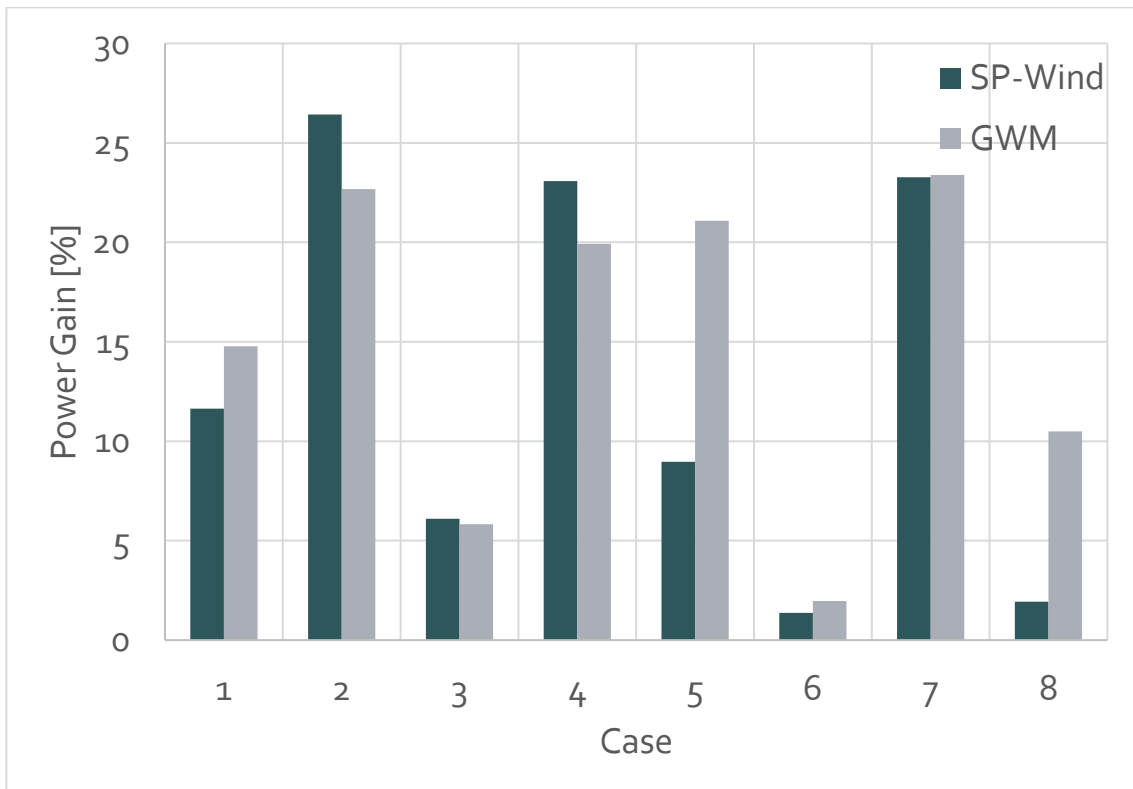


Figure 4-21 COMPARISON OF TOTAL WINDFARM POWER GAINS PREDICTED BY GWM VERSUS POWER GAINS OBTAINED FROM SP-WIND USING OPTIMAL YAWING SETPOINTS

Flow field results using the optimal yawing setpoints obtained from two of the eight cases listed in Table 4.2 are presented in Figure 4-20. Both case 2 and case 7 have fully aligned turbines for the TC RWP and the Lillgrund windfarm respectively, hence have a high capacity for power gains by steering the upstream turbine wakes away from downstream wakes, as seen by the time averaged flow field results from SP-Wind. A direct consequence of wake steering can be seen in Figure 4-21, exhibiting power gains up to 25% for both the TC RWP and the Lillgrund wind farm. For six of the eight cases, the power gains obtained via the high fidelity SP-Wind code are in good agreement with the predictions made by the low fidelity GWM, with cases 5 and 8 exhibiting larger errors. This can be attributed to two factors. First, the turbulence intensity model used in the GWM is an empirical expression proposed by (Niayifar and Porté-Agel). has been tuned for the range of $0.065 < TI < 0.15$, and fails to accurately capture the power generation of the extreme farm layout in case 5 with eight aligned turbines (Figure 4-22) and TI of 3.6%. Second, the wake expansion downstream of yawed turbines also depend on empirical parameters which need to be tuned for different windfarm layouts and wind speeds, and currently the model fails to accurately predict the power production at the low wind speed and tight layout configuration of the Lillgrund windfarm for case 8, in which majority of the wind turbines are operating in partial waked conditions (Figure 4-22). Thus, the results provided by the GWM model can further be improved by tuning the empirical parameters involved to cover a larger range of turbulence intensities and farm layouts, however that is beyond the scope of the current work. Nevertheless, the yaw setpoints obtained in both these cases from the GWM optimization still result in significant power gains when tested in the high fidelity environment of SP-Wind, resulting in power gains of 9% and 2% respectively.

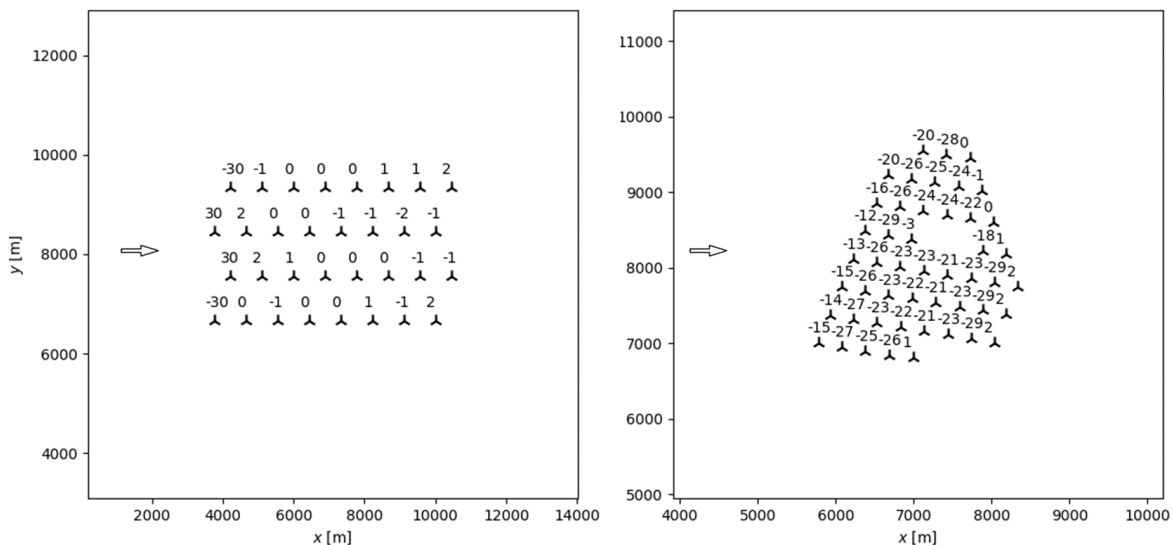


Figure 4-22 Turbine layout and optimal yaw setpoints for case 5 (left) and case 8 (right)

To determine the effect of yawing on the structural lifetime of the turbines, we use Damage Equivalent Loads (DELs) to compare the load histories of the turbines across the windfarm for the normal and optimal wake steering cases. DEL of each turbine is computed using the Palmgren-Miner rule and the Wöhler equation to account for accumulating fatigue damage caused to the wind turbine components by the fluctuating structural loads (Sutherland). The loads time series are counted and binned into individual cycles using the rainflow-counting algorithm (Socie, D.F. and Downing, S. D.), and for the wind turbine blades the components follow the Wöhler's curve with a

slope coefficient equal to 10. Total increase in cumulative windfarm blade root flapwise DEL is shown in Figure 4-23. It can be observed that for all the cases, the windfarm experiences significant increase in damage due to fatigue. The reason for increase in damage can be explained by two factors. First, individual turbines are subjected to higher fatigue loads while operating in yawed position than when compared to normal operation (Damiani, R. *et al.*). Second, downstream turbines operating in partially waked conditions are subjected to higher cyclic fluctuations in moments, also increasing the fatigue damage. Hence, while wake steering can result in an increase in overall windfarm power production, it is important to do a cost benefit analysis when using this control strategy due to the large impact on the structural lifetime of the turbines due to increased fatigue loading.

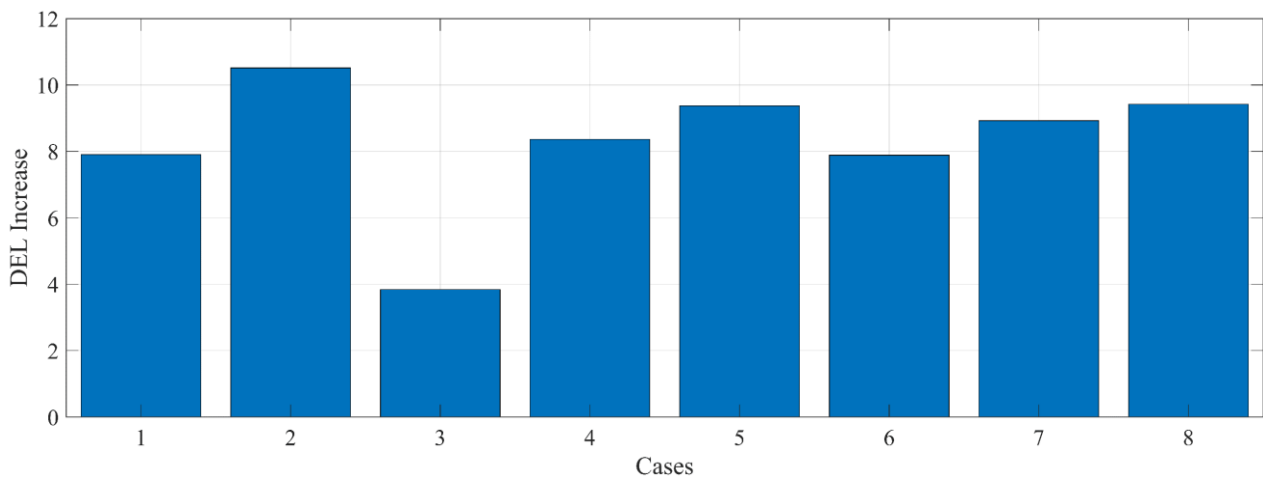


Figure 4-23 Total WINDFARM blade root flapwise moment DEL gain for power maximization wake steering

4.3 DNV

This section describes the procedure used by DNV GL to calculate and test a wind farm controller based on optimised turbine setpoints. This makes use of the Bladed and LongSim codes, which respectively model the performance of the turbine and the wind farm, and requires the following inputs:

- An aeroelastic model of the turbine set up to use with Bladed
- Information relating to the wind conditions at the site
- The turbine layout at the site

This information is described in the following subsections, followed by a discussion of different design options for the wind farm control. Steady-state setpoint optimisations using LongSim are demonstrated for selected schemes. The design of a practically realisable dynamic wind farm control algorithm which uses these setpoints is described, and LongSim is then used to run dynamic time-domain simulations to evaluate the performance of the controller in realistic time-varying conditions.

THE BLADED MODEL

A Bladed model of the Lillgrund turbine was constructed using information provided directly by the turbine manufacturer SGRE, and indirectly by DTU. Although some assumptions had to be made where the information supplied was uncertain or insufficient, the model gave a reasonable match to information which was provided on turbine performance, natural frequencies etc. Further details are not publicly available.

OPTIMAL THRUST REDUCTION SETTINGS

For the purposes of axial induction control, turbine control settings should be found which reduce rotor thrust to mitigate wake losses, while reducing power as little as possible.

The DNV GL approach uses the following steps:

1. Define a thrust reduction level. This is defined as a fractional reduction in rotor thrust coefficient (C_T).
2. For any given pitch angle, find the tip speed ratio which achieves the desired C_T .
3. Calculate the power coefficient (C_p) for this pitch angle and tip speed ratio.
4. Choose the (pitch angle, tip speed ratio) combination which maximises C_p .
5. Calculate the standard control law as defined in (Burton *et al*, 2011) for demanded generator torque Q as a function of the measured generator speed ω which achieves the desired values of C_p and tip speed ratio λ :

$$Q = K\omega^2 - L, \text{ where } K = \frac{\pi \rho R^5 C_P}{\lambda^3 G^3}$$

Here ρ is the air density, R the rotor radius, G the gearbox ratio and L represents any mechanical drive train losses referred to the high speed shaft. Here, K is referred to as the 'optimal mode gain'. The thrust reduction setpoint is then defined simply by the pair of controller parameters (K, β_0) where β_0 (the fine pitch angle) is set to the pitch angle chosen above. These are usually standard parameters in a wind turbine controller, so it is very easy to command the desired thrust reduction setting by changing these two parameters, without any changes to the actual controller software. (In practice, it may not be quite as simple; for example, the 7 MW turbine on which field tests carried out for Work Package 3 of this project has a speed exclusion zone for avoidance of tower resonance, and some adjustments were also required to the parameters controlling crossings of the exclusion zone. For the Lillgrund turbines, the control law consists of a look-up table of power demand as a function of rotor speed, but the parameter K is easy to convert into such a table: the power demand is given by $Q\omega\varepsilon$ where ε is the electrical efficiency.

Figure 4-24 show the current nominal controller settings in this form, together with some adjusted settings which were used for a trial conducted in the wind farm in 2012.

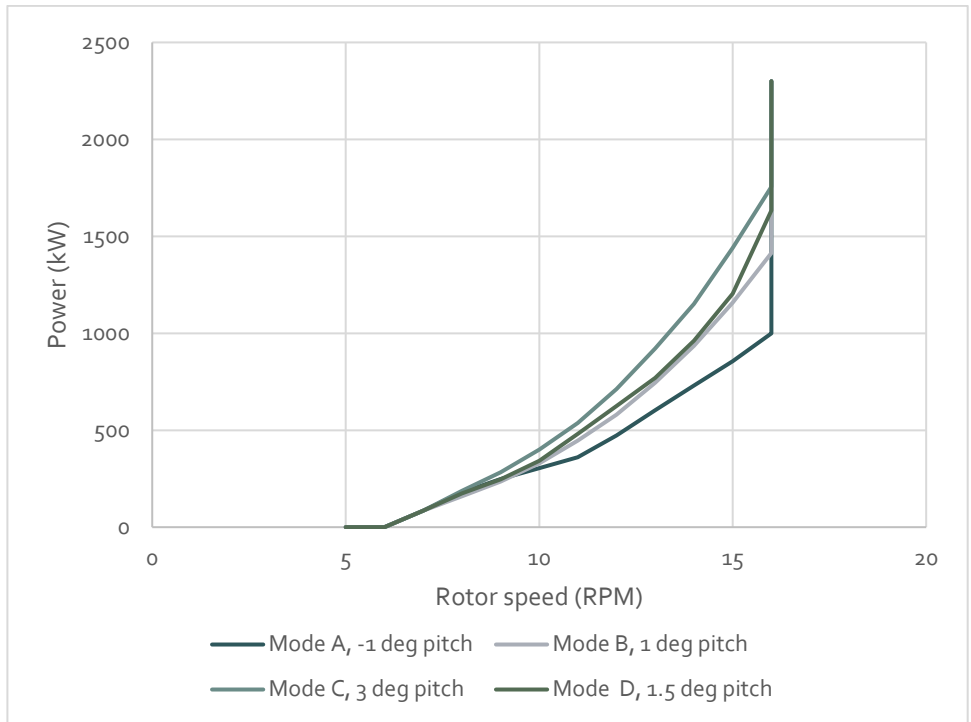


Figure 4-24: CONTROLLER SETTINGS AS USED IN 2012 TESTS

The corresponding power and thrust coefficients are shown in Figure 4-25 and Figure 4-26.

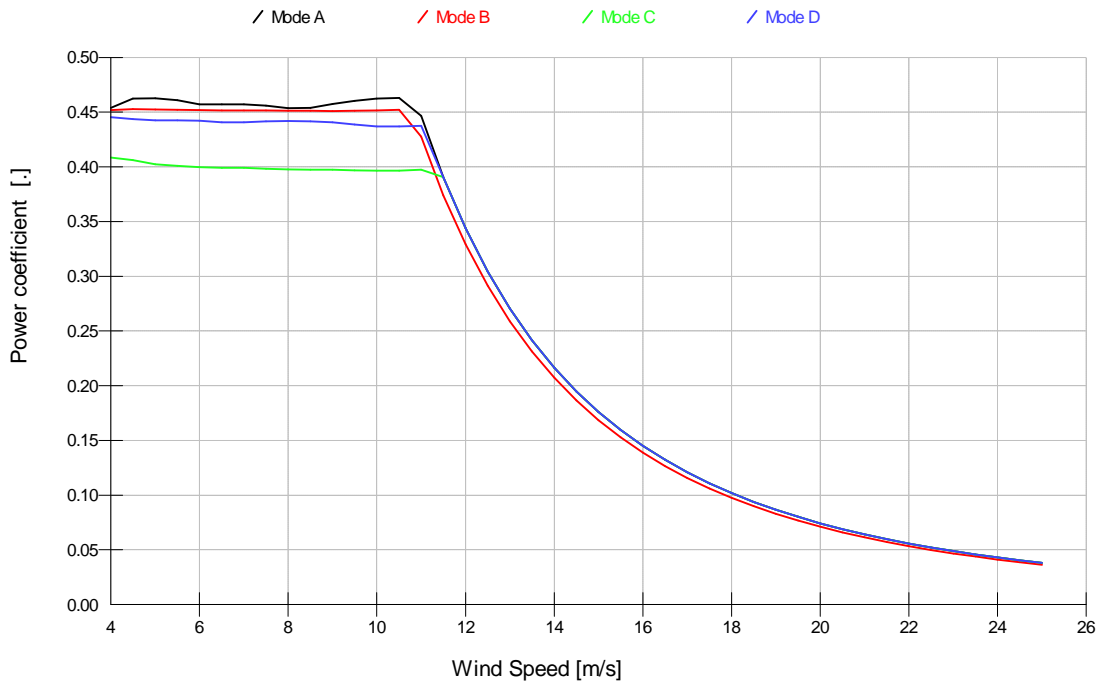


Figure 4-25: CONTROLLER SETTINGS AS USED IN 2012 TESTS – POWER COEFFICIENT

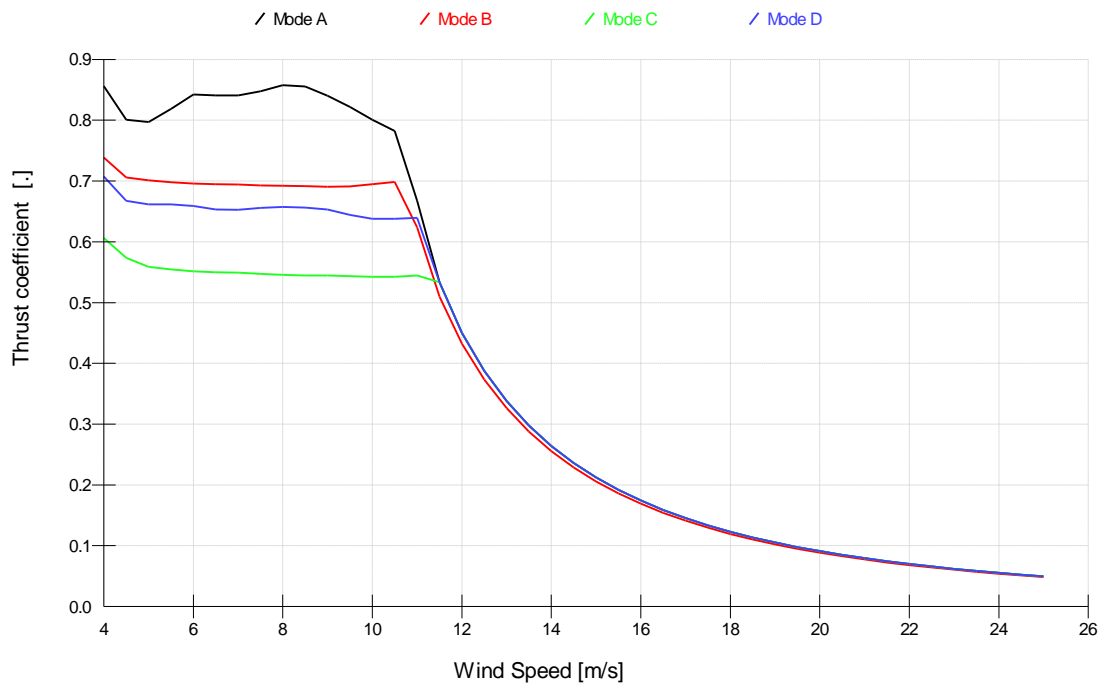


Figure 4-26: CONTROLLER SETTINGS AS USED IN 2012 TESTS – THRUST COEFFICIENT

As already mentioned in Section 3.3, one of the tests used to compare wake models was a toggle test performed in 2012 using three turbines at the Lillgrund site, dynamically changing operational modes at the turbines upstream. The results of this test, although uncertain, revealed a slight power gain for the downstream turbine (the third in the row being tested) if compared to the third turbine of the next row (operated at the normal operation mode), but however it showed no quantifiable power gain for the whole group of three turbines, since showing no clear difference between the toggle-on and toggle-off tests. Below, more efficient controller settings are proposed and discussed in details.

New proposed controller settings calculated as above are illustrated in Figure 4-27 for several different thrust reduction setpoints, along with the resulting power and thrust curves in Figure 4-28. Note that the power and thrust coefficients are not exactly constant during the period of optimal tip speed ratio operation – this is because the flexibility of the turbine has been taken into account in the calculations, so the rotor, for example, distorts differently at different wind speeds. Rotor speed and pitch angle are shown in Figure 4-29.

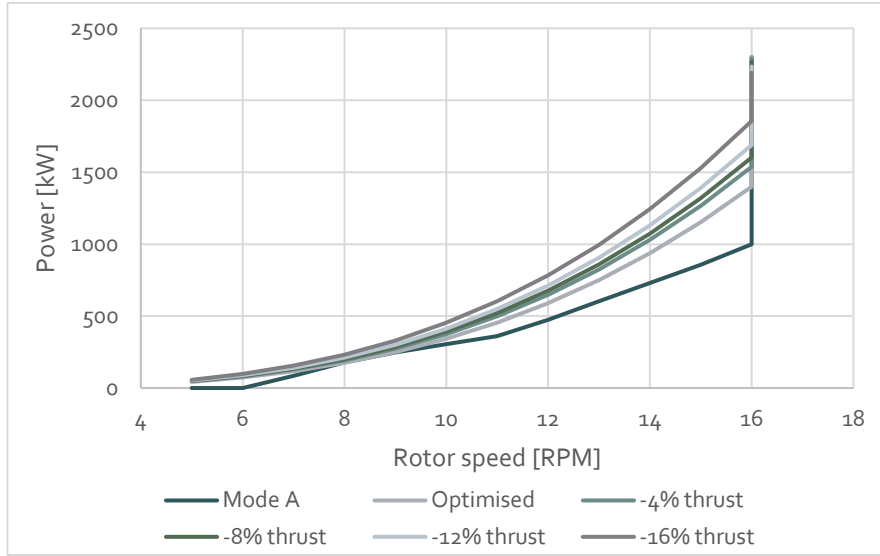


Figure 4-27: ORIGINAL AND PROPOSED CONTROLLER SETTINGS

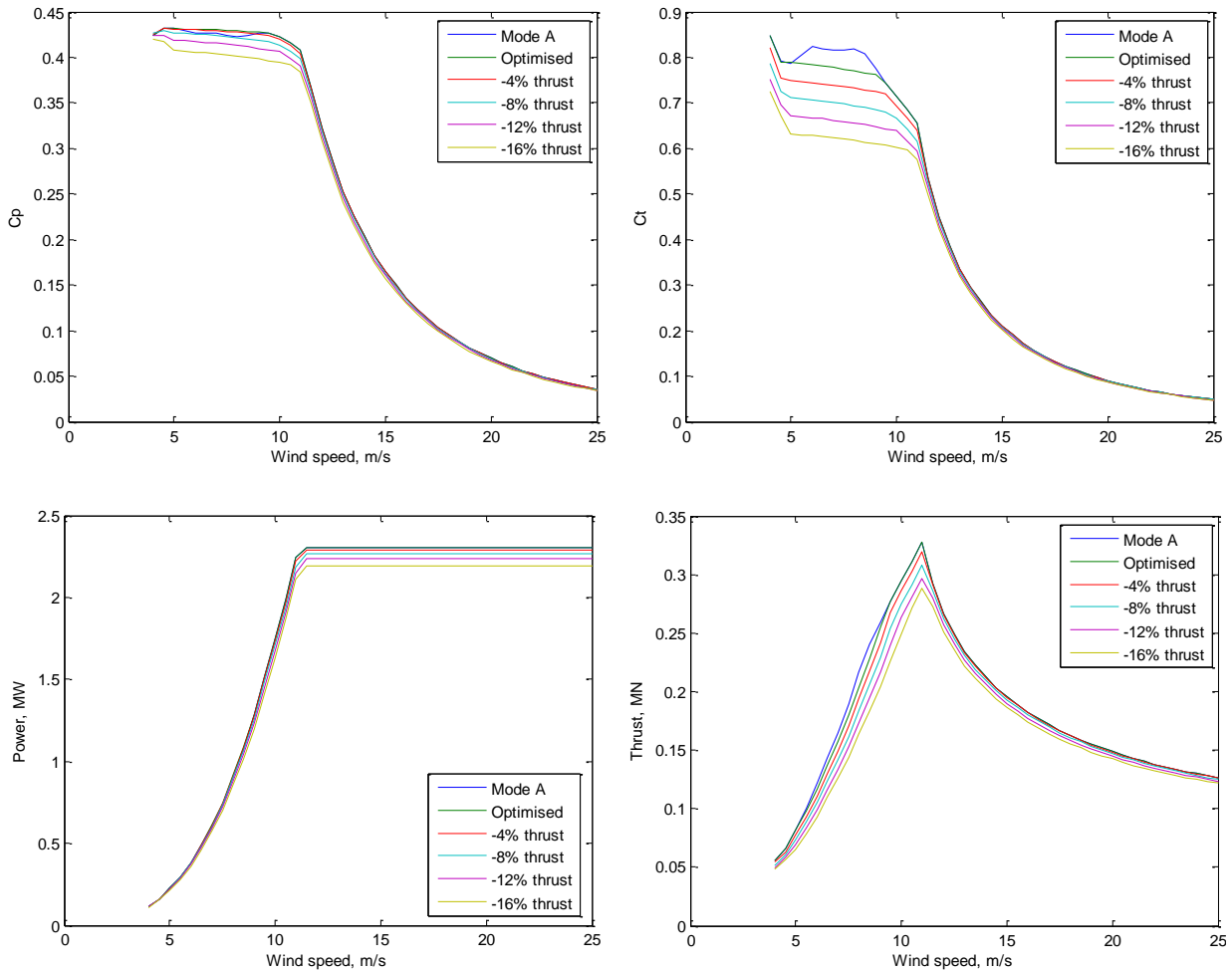


Figure 4-28: ORIGINAL AND PROPOSED CONTROLLER SETTINGS: POWER AND THRUST

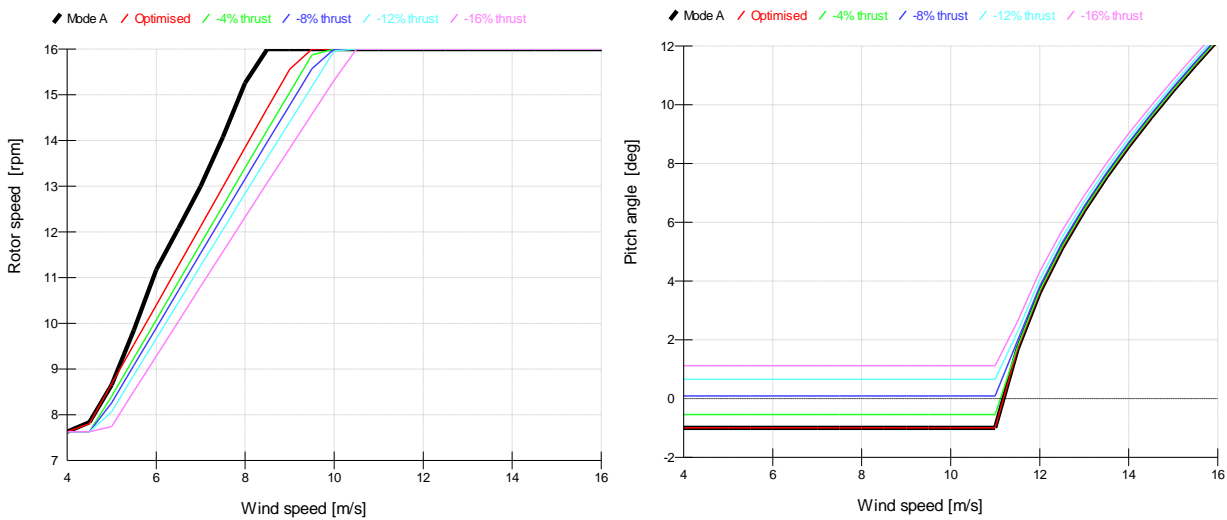


Figure 4-29: Original and proposed controller settings: Rotor speed and pitch angle

These controller settings apply to the variable speed range of the turbine operating envelope. It is also possible to extend the thrust reduction up to and above rated wind speed. This done by calculating the power reduction at the wind speed at which maximum rotor speed is reached, and applying the same power reduction at higher wind speeds simply by setting a third controller parameter, namely the maximum torque or power setpoint, to the corresponding value. The effect of this can be seen in Figure 4-28 above. (This allows induction control to be used at the higher wind speeds if it should prove to be beneficial; of course, if it is not beneficial the setpoint optimiser will simply choose the nominal setting for these wind conditions.)

A more complete set of controller settings is given in Tabel 4.4.

Table 4-4: SUMMARY OF CONTROLLER SETTINGS

Setpoint	Thrust (C_T) reduction from optimal (%)	Fine pitch (deg)	Optimal mode gain, K ($\text{Nms}^2\text{rad}^{-2}$)	Rated torque (Nm)
0	0	-1	0.422	16076
1	2	-0.83	0.449	16063
2	4	-0.54	0.464	16023
3	6	-0.20	0.471	15955
4	8	0.09	0.483	15872
5	10	0.38	0.496	15771
6	12	0.66	0.509	15654
7	14	0.89	0.533	15528
8	16	1.12	0.560	15388
9	20	1.69	0.602	15052
10	25	2.55	0.633	14563
11	30	3.47	0.672	14004
12	40	5.36	0.925	12688
13	50	8.63	0.933	11143

EFFECT OF YAW MISALIGNMENT

For wake steering control, the effect of yaw misalignment α on the power, thrust and fatigue loads needs to be known. The effect on fatigue loads is already included in the surrogate loads model described in Section **Error! Reference source not found.** LongSim has various options for modelling the turbine power and thrust, including the effect of yaw. A simple and convenient model has been used for the current work, in which the power and thrust at wind speed V are calculated from the zero-yaw power and thrust curves assuming that the effective wind speed is reduced to $V \cdot (\cos(\alpha))^p$, where the exponent p must be specified for the particular turbine. Here, a value of $p=0.65$ has been found to fit well when compared to Bladed simulation results. Some example fits are shown in Figure 4-30 for power and Figure 4-31 for thrust, showing that this model gives good results over the range of yaw angles likely to be used for wake steering, and equally well for the different thrust reduction settings described above. This makes this model particularly convenient to use when wake steering and axial induction control are combined (see below). The Bladed results for negative yaw angles are almost identical, so the model can be used for both positive and negative angles. At first, the thrust results might seem surprising above rated, but the thrust increases because the blade pitch is reduced compared to the zero-yaw case at the same wind speed, with rated power only reached at a higher wind speed.

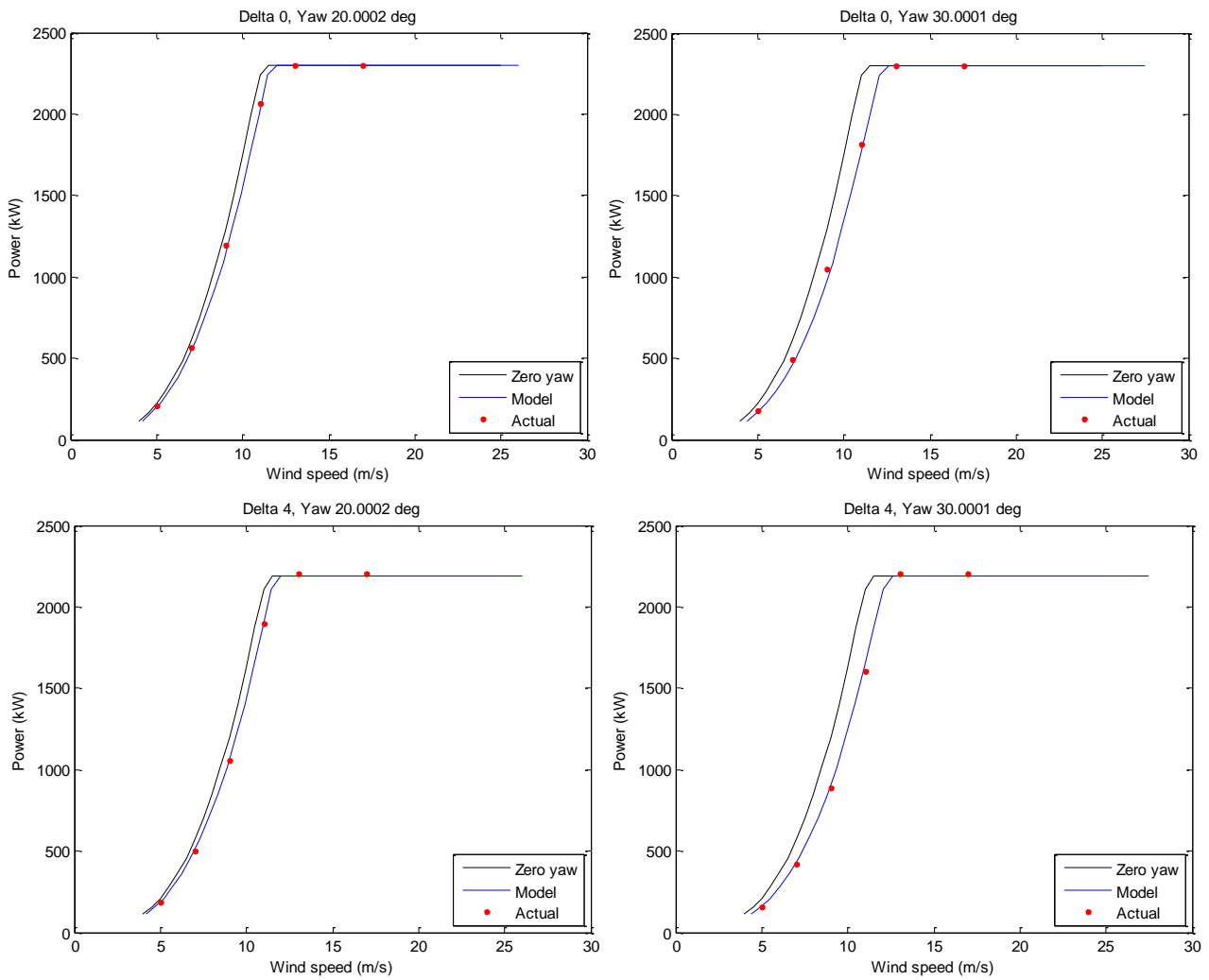


Figure 4-30: EFFECT OF YAW ON POWER CURVE: MODEL FITS TO BLADED RESULTS

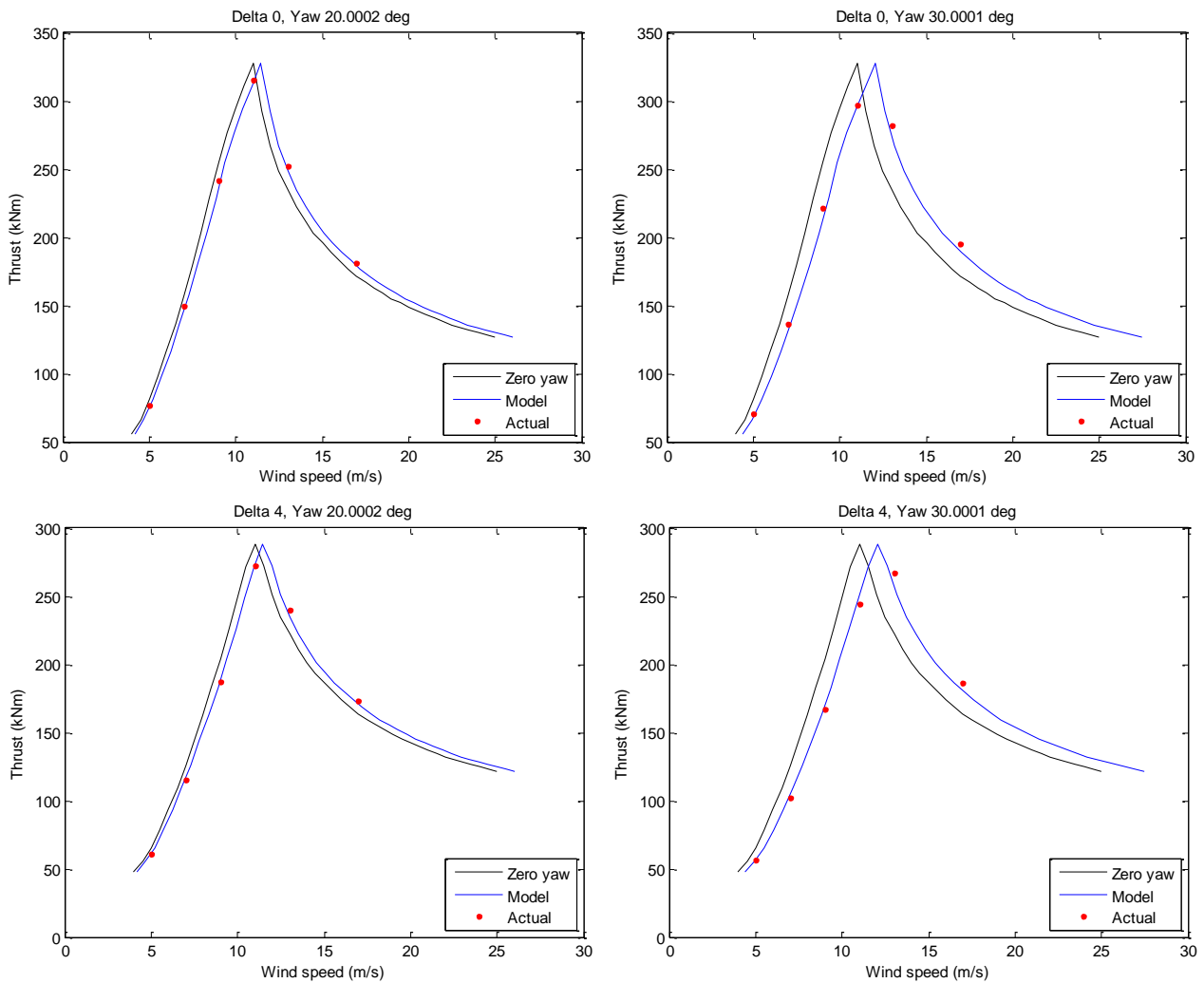


Figure 4-31: EFFECT OF YAW ON THRUST CURVE: MODEL FITS TO BLADED RESULTS

WIND CONDITIONS AT LILLGRUND

The overall atmospheric conditions at the Lillgrund site have already been summarised in Section 3.3. For the purposes of this report, a representative period of historical Lillgrund SCADA data has been selected which covers a range of below-rated wind speeds in the prevailing south-westerly sector – conditions which are being targeted for a possible field test later in the project. The wind conditions for this 22-hour period are shown in Figure 4-32. In the following sections, setpoint optimisations have been calculated to cover this range of conditions, and the same data has been used as input for time-domain simulations to test controller performance.

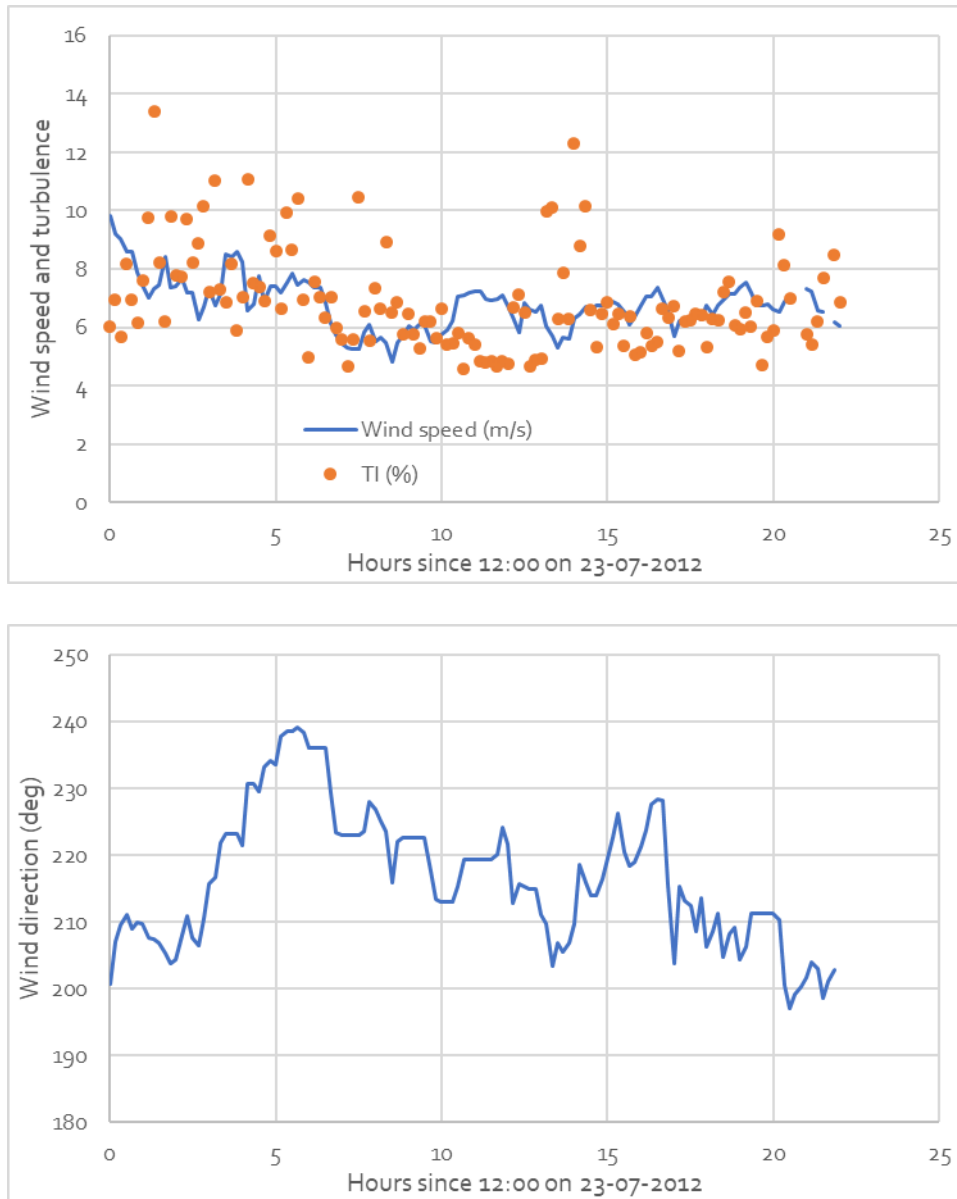


Figure 4-32: WIND CONDITIONS SELECTED FROM SCADA DATA

WAKE MODEL

A wake model appropriate to Lillgrund has been used in the remainder of this section, and also in Chapter **Error! Reference source not found.**. This is the 'exact' stability-dependent Ainslie wake deficit model (Ruisi and Bossanyi, 2019) with Obukhov length -zoom, Quarton-Ainslie added turbulence, sum-of-deficits superposition, and EPFL/Bastankah wake deflection (as defined in Bastankhah and Porté-Agel, 2016), with implicit wake meandering (i.e. no wake smearing is applied for steady-state optimisations, and inverse wake smearing for time-domain simulations where the wind field causes meandering).

The selected wake model has been compared to measured power data in Chapter 3, showing to represent well Lillgrund turbines' power output. For this specific segment of data, the model was tuned to run for unsteady conditions according to the preponderance of this condition in the period in question: a comparison is shown in Figure 4.33.

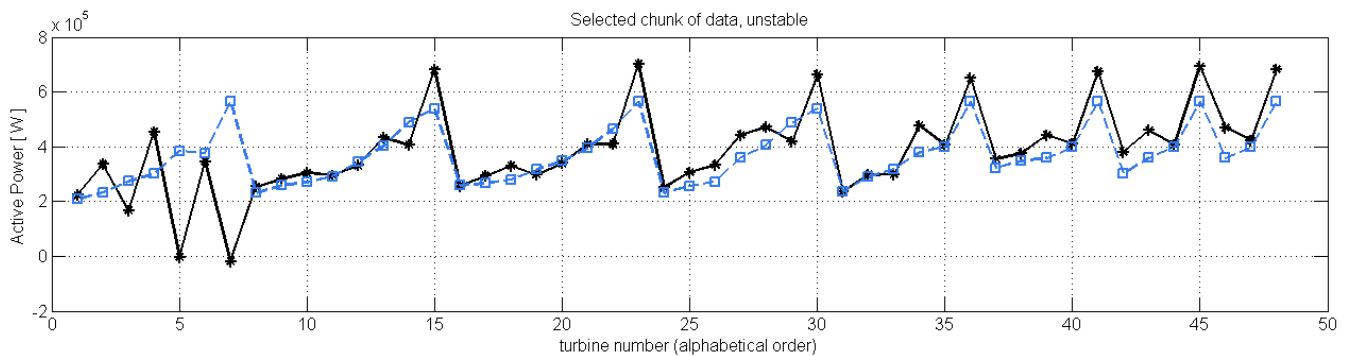


Figure 4-33: SCADA active power compared to modelled power, for the specific portion of data used for dynamic simulations.

INDUCTION CONTROL

This section calculates controller setpoints defined as in Figure 4-27 optimised to maximise the total wind farm power output. The effect on loads is also evaluated. The setpoints are calculated for steady-state conditions. The resulting setpoints are used as the basis for a dynamic control algorithm, and time-domain simulations are used to evaluate the performance of such a controller in realistic time-varying conditions.

The optimal setpoints will change with wind speed and direction, and also with turbulence intensity, and will be different for each turbine. However, before doing this full optimisation, a simpler scheme is investigated first, motivated by the idea that in the 'greedy' controller settings of the baseline turbine, although optimal for a stand-alone turbine, are not optimal in a wind farm context, and that a setting which sacrifices a small amount of power to achieve a significant thrust reduction might lead to overall better wind farm performance due to reduced wake losses. The simplest way to exploit this is to find a single controller setting applied to all turbines which maximises total farm output.

To illustrate this, optimisations have been performed for one particular wind condition (9 m/s with 6% turbulence intensity and wind direction 222° , i.e. blowing directly along the principal rows), and the power and loads are compared to the base case with nominal controller setting. In the 'Uniform optimised' case, the same setpoint is applied to all turbines, whereas the 'Fully optimised' case allows each turbine to have a different setpoint. In addition to the power, two key fatigue loads are shown as damage equivalent loads (DELs): the blade root out of plane moment with Wöhler exponent 10 (representing GRP composite for the blades) and the tower base fore-aft moment with Wöhler exponent 4 (representing steel). Also shown are two further optimisations, again Uniform and Optimised but now optimised against a merit function which includes weighted terms representing the fatigue loads: the total power has a 90% weighting in the merit function, with

weightings of 5% each for the blade root and tower loads. The loading terms represent the coefficient of variation (CoV) of each DEL across the wind farm, i.e. the standard deviation across all turbines divided by the mean; reducing the CoV has the effect of reducing the highest DELs by making the damage more uniform across the farm. The maximum DEL across all turbines could have been included directly in the merit function, as could other terms such as the mean, if deemed useful. However, using the maximum on its own gives a poorly-behaved optimisation, since the turbine experiencing the maximum is often unaffected by setpoint changes at other turbines.

The results for each turbine are shown in Figure 4-34 to Figure 4-37 and the summary for the whole farm is in Figure 4-38 and Table 4.5. Figure 4-34 shows the optimal setpoints: for the uniform optimisation for power, the optimal setpoint is 5.04, representing a thrust reduction of just over 10% from the base case 'greedy' setting (see Table 4.5). Although this represents a reduction in power coefficient for each turbine, the total wind farm power increases by 2.2% due to reduced wake losses. This is already most the gain obtained by the full optimisation (2.75%), and the maximum loads are reduced significantly more than in the fully optimised case. The weighted optimisation for power and loads shows that, if desired, the maximum loads can be further reduced in exchange for a small reduction in the power gain.

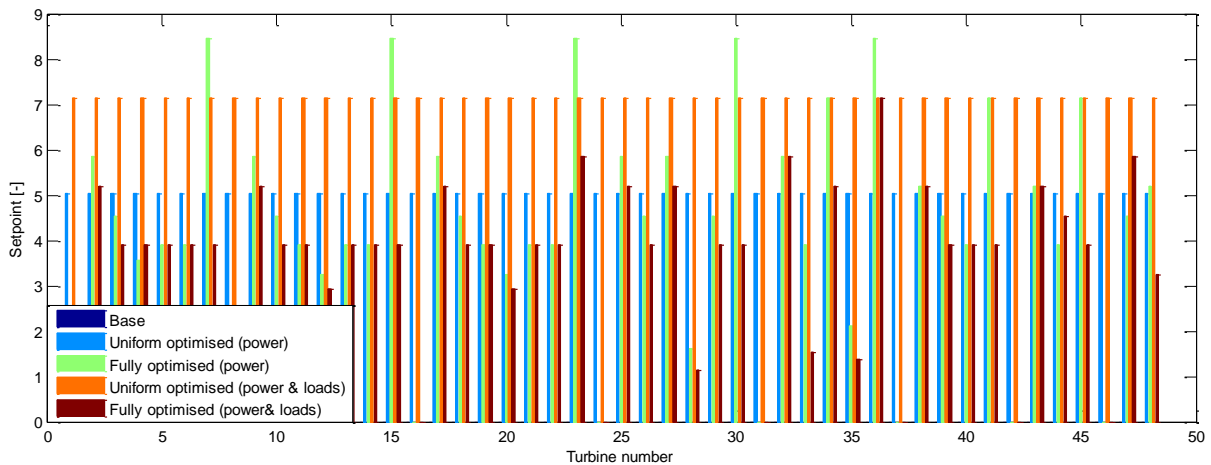


Figure 4-34: INDUCTION CONTROL SETPOINTS FOR THE DIFFERENT SCHEMES

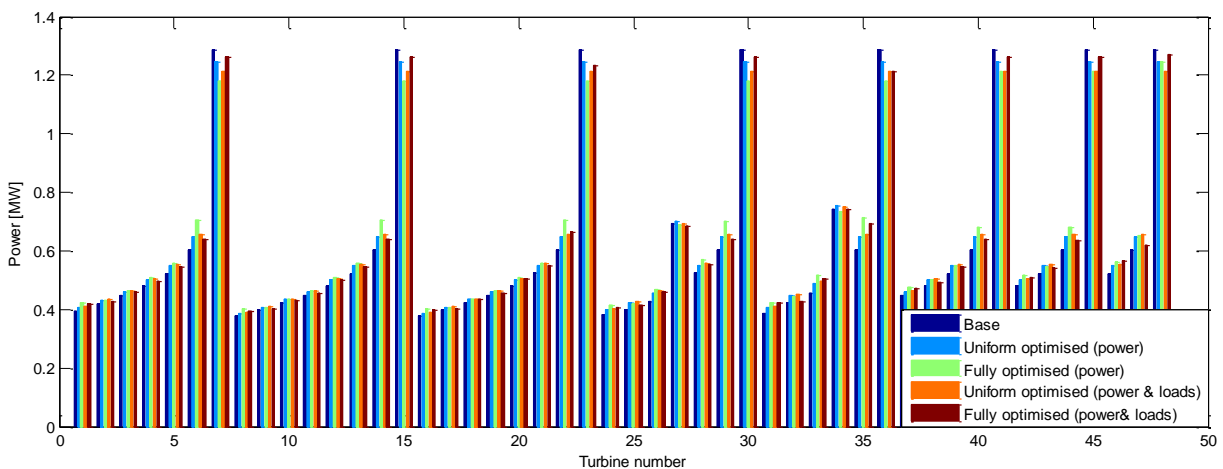


Figure 4-35: POWER AT EACH TURBINE

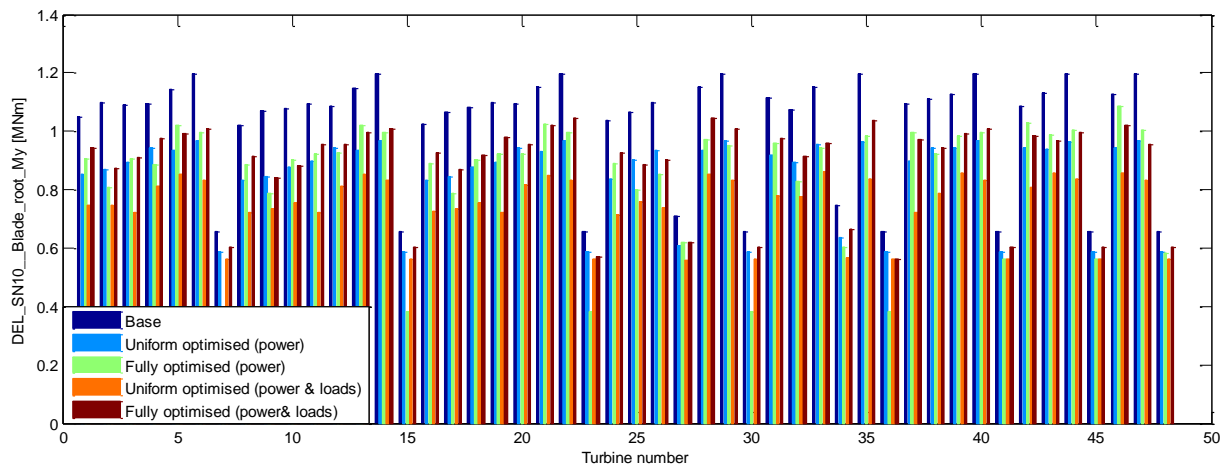


Figure 4-36: BLADE ROOT DEL AT EACH TURBINE

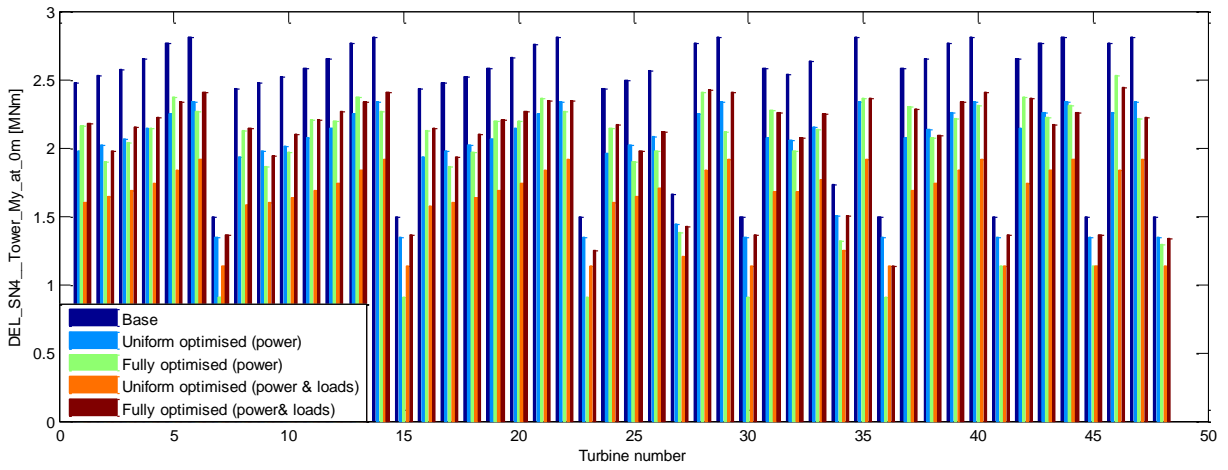


Figure 4-37: TOWER BASE DEL AT EACH TURBINE

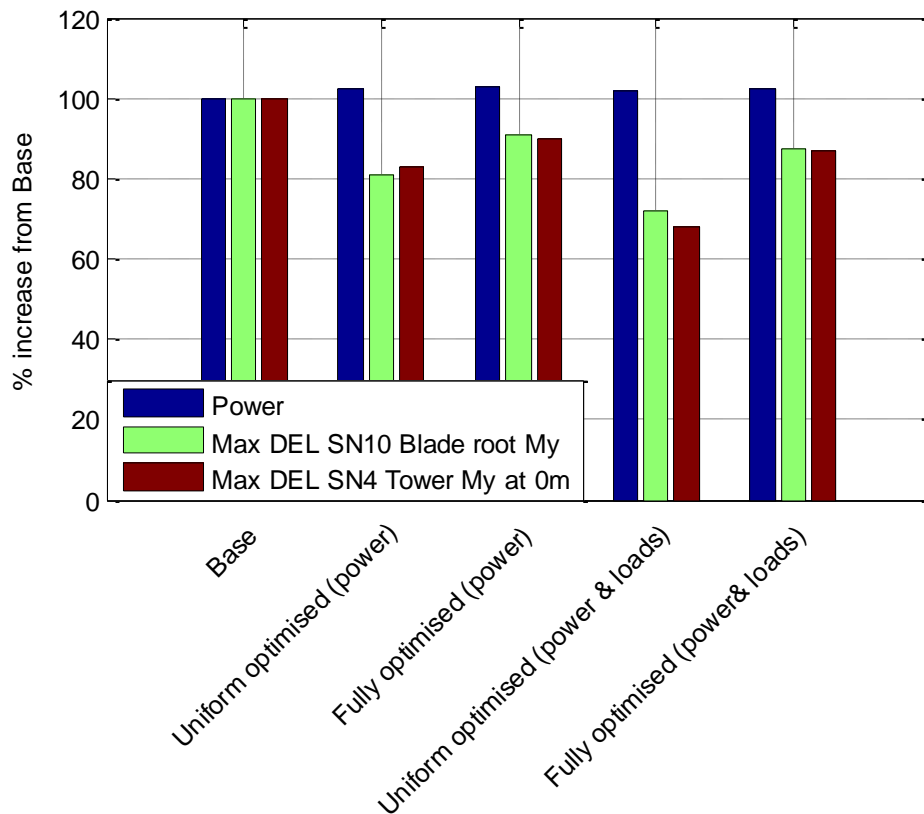


Figure 4-38: OVERALL RESULT OF DIFFERENT INDUCTION CONTROL SCHEMES

Table 4-5: Overall result of different induction control schemes

	Power	Blade root load		Tower base load	
		CoV	Max	CoV	Max
Base case	1.0000	1.00	1.00	1.00	1.00
Uniform optimised (power)	1.0220	0.88	0.81	0.88	0.83
Fully optimised (power)	1.0275	1.30	0.91	1.27	0.90
Uniform optimised (power & loads)	1.0193	0.77	0.72	0.84	0.68
Fully optimised (power & loads)	1.0234	0.94	0.87	0.96	0.87

WAKE STEERING AND COMBINED CONTROL

For the same wind condition as in Figure 4-38, blowing directly along the main rows, optimisations were carried out for the case of wake steering, allowing yaw angles up to $\pm 35^\circ$, and also for the combination of induction control and wake steering. For the combined case, it was found helpful for the optimiser to start from the optimal induction control setpoints, and then allow the optimiser to further adjust these setpoints and the yaw offsets simultaneously for each turbine. Once

again, optimisations were carried out first for power only, and then for power and loads using the same weightings as before.

The resulting total power and maximum DELs are shown in Figure 4-39 and Table 4-6. The labelling uses IC for induction control and WS for wake steering, with the optimisation criterion in brackets. Clearly, wake steering on its own is capable of a much greater power gain in this wind condition, but at the expense of much higher maximum blade root and tower base fatigue. With loads included in the optimisation criterion the power gain is roughly halved, though slightly greater than with induction control, but the maximum fatigue loads are still 20% above the base case.

When wake steering is used in addition to induction control, the power increase is even higher than with wake steering on its own, as expected, and the loads increase is not quite as great. By including loads in the optimisation criterion, the maximum loading is brought back below the base case and is now similar to induction control on its own, but with a slightly high power gain.

The induction control and wake steering setpoints for each turbine are plotted in Figure 4-40, along with the power. It can be seen that the amount of yawing is much reduced in the combined case when loads are included in the optimisation.

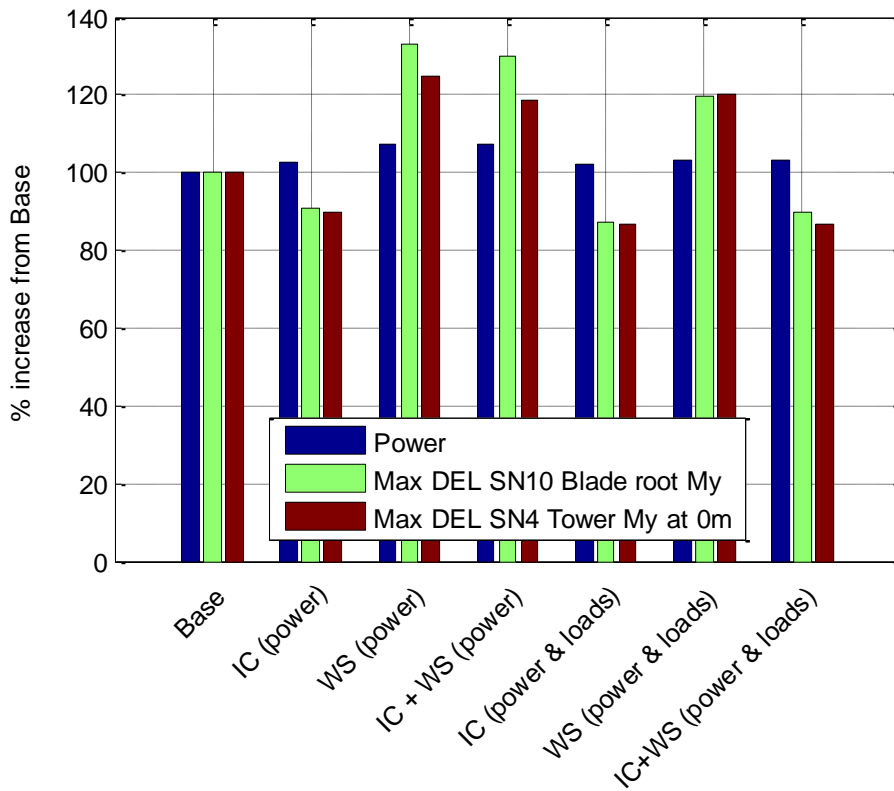


Figure 4-39: Comparison of induction control and wake steering optimisations

Table 4-6: Results of induction control and wake steering optimisations

	Power	Blade root load		Tower base load	
		CoV	Max	CoV	Max
Base case	1.0000	1.00	1.00	1.00	1.00
IC (power)	1.0275	1.30	0.91	1.27	0.90
WS (power)	1.0722	1.04	1.33	1.26	1.25
IC + WS (power)	1.0727	1.27	1.30	1.34	1.19
IC (power & loads)	1.0234	0.94	0.87	0.96	0.87
WS (power& loads)	1.0335	1.02	1.20	1.14	1.20
IC + WS (power& loads)	1.0313	1.04	0.90	1.02	0.87

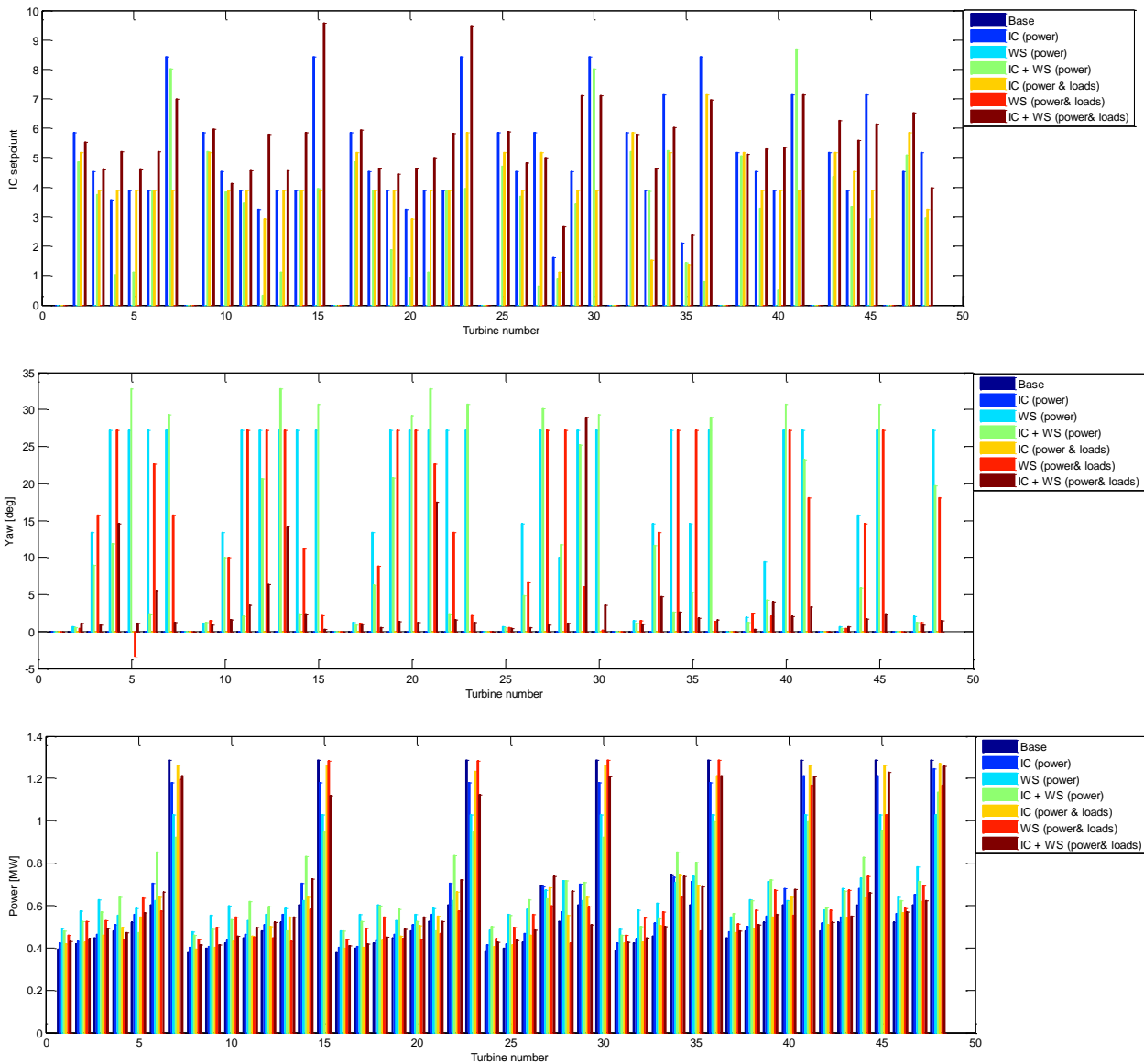


Figure 4-40: SETPOINTS AND POWER FOR EACH TURBINE

These results indicate that if wake steering is to be used on this particular wind farm, it should probably be combined with induction control, unless a significant increase in maximum fatigue loads is acceptable. The energy gain is improved compared to induction control alone, and a reduction in maximum fatigue loads can still be achieved.

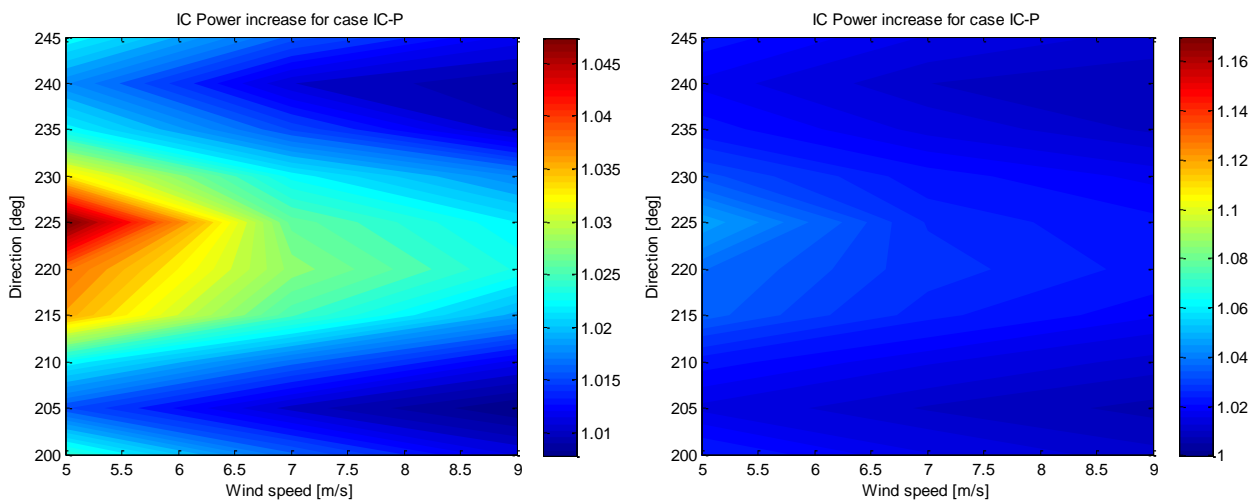
OPTIMISATION FOR A RANGE OF WIND CONDITIONS

These optimisations were performed for a single wind condition, with wind direction exactly aligned with the long turbine rows. For a practical wind farm controller they should be repeated for a range of conditions, leading to tables of setpoints which vary with wind speed and direction, and ideally turbulence as well. This has been done for the wind conditions shown in Figure 4-32, as follows:

- Wind speeds: 5, 7 & 9 m/s
- Wind directions: 200° – 245° in steps of 5°
- Turbulence intensities: 7%

For a real case one would ideally interpolate setpoints over a range of turbulence intensities – and better still, also to atmospheric stability, with the wake model changing appropriately, but for simplicity this has not been done here, as these variations are usually of lesser importance to the effectiveness of the control.

Figure 4-41 shows the power increase as a function of wind speed and direction. The top left plot is for induction control optimised for power only, showing gains from under 1% to over 4.5% for the lowest wind speed when the direction is aligned with the turbine rows. The top right plot shows the same data but with the colours scaled to match the other two plots, which show the effect of including wake steering in addition to induction control. Bottom left is optimised for power only, and bottom right for power and loads (with weightings as above).



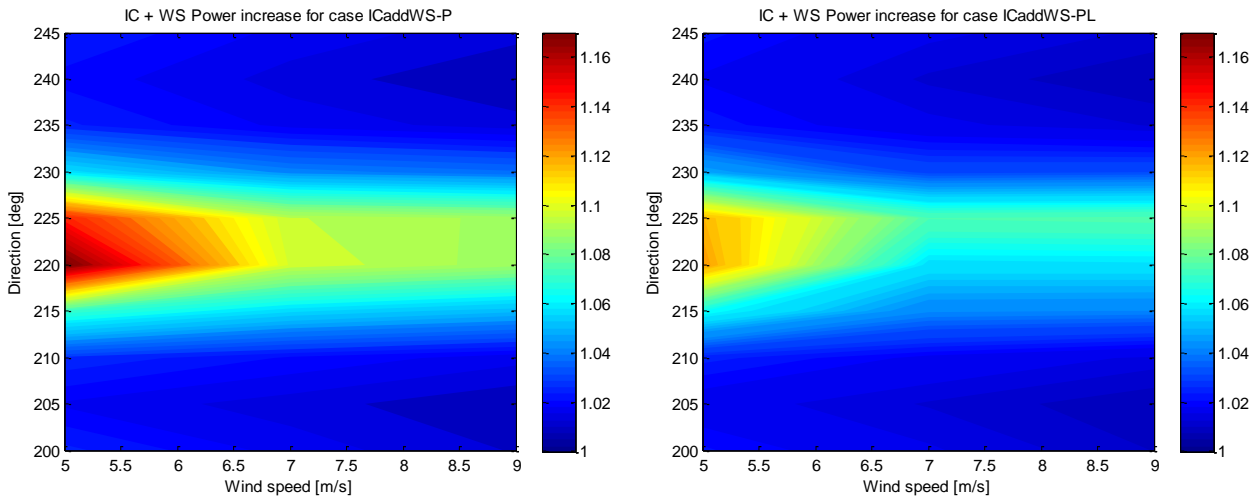
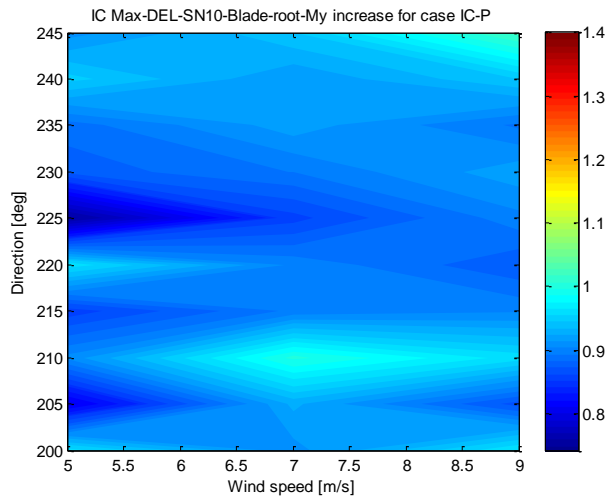


Figure 4-41: Power gains for a range of wind speeds and directions. The top left plot has a different colour scale; top right shows the same data with colour scale matching the bottom two plots

These plots show that adding wake steering can result in much higher gains when the wind is blowing along the rows, but makes very little difference in other directions.

The maximum blade root and tower base DELs for these cases are shown in Figure 4-42 and Figure 4-43 respectively. The same cases as Figure 4-41 are shown, but only one plot is shown for the induction control case, with the same colours scales used for each case.



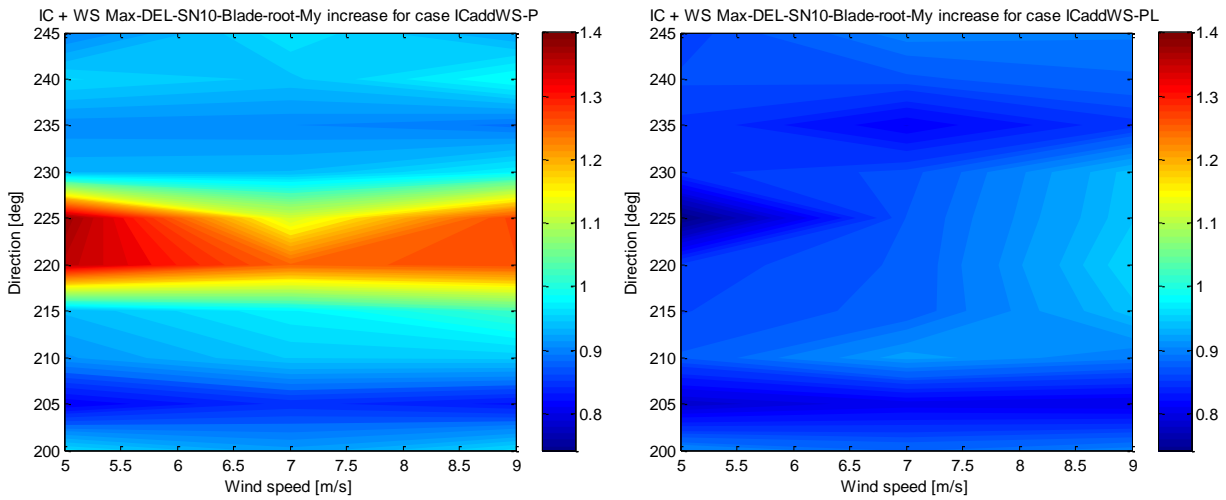


Figure 4-42: BLADE ROOT DELS FOR A RANGE OF WIND SPEEDS AND DIRECTIONS.

These figures clearly show the significant loading increases caused by wake steering, and how these can be entirely mitigated by optimising for power and loads, albeit with a reduction in the power gain (although it is still higher than with induction control alone).

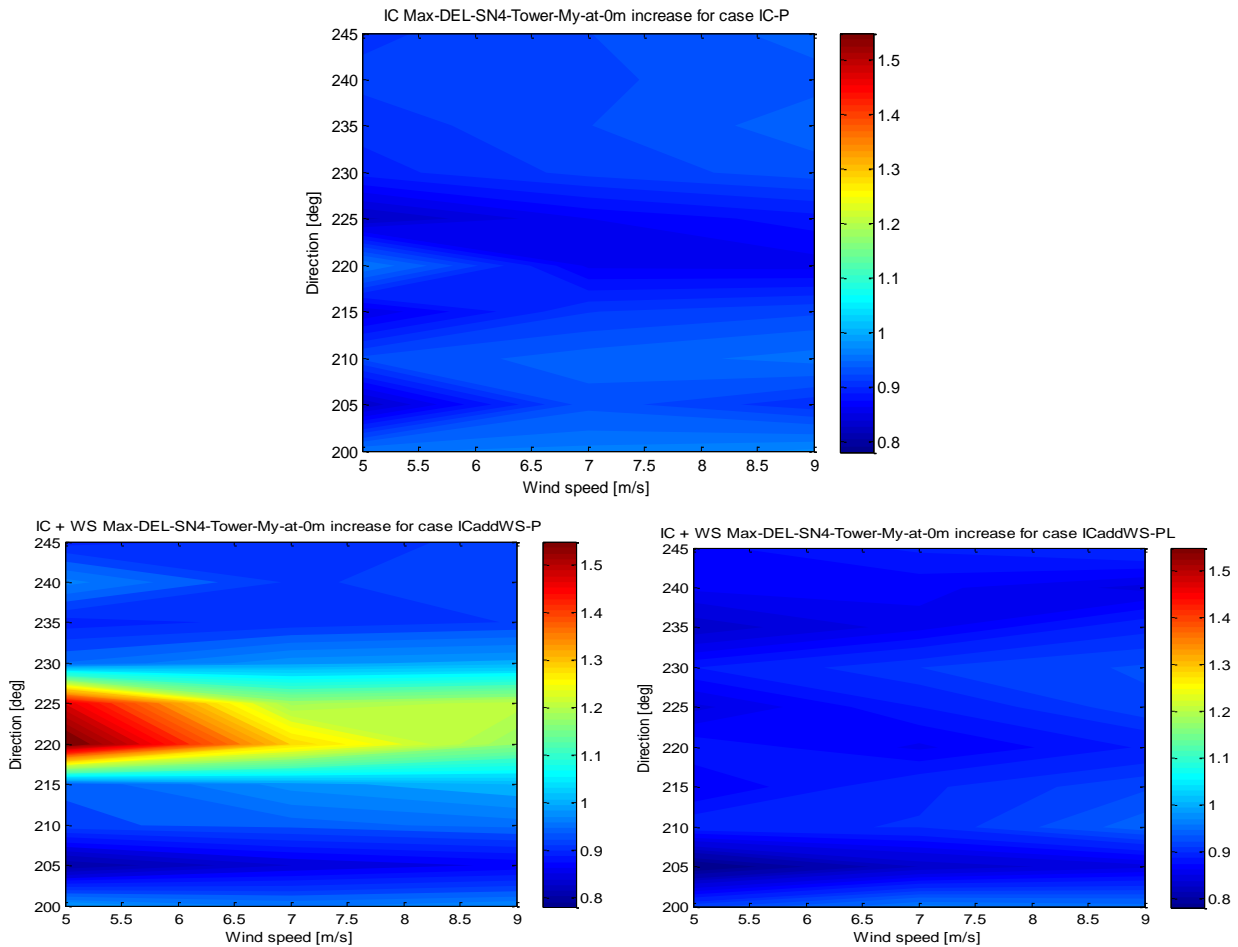


Figure 4-43: TOWER BASE DELS FOR A RANGE OF WIND SPEEDS AND DIRECTIONS.

DYNAMIC TIME-DOMAIN SIMULATIONS

Having generated tables of optimised setpoints, these are used to construct a wind farm controller capable of being implemented dynamically in real time. The control algorithm has three steps (described below in more detail): first, the estimation of the wind conditions using any available measurements (for which estimates of wind speed and direction are assumed to be available from all the turbine controllers); second, using the wind conditions to interpolate all the turbine setpoints from the lookup tables produced by the optimiser; and thirdly, implementing the thrust reduction and/or wake steering setpoints at all the turbines.

Using the time-varying sample of wind conditions taken from historical SCADA data shown in Figure 4-32, four simulations have been run:

1. Base case with no wind farm control
2. Induction control, optimised for power only
3. Combined control, optimised for power only
4. Combined control, optimised for power and loads

The simulations were run with a time step of 10s. This is too long to allow turbine pitch and torque controller dynamic response to be modelled, but the yaw dynamics were included to allow the turbines to respond to wind direction variations in a realistic way. In the absence of manufacturer's details on the yaw control algorithm, this was modelled using a 30s first-order filter on the wind direction calculated from the instantaneous wind vane signal and the nacelle position, 8° of hysteresis on the filtered yaw misalignment, and a yaw rate of 0.3°/s. With wake steering control this yaw strategy was overridden as explained below.

For cases 2, 3 and 4, the setpoint tables arising from the steady-state optimisations were converted into an implementable dynamic wind farm controller in the following way:

- a) The setpoint lookup tables were first smoothed to account for the inevitable uncertainties in measured wind conditions, which cannot be measured exactly, and which in any case are not the same everywhere in the wind farm at any one instant. This has been shown to be a beneficial step, tending to slightly increase the benefits while reducing the amount of control action (Bossanyi and Ruisi, 2021). Only direction smoothing was used, with an assumed uncertainty of 5°.
- b) The wind conditions needed to find the turbine setpoints at any time were calculated in the simulation by an algorithm which determines which turbines are currently unwaked, and calculates the mean of the wind speed, direction and turbulence intensity measured at each of these turbines. The wind conditions are filtered using a first-order low-pass filter, which provides additional smoothing to make the wind conditions more representative of the whole wind farm, and also introduces a time lag. The filter time constant of 200s has been chosen to represent roughly the time taken for the measured wind to advect to the centre of the wind farm.
- c) Using these filtered wind conditions, the setpoints for all turbines are interpolated from the lookup tables. The setpoints are updated at intervals of 1 minute.

- d) The setpoints are implemented at the turbines in a realistic fashion. The induction control setpoints are implemented with a first-order lag of 5s, which is realistic for the rate at which blade pitch and speed-torque gain would be allowed to change (in principle, LongSim can model these dynamics explicitly, but the required controller details were not made available for this turbine). The yaw setpoint was implemented by sending a demanded nacelle position to each turbine, which works slightly better than merely sending a yaw offset to the turbine's standard yaw controller. To reduce yaw drive duty, a hysteresis of 2° was introduced, so that yawing only occurs if the (slowly-varying) position demanded is more than 2° different from the actual position, and the turbine then yaws to its new position at a rate of $0.3^\circ/\text{s}$. This overrides the turbine's individual yaw controller response.

Parameters such as the filter time constant, controller update interval and yaw hysteresis could be optimised by running a few simulations and evaluating the results in terms of energy gain, loading changes and yaw drive and pitch actuator duty. This has not been done here, but would be a useful exercise for any controller design which will be used in practice.

The wind conditions of Figure 4-32 were used to generate a stochastic wind field, varying in time and space, covering the whole wind farm, using LongSim's default spatial correlation settings. This wind field was then used to run the four simulations described above.

DYNAMIC TIME-DOMAIN SIMULATIONS

Having generated tables of optimised setpoints, these are used to construct a wind farm controller capable of being implemented dynamically in real time. The control algorithm has three steps (described below in more detail): first, the estimation of the wind conditions using any available measurements (for which estimates of wind speed and direction are assumed to be available from all the turbine controllers); second, using the wind conditions to interpolate all the turbine setpoints from the lookup tables produced by the optimiser; and thirdly, implementing the thrust reduction and/or wake steering setpoints at all the turbines.

Using the time-varying sample of wind conditions taken from historical SCADA data shown in Figure 4-32, four simulations have been run:

5. Base case with no wind farm control
6. Induction control, optimised for power only
7. Combined control, optimised for power only
8. Combined control, optimised for power and loads

The simulations were run with a time step of 10s. This is too long to allow turbine pitch and torque controller dynamic response to be modelled, but the yaw dynamics were included to allow the turbines to respond to wind direction variations in a realistic way. In the absence of manufacturer's details on the yaw control algorithm, this was modelled using a 30s first-order filter on the wind direction calculated from the instantaneous wind vane signal and the nacelle position, 8° of hysteresis on the filtered yaw misalignment, and a yaw rate of $0.3^\circ/\text{s}$. With wake steering control this yaw strategy was overridden as explained below.

For cases 2, 3 and 4, the setpoint tables arising from the steady-state optimisations were converted into an implementable dynamic wind farm controller in the following way:

- e) The setpoint lookup tables were first smoothed to account for the inevitable uncertainties in measured wind conditions, which cannot be measured exactly, and which in any case are not the same everywhere in the wind farm at any one instant. This has been shown to be a beneficial step, tending to slightly increase the benefits while reducing the amount of control action (Bossanyi and Ruisi, 2021). Only direction smoothing was used, with an assumed uncertainty of 5° .
- f) The wind conditions needed to find the turbine setpoints at any time were calculated in the simulation by an algorithm which determines which turbines are currently unwaked, and calculates the mean of the wind speed, direction and turbulence intensity measured at each of these turbines. The wind conditions are filtered using a first-order low-pass filter, which provides additional smoothing to make the wind conditions more representative of the whole wind farm, and also introduces a time lag. The filter time constant of 200s has been chosen to represent roughly the time taken for the measured wind to advect to the centre of the wind farm.
- g) Using these filtered wind conditions, the setpoints for all turbines are interpolated from the lookup tables. The setpoints are updated at intervals of 1 minute.
- h) The setpoints are implemented at the turbines in a realistic fashion. The induction control setpoints are implemented with a first-order lag of 5s, which is realistic for the rate at which blade pitch and speed-torque gain would be allowed to change (in principle, LongSim can model these dynamics explicitly, but the required controller details were not made available for this turbine). The yaw setpoint was implemented by sending a demanded nacelle position to each turbine, which works slightly better than merely sending a yaw offset to the turbine's standard yaw controller. To reduce yaw drive duty, a hysteresis of 2° was introduced, so that yawing only occurs if the (slowly-varying) position demanded is more than 2° different from the actual position, and the turbine then yaws to its new position at a rate of $0.3^\circ/\text{s}$. This overrides the turbine's individual yaw controller response.

Parameters such as the filter time constant, controller update interval and yaw hysteresis could be optimised by running a few simulations and evaluating the results in terms of energy gain, loading changes and yaw drive and pitch actuator duty. This has not been done here, but would be a useful exercise for any controller design which will be used in practice.

The wind conditions of Figure 4-32 were used to generate a stochastic wind field, varying in time and space, covering the whole wind farm, using LongSim's default spatial correlation settings. This wind field was then used to run the four simulations described above.

The total power for the four simulation cases is shown in Figure 4-44. The four lines are difficult to distinguish, but the mean percentage power increase over the whole period compared to the base case is tabulated.

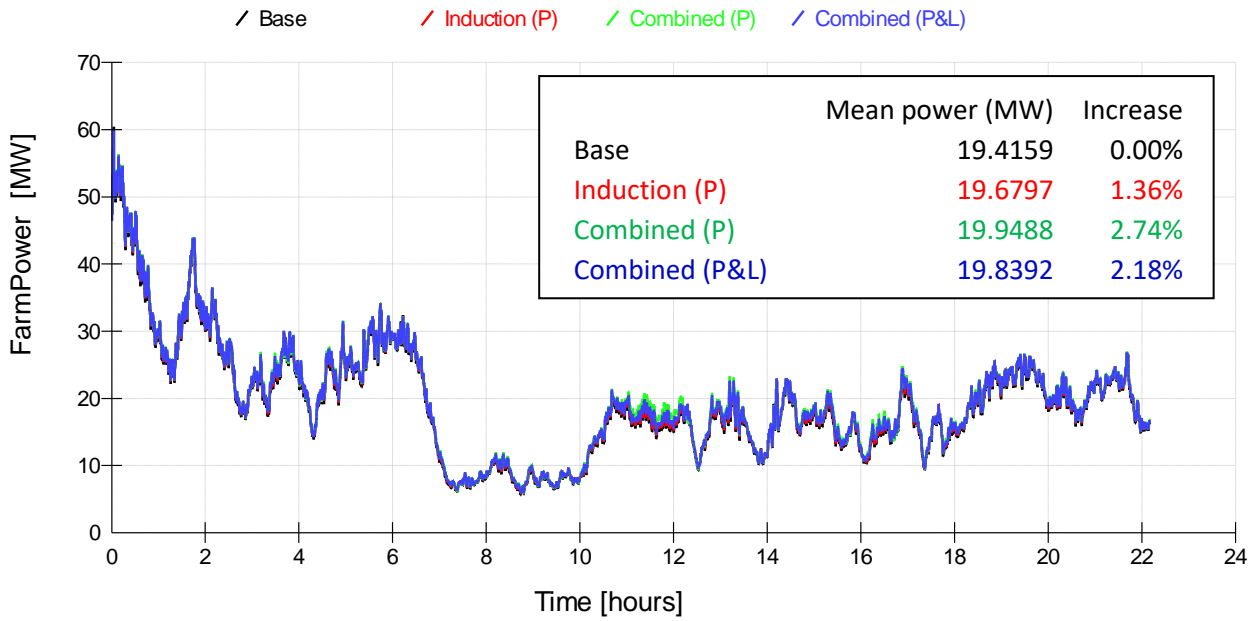


Figure 4-44: TOTAL POWER FOR THE FOUR SIMULATION CASES

The damage equivalent loads, calculated every 10 minutes, are shown for one of the turbines (Do8) in Figure 4-45 for the blade root out-of-plane bending moment at Wöhler exponent 10 (for glass fibre), and Figure 4-46 for the tower base fore-aft moment at Wöhler exponent 4 (for steel). Both loads are consistently reduced by an appreciable amount relative to the base case, except in one or two short periods for the tower base moment at low wind speed.

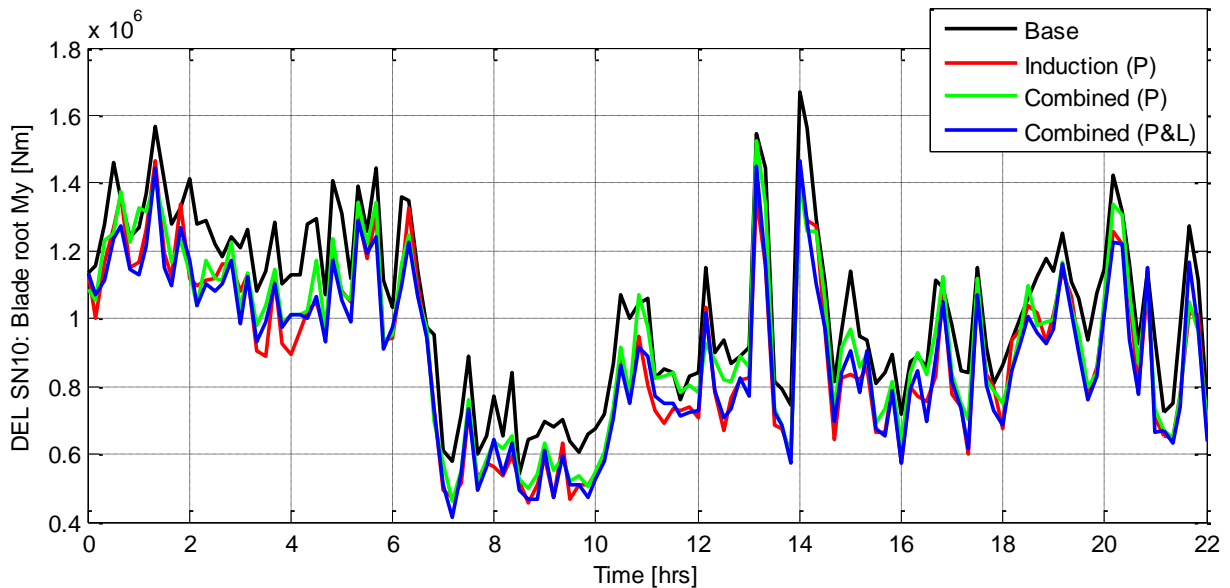


Figure 4-45: 10-MINUTE BLADE ROOT MOMENT DELS

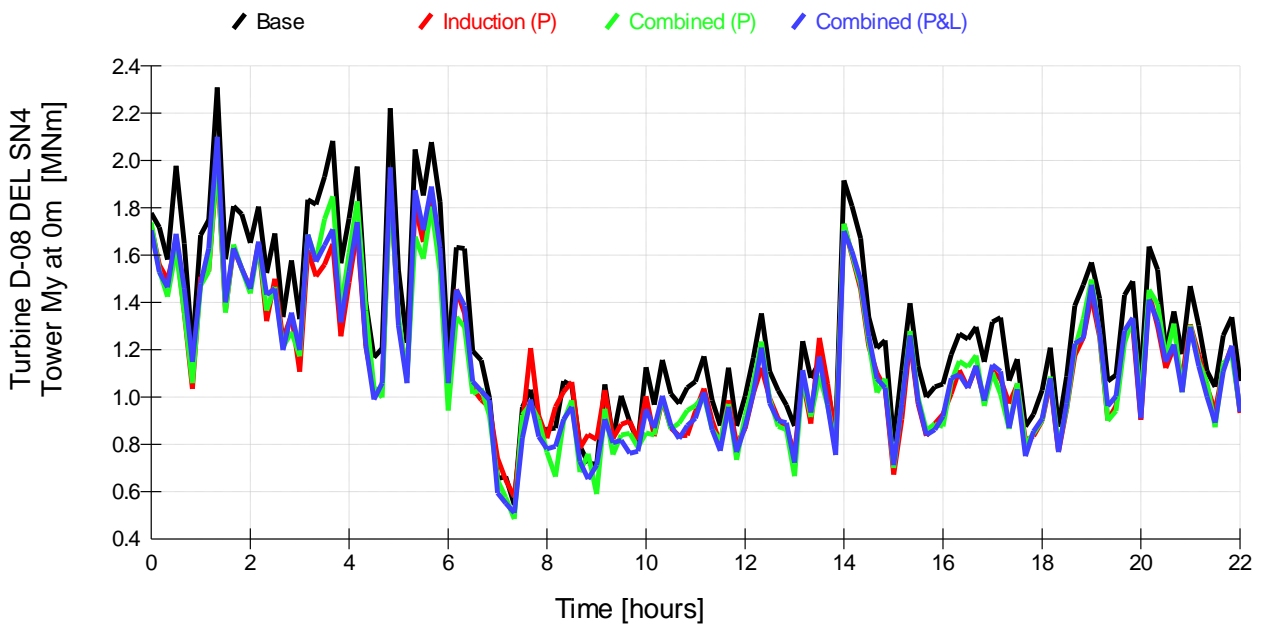


Figure 4-46: 10-MINUTE TOWER BASE MOMENT DELS

LongSim can also output the detailed, in this case 20 Hz, time-domain loads at each turbine in the wind farm. For example, to try to understand why the tower base fatigue briefly increase in the induction control case around 7 hours we can examine the 20Hz tower moment as shown in Figure 4-47, and we can see that the cause of the increase in fatigue is the increased tower vibration at the first tower mode frequency. This would be a result of 3P tower excitation at the low rotor speed and reduced damping due to the increased fine pitch angle.

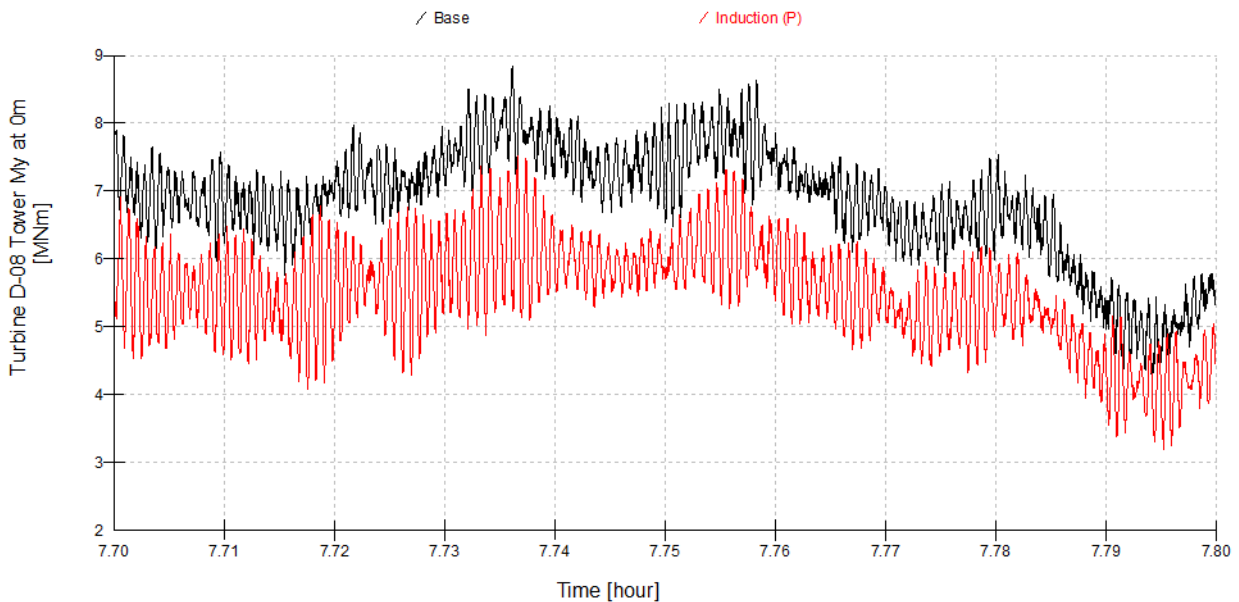


Figure 4-47: 20HZ SAMPLE TOWER BASE MOMENT SHOWING TOWER RESONANCE

More importantly, we should look at the maximum DEL across all the turbines, shown in Figure 4-48 (blade root) and Figure 4-49 (tower base). In all three controlled cases the maximum fatigue loads are always lower than the base case.

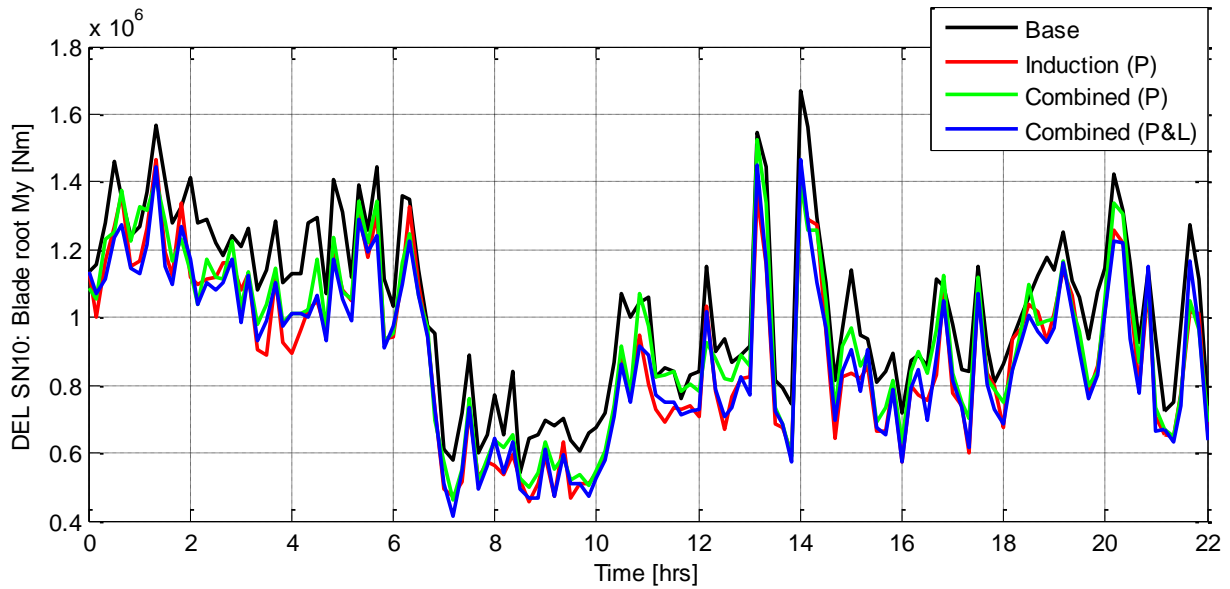


Figure 4-48: MAXIMUM OF 10-MINUTE BLADE ROOT MOMENT DELS

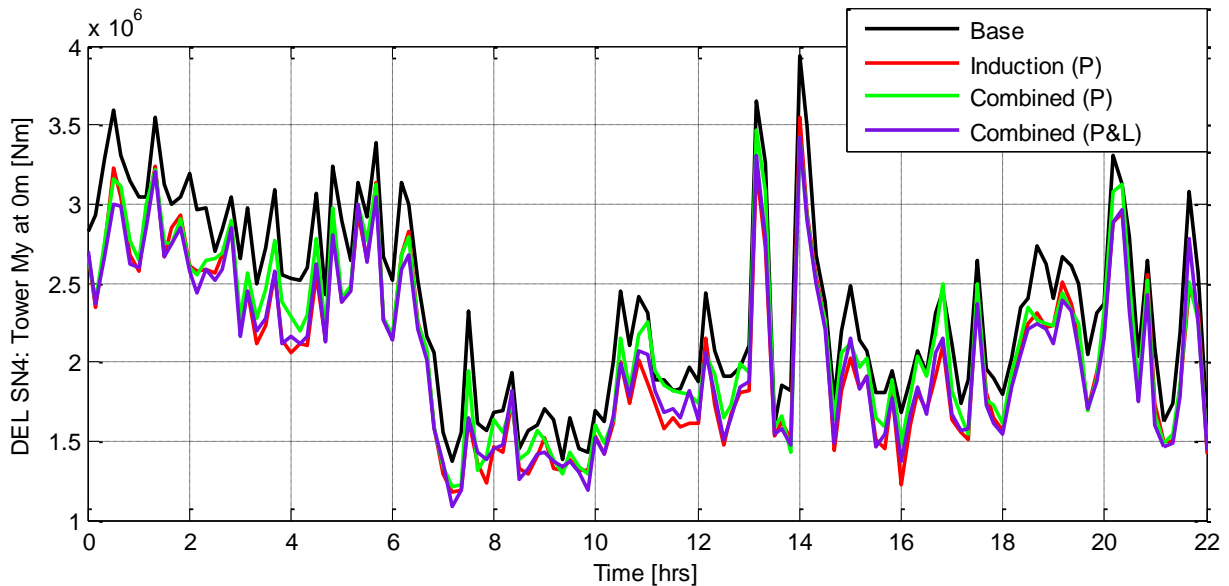


Figure 4-49: MAXIMUM OF 10-MINUTE TOWER BASE MOMENT DELS

The simulation results also provide the amount of yaw travel and the number of yaw manoeuvres occurring in each case. These are shown in Table 4-1. Interestingly, the two later cases which include wake steering show a much smaller total yaw travel. This is because each turbine’s own yaw controller, which relies only on that turbine’s wind vane, is replaced by a centralised yaw control strategy where the wind farm controller commands each turbine to move to a given nacelle position, using information from all the upstream turbines. This is a strategy which could be used also in the cases where there is no wake steering, and is likely to be beneficial – see also Bossanyi (2019). The combined strategy optimised for power and loads results in a further reduction in the amount of yawing. The number of yaw manoeuvres tells a slightly different story because the

strategy used for wake steering used a 2° deadband rather the 8° used for the turbine yaw controller. The smaller deadband would be expected to result in a larger number of smaller yaw manoeuvres. The number is indeed larger in the Combined (P) case, but not by as much as might be expected because of the central yaw control strategy. The Combined (P&L) case has slightly fewer yaw manoeuvres than the base case, and only one third of the total yaw travel. Clearly LongSim could be used to optimise the yaw strategy further, to find the best compromise between energy gain and yaw system duty. One of the original reasons for developing LongSim in the first place was actually for optimisation of single-turbine yaw strategies.

Table 4-1: YAW ACTIVITY FOR THE SIMULATED CASES

Case	Total yaw travel [deg]	No. of yaw manoeuvres
Base	106960	8228
Induction (P)	106960	8228
Combined (P)	43398	11743
Combined (P&L)	28191	8179

CONCLUSIONS FROM SECTION 4.3

This section of the report has demonstrated the possibilities of axial induction control and wake steering, and also the combination of the two, using the Lillgrund wind farm as an example. The main points to highlight are:

- The definition of axial induction control setpoints which which reduce rotor thrust as much as possible while the power output reduces as little as possible
- The method for correcting power curves for the effect of yaw misalignment
- The possibility of a very simple form of induction control in which all the turbines use the same setpoint, but one which is optimised for the wind farm and not for the turbine
- The steady-state calculation of optimal setpoints for induction control, wake steering, and both together, using LongSim, with the possibility to include loading in the merit function so that the optimal setpoints take account of fatigue loading as well as power production
- Induction control has the capability to increase power production by one or two percent while significantly reducing fatigue loads
- Wake steering has the capability to give significantly higher power gains than induction control, but at the expense of significantly increased loading
- Combined control, especially when optimised to take account of loads, could be a useful solution
- Time-domain simulation with LongSim using realistic time-varying conditions provides the capability to evaluate the performance of different wind farm control algorithms in significant detail, including the possibility to examine the loading effects overall and at each individual turbine.

4.4 COMPARISON OF RESULTS WITH DIFFERENT LOW FIDELITY WAKE MODELS

Compare power production increase with different set-points using FUGA, LongSim and Gaussian wake

DNV, KUL, FUGA SETPOINT COMPARISON

To compare the performance of different low fidelity models for optimal wake steering, a direct comparison is made between the results obtained from the KU Leuven code GWM and DNV GL code LongSim. Using the same inflow conditions for the Lillgrund windfarm, optimal yawing setpoints are obtained using the optimization methodology for both the models outlined in Sections 4.2 and 4.4. Yaw setpoints for power maximization for the two models for cases 6 and 7 of Table are shown in Figure 4-50Figure 4-23. Besides minor discrepancies, both the GWM and LongSim result in very similar setpoints across with the windfarm for the inflow cases considered. However, LongSim reports lower power gains of 7.91% and 0.16% compared to GWM gains of 23.26% and 1.36% for cases 6 and 7 respectively. A possible reason for this discrepancy could be the difference in the turbulence intensity models or power curve models used, resulting in different inflow velocities and turbulence intensities for the downstream turbines even though similar yaw settings are used. An in depth analysis of the velocity fields obtained from these two codes should be conducted to determine the exact cause for the discrepancy, however that is beyond the scope of the current work.

Since LongSim uses a surrogate model and has the capability of combined power and structural optimization, the setpoints obtained from LongSim for Case 6 are verified in KU Leuven's high fidelity aeroelastic LES code, SP-Wind. The LongSim setpoints for optimal power and loads are shown in Figure 4-51, along with the difference in power and DEL gains when compared to power optimization alone. From the figure, it is evident that for the combined power+loads optimization, while the new setpoints lead to a reduction in overall power gain compared to power optimization alone, by incorporating loading in the optimization framework significant savings on turbine operating lifetime can be obtained while still retaining gains in power.

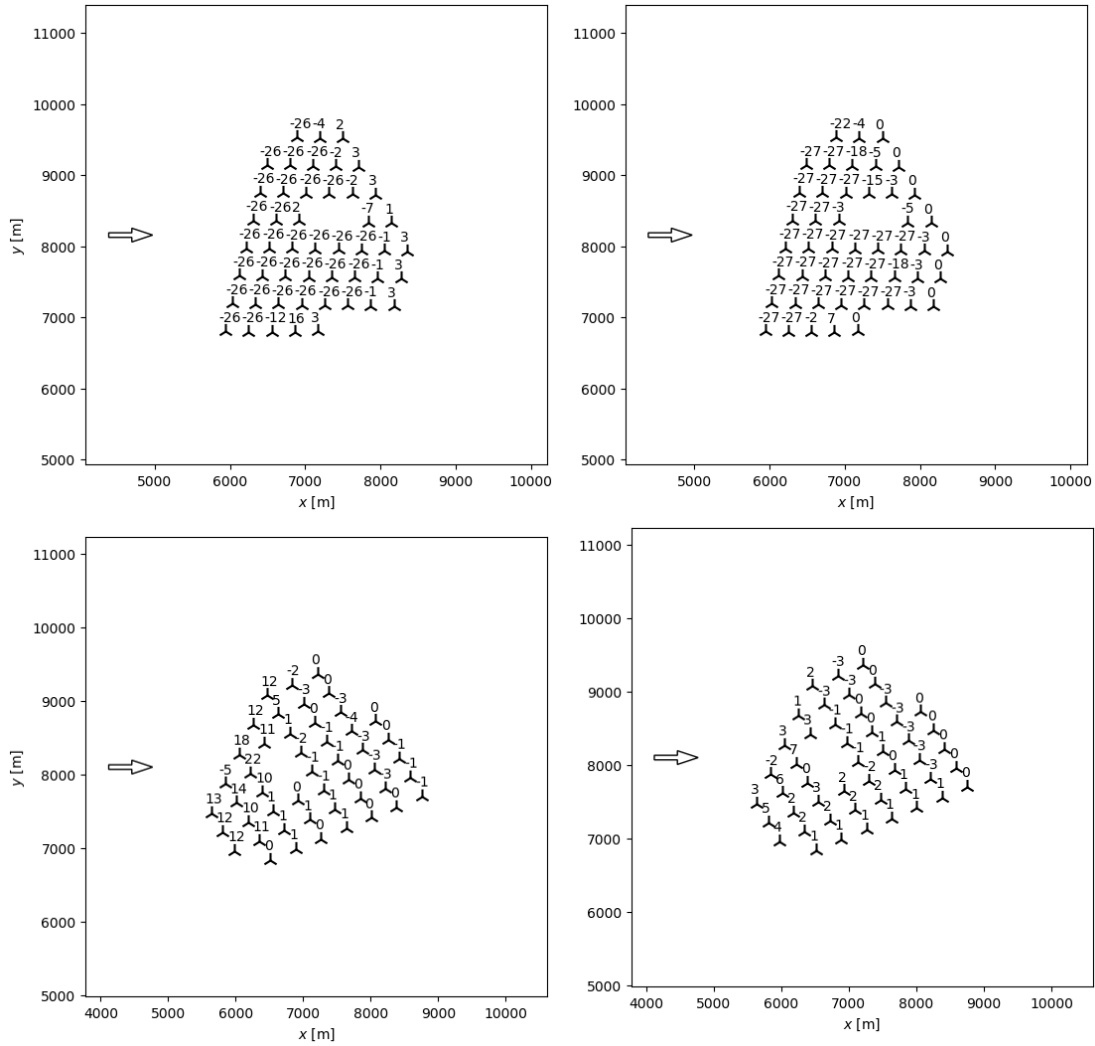


Figure 4-50 POWER maximization Optimal setpoint comparison between GWM (left) and LongSim (right) for case 6 (top) and case 7 (bottom) from Table 4.2.

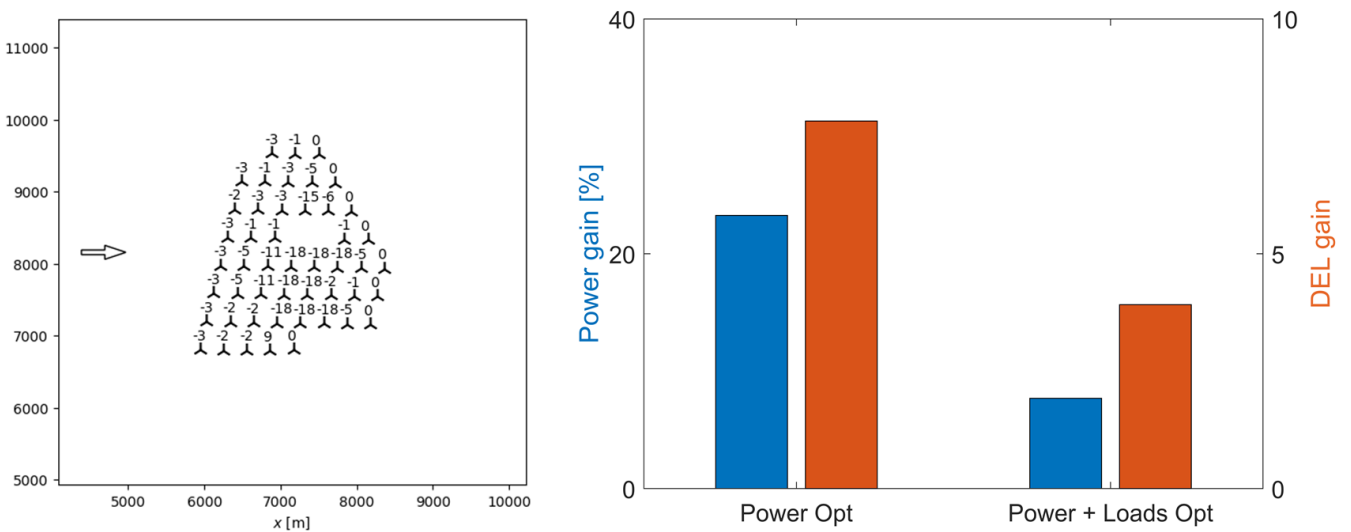


Figure 4-51 LongSIM yaw setpoints for combined power+loads optimization (left), comparison of power and DEL obtained using SP-Wind for Power optimization and combined power+loads optimization (Right).

FUGA Setpoints

The FUGA low fidelity model setpoints were based on the one-parameter version of the platform that demonstrated that production gains are feasible through selective de-rating of the Lillgrund WT's over different prevailing wind directions. The power gains can be obtained for virtually no cost since no extra control system tuning is needed and 5% gain in AEP was obtained in wind sectors with large wake effects. The WT loads is not considered but, given the fact that wake losses are reduced, it can be assumed that the load level in general is not increased as a result of the developed WPP control optimization. Yaw steering may cause increase in loads, but herein as opposed to yaw steering done in LongSim and GWM, the results from FUGA are only based on de-rating, increase in loads is not a concern.

In a future perspective, besides de-rating, active yaw control of WPP WT's would be included in FUGA simulations, whereby load constraints would also be required to be prescribed in the optimization to ensure that the yaw deflection does not result in increase of mechanical loading.

5. SETPOINT OPTIMIZATION WITH THE DYNAMIC WAKE MEANDERING APPROACH (DTU)

The low-fidelity approaches discussed in the previous sections of this report have the advantage of simplicity and computational efficiency. However, they also have limitations as the dynamics of the wake are only considered in a quasi-static way, and typically, the low-fidelity models do not provide outputs in terms of load estimates.

The dynamic loading on wind turbines, including the effect of wakes impacting the rotor, can be simulated using aeroelastic load simulation tools such as e.g. Hawc2 (Larsen T J and Hansen A M). Specifically, the effect of wakes is considered through the Dynamic Wake Meandering (DWM) model, which simulates a moving wake deficit that is propagated downwind based on the lateral components of the wind fields used in the simulation (Larsen G C, Madsen H A, Thomsen, K. and Larsen T J). Due to the computational requirements of this model setup (approximately 3 times slower than real-time on a single CPU), it is impractical to directly include the aeroelastic simulations in the optimization procedure. Instead, the wind turbine response is mapped to a simpler surrogate model which is trained on a large database of pre-computed simulation outputs. The surrogate model approach is popular and used in various applications such as uncertainty propagation (Murcia Leon, J. P., Réthoré, P-E., Dimitrov, N. K., Natarajan, A. et.al.) and prediction of wind farm power output (Dimitrov, N. K., and Natarajan, A., 2019). The present study introduces a novel application of surrogate models for wind farm control set-point optimization.

A major part of the work towards the objectives in this section is reported in an open-access paper which is due to be published in the Journal of Physics: Conference series (Dimitrov, N. K., and Natarajan, A, 2021). The present section provides a summary of the methods, presents the findings, and discusses the benefits and challenges with using the DWM model within wind farm set-point optimization.

5.1 FATIGUE VS. POWER PRODUCTION

Having a model that can quickly provide both load and power estimates means that the set-point optimization can be carried out under more advanced objectives where the power maximization can be balanced against a reduction of fatigue damage accumulation. The mathematical formulation of these optimization problems uses the following definitions:

- The number of turbines in a wind farm equals N_T ;
- The individual turbine power output is denoted as P_i , $i = 1 \dots N_T$;
- The fatigue is considered in terms of damage-equivalent loads, $DEL_i \propto (\Delta D)^{\frac{1}{m}}$, where ΔD denotes the fatigue damage accumulated at a single location on the wind turbine over a reference period of ten minutes, and m is the slope of the material $S - N$ curve.

Based on these definitions, two types of optimization problems are considered:

- 1) Power maximization subject to load constraints:

$$\begin{aligned} & \text{Maximize } \sum_{i=1}^{N_T} P_i \\ & \text{Subject to: } DEL_i \leq DEL_{max}, \text{ for all } i = 1 \dots N_T \end{aligned}$$

2) Fatigue minimization at target total farm power output P_{target} :

$$\begin{aligned} & \text{Minimize } \sum_{i=1}^{N_T} DEL_i \\ & \text{Subject to: } 1) \sum_{i=1}^{N_T} P_i = P_{target} \\ & \quad \quad \quad 2) DEL_i \leq DEL_{max}, \text{ for } i = 1 \dots N_T \end{aligned}$$

The rationale behind the first approach is to maximize the power output while ensuring that none of the turbines would experience a load increase that would bring the total lifetime fatigue accumulation beyond the turbine design limits. In order to fulfil this goal, the load constraints need to be set as the fatigue design limits of each turbine, or to other maximum acceptable fatigue load limit, e.g. the maximum expected fatigue accumulation, for a turbine in the same wind farm, under operation without optimization of control strategies.

The second optimization approach becomes relevant mainly in situations where increased power output is not relevant or not desired – e.g., in operation under power curtailment where the total power output of the wind farm may be limited by the grid demand. In such cases it would be beneficial to provide the target output power at the lowest cost.

5.2 DE-RATING STRATEGIES AND SURROGATE MODEL IMPLEMENTATION

The present set-point optimization method requires a process where the actual optimization is the final step and is preceded by several other steps required to generate inputs and train the surrogate models used in the optimization. The entire procedure is illustrated in Figure 5-1.

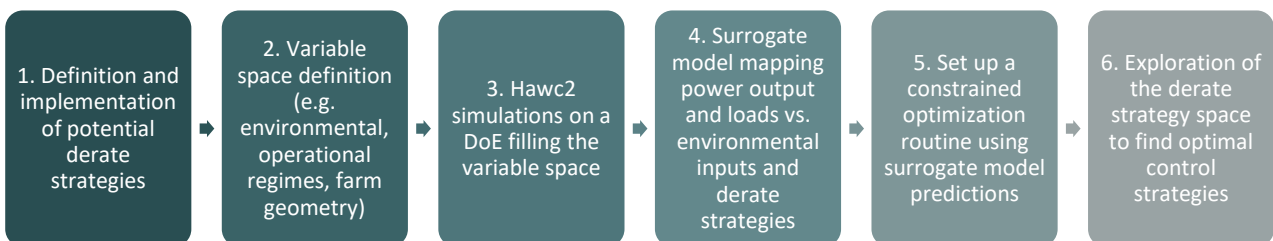


Figure 5-1 steps in the Procedure for set-point optimization including load assessment

The specific solutions for each of the steps shown in Figure 5-1 are explained in details in (Dimitrov, N, 2019). Key elements of the procedure are the choice and implementation of the de-rating strategy in the aeroelastic code, and the definition of variable space that allows the use of standard supervised learning techniques for training a regression model. The de-rating strategy consists of

applying changes to the generator torque demand and to the minimum blade pitch angle, which result in lower rotor speed and reduced power, along with reduced rotor thrust and hence a reduction in the rotor induction and the strength of the wake behind the turbine. For convenience, the de-rate strategy is described by a single variable denoted as “derate index”, $DI \in [0,1]$. $DI = 0$ means the turbine runs at nominal settings, while $DI = 1$ corresponds to maximum de-rating. The minimum pitch angle φ_{min} and the torque demand multiplier K are linear functions of DI :

$$\varphi_{min} = -1 + 5DI$$

$$K = K_{nominal} * (1 + 0.57DI)$$

This de-rating strategy results in up to 40% reduction in the rotor thrust, and it affects the power output in a similar way, with up to 30% reduction in power output below rated. The power and thrust curves under different DI values are shown in Figure 5-2. This de-rating approach only has an effect below rated wind speeds. Above the rated wind speed, the power and thrust curves are equivalent to the nominal curves without de-rating.

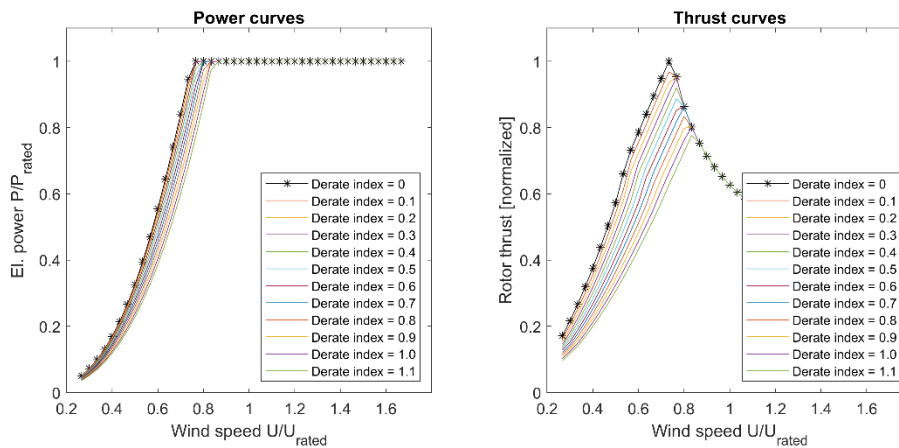


Figure 5-2 effect of thrust-reduction based de-rating strategy on power output and thrust force

The variables used to describe the farm effects (the influence of upwind turbines on the power output and loads on the downwind turbine) are defined in terms of the farm geometry. The relative position of each upwind turbine considered, is defined in terms of two variables: the relative upwind distance in terms of rotor diameters, R_D , and the relative angle between the upwind turbine direction and the free wind direction, θ . This is illustrated in Figure 5-3. Since the upwind turbines may have different de-rate settings which will influence their wakes, an additional variable defining the DI of each upwind turbine is introduced. This results in 3 additional variables in total for every upwind turbine considered. Most surrogate modelling approaches, including the currently used feedforward neural networks, require a fixed number of input variables. In order to satisfy this condition while maintaining the variable description discussed above, we define an upper limit of the number of upwind turbines to be considered, N_{upwind} . Then the surrogate model will have a fixed number of input variables, equal to 3 (the number of environmental variables) + 1 (the derate index of the currently simulated turbine) + $3N_{upwind}$. Then, for situations where there is less than N_{upwind} disturbing turbines, the irrelevant variables are simply set to 0.

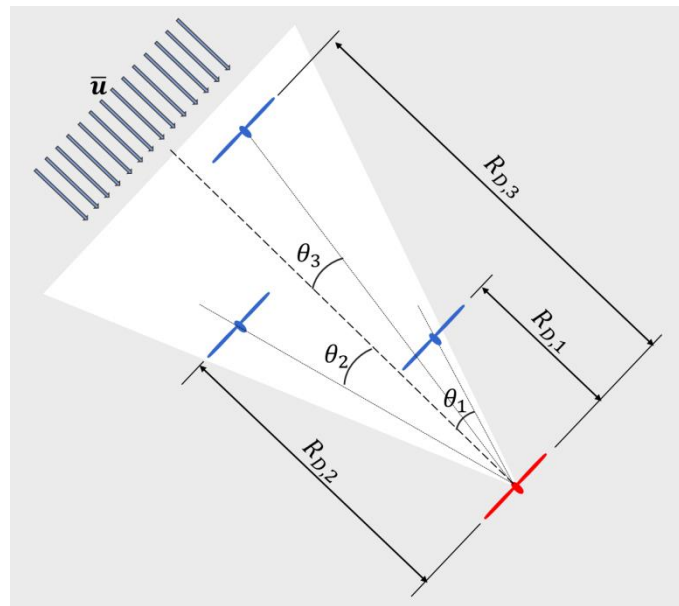


Figure 5-3 Parameterization of wake-related conditions in the wind farm

The distribution of the data sample for training the surrogate model should be chosen so that it covers the range of situations (e.g. site-specific climate, wind farm geometries) where the model is going to be used. If the intended use is for a specific wind farm or a few wind farms, an efficient sampling approach is to randomly pick scenarios representing these particular wind farms. Hawc2 simulations with the DWM model can include the wake effects of all wind turbines in a wind farm, however load time series are calculated on a single turbine only. Therefore, the sampling strategy is as follows: 1) environmental conditions (wind speed, turbulence and shear exponent) are sampled from their respective distributions, and a random DI level is selected for each turbine in the wind farm, 2) a random wind direction is picked from a uniform distribution between 0 and 360deg; 3) a random turbine position within the wind farm is selected; 4) a Hawc2 simulation for the selected turbine is carried out, under the wind direction, environmental conditions, and operating status of neighboring turbines as selected. The simulation results are then applied as the target data in the surrogate model training process, while the input variables are defined from the simulation inputs using the procedure described above. A large database of Hawc2 simulation results is generated, covering the relevant ranges of input conditions as well as varying combinations of de-rating strategies. The simulations in this database are used as inputs for training the surrogate model.

The aeroelastic simulations use randomly generated turbulent fields as inputs. This introduces a realization-to-realization uncertainty due to the different seeds used in the random number generation process. This means the models based on simulations with the DWM model will have an additional uncertainty compared to quasi-steady models such as the engineering wake models available in PyWake ((Pedersen, M.M., van der Laan,P., Friis-Møller, M., Rinker, J. et.al.). It could therefore be relevant to run quasi-steady simulations with low-fidelity models to obtain the predictions of power output, and only use the DWM for the load predictions. In the present study we use both approaches, and generate three types of surrogate models – a power-prediction surrogate model based on PyWake with the Bastankhah wake deficit model (Bastankhah M and

Porté-Agel F.), a power-prediction surrogate model based on Hawc2 simulations with the DWM, and a load prediction surrogate model based on Hawc2 simulations with the DWM (see Dimitrov, N., and Natarajan, A. (2021)) for additional details on the implementation).

5.3 COMPARISON OF RESULTS WITH LOW FIDELITY APPROACH

The first application of the surrogate model based set-point optimization that we present is pure power maximization, which allows a direct comparison with the low-fidelity approaches presented in Section 4.1 in this report. The optimization problem aims at maximizing the total wind farm power output, by varying the *DI* of each turbine between 0 and 1. Separate optimizations are run for wind speeds from 4 to 25m/s in 1m/s steps, and wind directions from 0 to 359deg in 1deg steps. The resulting power outputs and the potential gains due to the change in suggested operating strategy are then probability-weighted according to the wind speed and wind direction probability given in Table , to find the potential gains in AEP due to the updated operating strategy. A summary of this calculation is shown in Figure 5-4. The polar plot on the left hand side shows the relative power gain over all wind speeds (with probability weighting according to the wind speed probability in that sector), as function of the wind direction. This plot can be compared with the polar plot in Figure 16 in section 4.1. The gain patterns are similar in both plots, and as expected the highest gains are in the wind directions where the wind turbine alignment means there are significant wake effects. The plot on Figure 5-4 shows more irregular patterns which is due to the increased uncertainty with the use of a surrogate model. This uncertainty is discussed further in Section 5.4. The overall gain in AEP predicted with this optimization approach is 0.7%, which is similar but slightly lower than the gains predicted with the methods presented in Section 4.1.

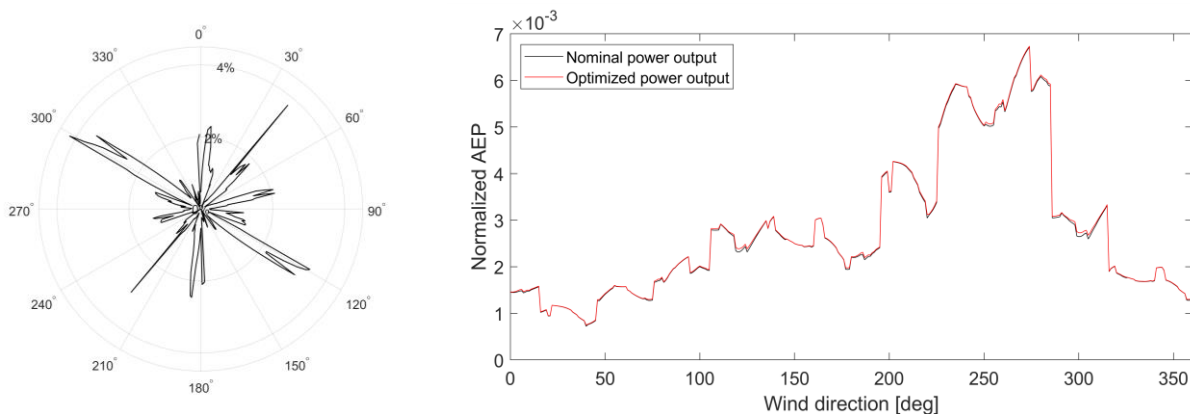


Figure 5-4 relative power gain as function of wind direction, based on power maximization approach. All quantities are weighted according to the wind speed probability distribution for the given wind direction. LEFT: Polar plot of power gain in percent. Right: comparison of the probability-weighted power outputs of the nominal and optimized strategies at different wind directions

The set-points suggested by the optimization procedure described above were compared to the nominal operating strategy in terms of the impact on blade root flapwise damage equivalent loads. The overall load change over all wind turbines in the wind farm as function of wind direction is shown in Figure 5-5. Evidently, even a de-rating strategy aimed at pure power maximization is also expected to result in a decrease in fatigue loads. The total decrease of blade fatigue DEL over the lifetime is predicted to be in the order of 3.6%. Given the nonlinearity of the fatigue damage calculation defined by the slope of the fatigue S-N curve, a 3.6% decrease in DEL could be

equivalent to between 10% and 40% increase in the fatigue lifetime compared to the design lifetime defined by the nominal operating strategy. These results mean that optimal strategies can be defined by balancing (i.e., finding the best synergy) between the economic benefits of power increase and lifetime extension.

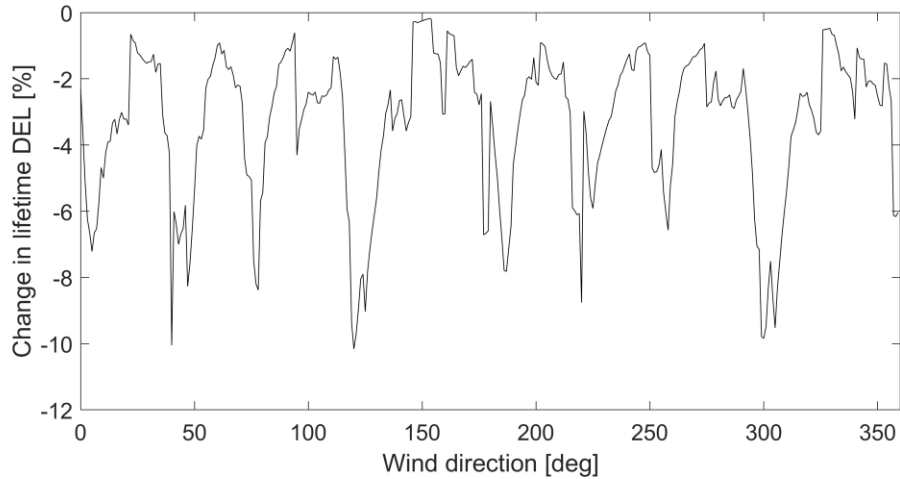


Figure 5-5 change in fatigue del accumulation over the farm lifetime due to implementing de-rating based power output optimization

Figure 5-6 shows an example of the distribution of the de-rating applied to turbines in a suggested optimal set point, for mean wind speed of 9m/s and wind direction of 299deg which coincides with the wind turbine alignment. There is no specific regular pattern in the location of the de-rated turbines. This can be attributed to the possibility of having multiple (non-unique) solutions with different set-ups but similar total power outputs, as well as due to uncertainty/irregularity in the surrogate model predictions which may lead to the optimization procedure get stuck in a sub-optimal local minimum. The effect of these uncertainties is investigated in more detail in Section 5.4.

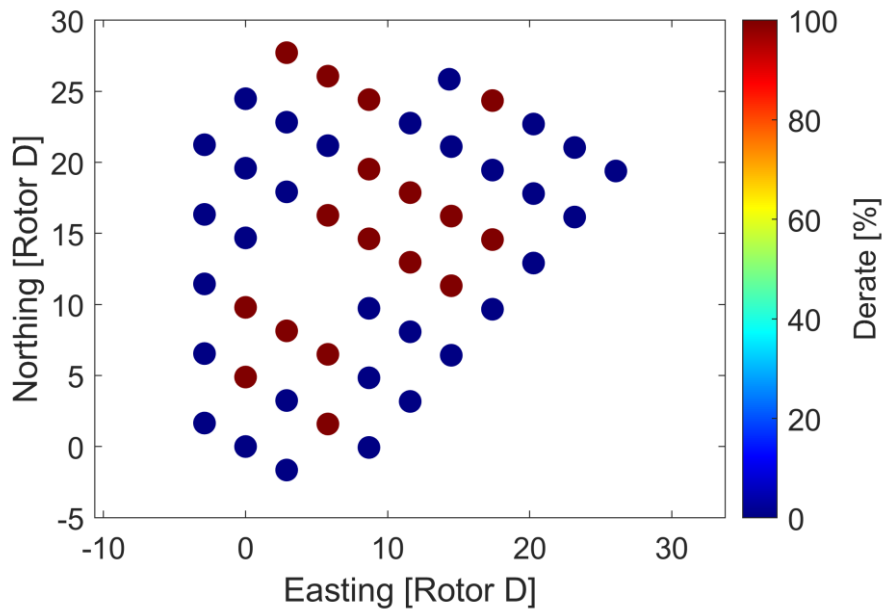


Figure 5-6 Example of the distribution of derating for a suggested optimal set-point at 9m/s mean wind speed and wind direction of 299deg.

The other optimization scenario considered in the present study aims at minimizing the total load accumulation over the wind farm, while maintaining nominal power output (i.e., power output equal to the output expected without any de-rating). This scenario can show if it is possible to lower the damage accumulation further while keeping a high power output. In addition to maximum lifetime extension at nominal power output without grid constraints, such an approach could be useful to determine an optimal strategy for situations when the grid restrictions means that the wind farm is curtailed (i.e., an upper limit on the farm power output is imposed). A set of optimizations based on this scenario is run for the same range of wind speeds and wind directions as in the power-maximization scenario. Figure 5-7 shows a comparison of the relative load reduction achieved with the two scenarios, as function of wind direction. With this strategy, as expected the overall decrease of lifetime fatigue DEL is larger, in the order of 8%, which translates to between 25% and 120% increase in the fatigue lifetime of structural components, estimated for S-N curve slopes of 3 (steel) and 10 (load-carrying composite beams), respectively.

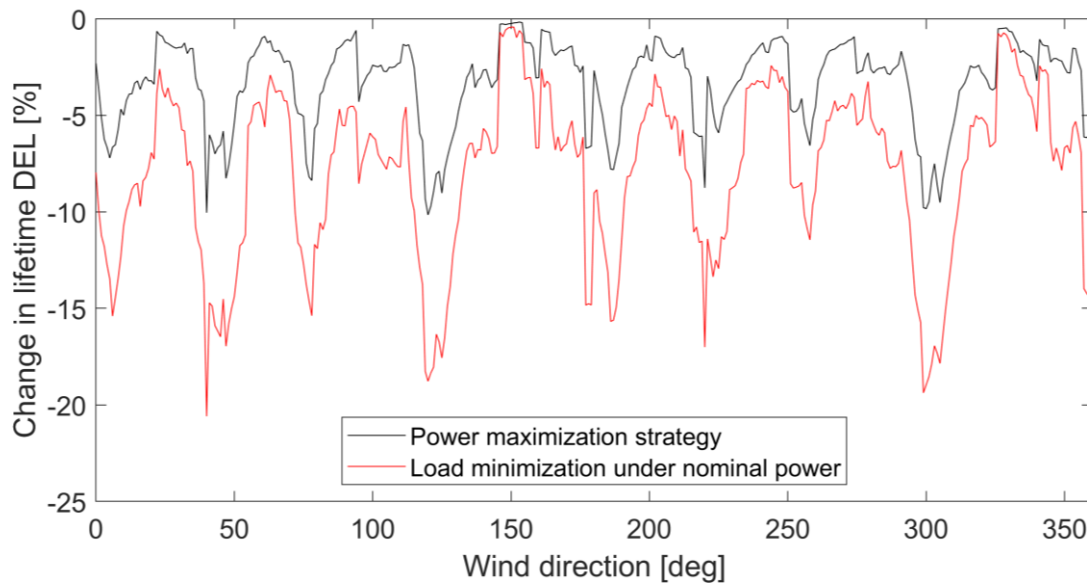


Figure 5-7 Comparison of the relative load reduction achieved with power maximization vs. load minimization under nominal power

5.4 UNCERTAINTIES IN THE SET-POINT OPTIMIZATION PROCESS

The set-point optimization procedure involves the use of several modelling steps (aeroelastic simulations, surrogate model training, and optimization) that will introduce uncertainties in the final power and load estimates and in the potential benefits of the optimized control strategy. The sources of these uncertainties, their ranges estimated from the present study, and their expected significance for the control optimization goals are explained in details in Table 5-1.

Table 5-1 uncertainties in the load surrogate model-based set-point optimization process.

Uncertainty type	Explanation	Observed range	Significance
Realization-to-realization uncertainty	Uncertainty due to the use of random turbulence seeds. Affects only dynamic simulations with turbulence	Power below rated wind speed: ~20% COV (95% confidence interval width of $\pm 40\%$ of the mean value) Blade DEL: ~15% COV (95% confidence interval width of $\pm 30\%$ of the mean value)	Behaves like standard error in a typical random sample (uncertainty decreases with \sqrt{N} for N number of realizations), meaning that running e.g. 12 seeds per sample would reduce the uncertainty in the estimate of the mean power output from 20% to ~6%. This uncertainty influences the accuracy of surrogate models trained on such data. Eliminating it requires either running multiple seeds per sampling point, or increasing the sampling point density – which in both cases increases the amount of data required for proper model training.
Surrogate model uncertainty	Uncertainty due to inaccurate mapping of the response by the surrogate model	Power below rated wind speed, HAWC2: ~7% COV, R-square = 0.985	When mapping a deterministic model like the static wake models included in Pywake, the uncertainty is just a few percent.

		Blade DEL, HAWC2: ~9.5% COV, R-square = 0.95 Power below rated wind speed, Pywake: ~1.6% COV R-square = 0.998	
Optimization uncertainty	Uncertainty due to the presence of local minima	~0.1% COV on the power output ($\pm 0.3\%$ total range).	Performing multi-start (multiple optimizations with different, random initial conditions) leads to slightly different optimal solutions (see (Dimitrov, N., and Natarajan, A. (2021))) for details). This is due to the presence of local minima where the optimization process finishes without finding the true global maximum. However, this uncertainty seems to be rather small compared to other factors.
Wake model uncertainty	Uncertainty due to the different flow assumptions in engineering wake models	0-30% bias in the power output predictions of waked turbines (varies according to wind speed and wake angle). 15% average difference between the predictions of the Bastankhah model in PyWake and the DWM model with Hawc2.	Engineering wake models, including the DWM, differ significantly in the assumptions about deficit depth, wake expansion, and recovery rates. This results in significant differences in the predictions of total power output in situations with strong wakes, especially with multiple turbine rows. Specifically, the standard settings of the DWM model result in stronger deficits than the Gaussian/Bastankhah wake models implemented in PyWake. This is illustrated in Figure 5-8. Such differences are mainly in terms of bias (the scatter in the figure is mainly due to seed-to-seed uncertainty). The main impact of such bias is that it will lead to inaccurate assessment of the power gains in absolute terms. In case the bias varies significantly throughout the analysis domain, the relative power gain estimation accuracy will also be affected.

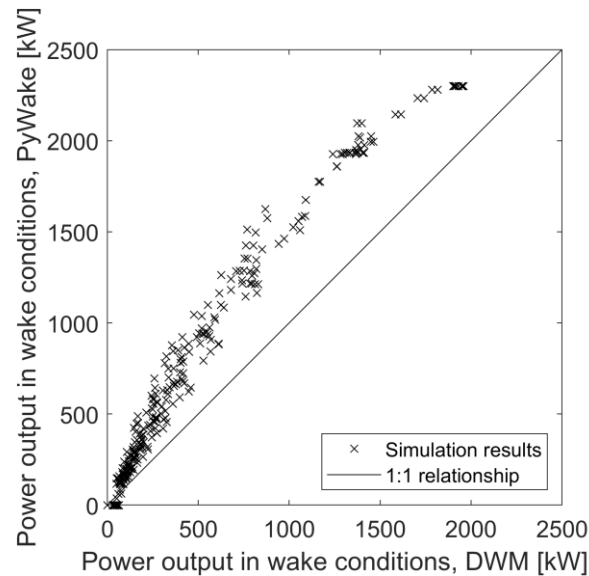


Figure 5-8 Comparison of power output predictions in wake conditions for the dwm model implemented in hawcz and the bastankhah model implemented in pywake.

5.5 CONCLUSIONS FROM THE SET-POINT OPTIMIZATION USING DWM

This is a summary of the findings and conclusions from the study on using the DWM model for wind farm set-point optimization:

- In order to make the optimization computationally feasible, it is necessary to map the aeroelastic model outputs to a more computationally efficient surrogate model;
- The total AEP gains estimated with this method are in the range of 0.75%, which is similar to the other studies which are part of this deliverable document;
- Lifetime-equivalent fatigue load decrease in the order of 3.6% was observed for the derate strategies aimed at pure power maximization. This could lead to 10-40% increase in the fatigue lifetime limits depending on the component. It means that pure power maximization could be a beneficial strategy, and that there could be optimal solutions which seek the best synergy between power increase and lifetime extension;
- For strategies aimed at obtaining a nominal power output at least possible fatigue load accumulation, a load decrease of up to 8% over the farm lifetime was observed;
- There is a significant uncertainty associated with the settings of wake deficit models, which is the main contribution to the uncertainty in the estimated total benefits of the optimized control strategies;
- There is an additional uncertainty associated with the use of the DWM model, mainly governed by the realization-to-realization uncertainty associated with using random turbulence fields in the load simulations. This requires that larger amount of data is used for surrogate model training;
- Due to the higher uncertainty associated with the DWM model, it could be beneficial to supplement the model training data with power predictions based on other models, e.g. to train a surrogate model for power prediction based on PyWake simulations and use the DWM results just for load predictions;

6. ANCILLIARY SERVICES (DNV)

This chapter is concerned with certain types of grid ancillary services where wake effects play a significant role. It is not concerned with the grid-facing aspects of wind farm control such as voltage and reactive power regulation, fast frequency response, or the provision of black start and grid-forming capabilities, which are only influenced by wake effects in a very peripheral way. LongSim has already been used in conjunction with a grid simulation model to investigate optimisation of fast frequency response strategies in this project (Deliverable D4.1: Bossanyi *et al*, 2020 and Schoot *et al*, 2020), and a field test of fast frequency response strategies on the 7MW demonstration turbine is planned as part of Work Package 3.

Wake effects are more important for those ancillary services which involve sustained changes to the level of active power production from the wind farm, such as curtailment of the total wind farm output, or delta control to provide a level of reserve power available at short notice. This chapter deals mainly with the issue of responding to grid curtailment demands, because to achieve the required curtailment level, an understanding of wake effects can allow the wind farm operator to distribute power reductions among the turbines in such a way as to minimise turbine fatigue loading, potentially helping to achieve a longer life of the farm. A brief section on delta control is also included.

Wake steering could be used for both curtailment and delta control, but it would be more appropriate to use the thrust reduction settings as defined for axial induction control in Section **Error! Reference source not found.** The induction control settings can be changed with a much faster response than the yaw misalignments, and the effect on turbine fatigue loading is very beneficial, unlike the effect of the large yaw misalignments which would otherwise be required.

Both curtailment and delta control algorithms will be field tested on the 7MW Levenmouth demonstration turbine in Work Package 3 of this project.

6.1 CURTAILMENT

This section shows how the LongSim setpoint optimiser can be used to adjust turbine setpoints to achieve a given level of curtailment, and goes on to evaluate the performance using time-domain simulations.

The optimisation has been done in three stages to aid convergence. This means that the optimum found may not be the true global optimum; but there is in any case no guarantee of finding the global optimum. The stages used were as follows:

- a) Using a uniform setpoint for all turbines as in Section **Error! Reference source not found.**, the setpoint is adjusted for maximum power production to give a good starting point, using a merit function which is just the total power.
- b) The uniform setpoint for all turbines is adjusted downwards until the correct curtailment level is achieved, using a merit function which minimises SCE, the square of the curtailment error (difference between total power and the curtailed power demand).

- c) As b) but using a merit function which includes blade root and tower base bending moment fatigue as in Section **Error! Reference source not found.**
- d) As c) but now optimising all turbine setpoints individually

The optimisation is first illustrated for one particular wind condition: 9 m/s with 6% turbulence intensity and wind direction 222°, with the curtailment level set to 25 MW (compared to the base case power level of just over 30 MW in this wind condition). Stage (a) is then the same as in Section **Error! Reference source not found.** Figure 6-1 shows the results of the four optimisations a) to d) described above, and a fifth case e) which is the same as c) but with increased weighting on the loads (60% on power error, and 10% each on the maximum and the CoV of the blade root and the tower base DEL).

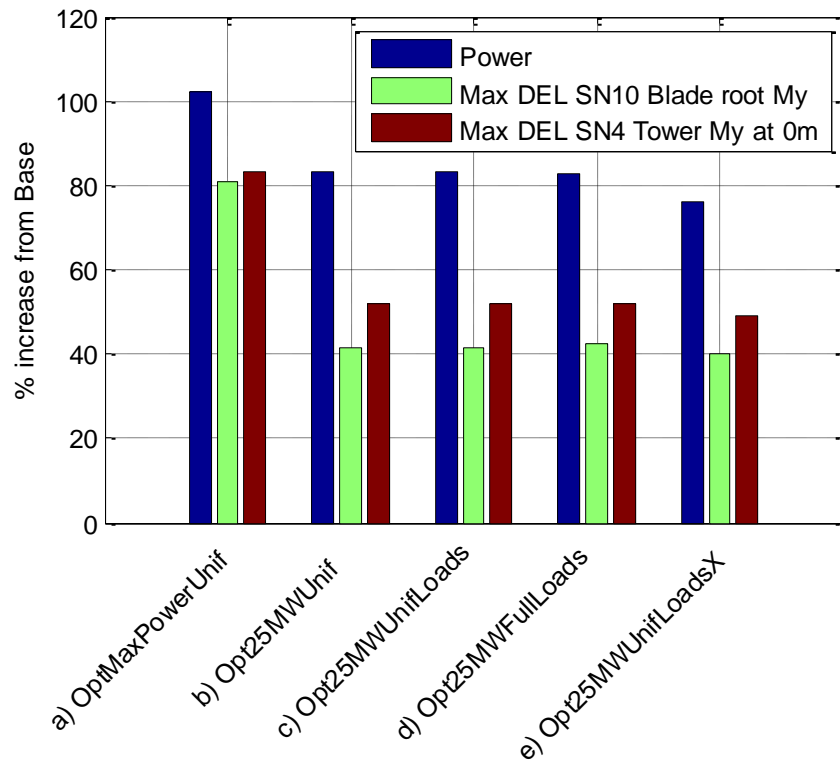


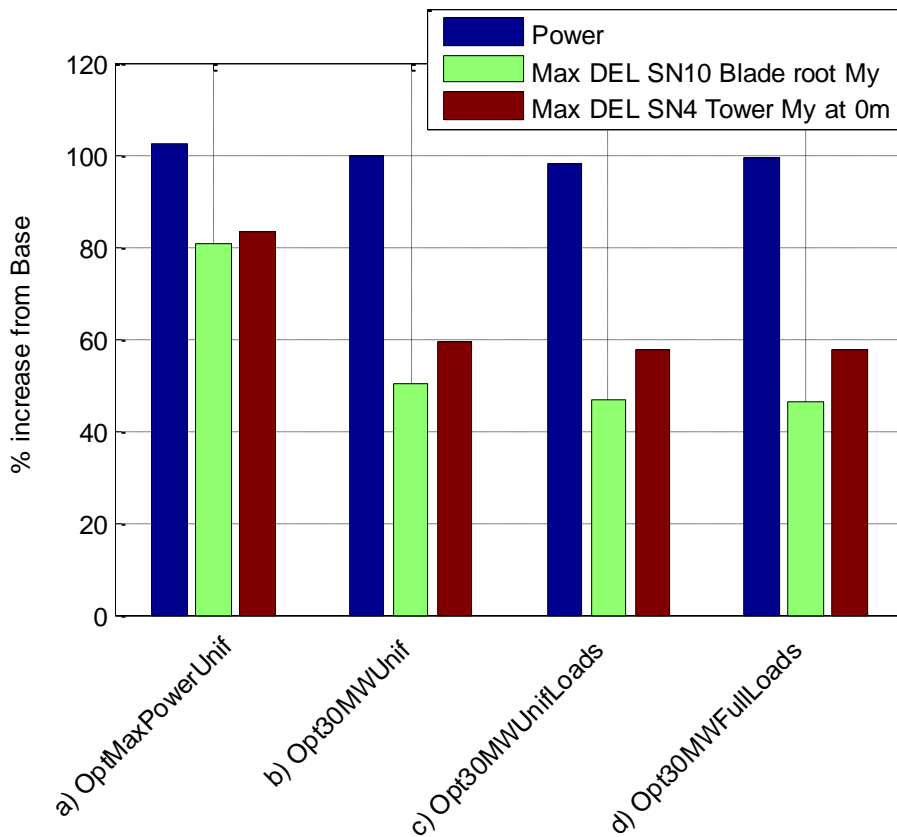
Figure 6-1: Optimisation results for at 9 m/s: uncurtailed case, and curtailment to 25 MW

This shows that the correct curtailment level is achieved in each of cases b), c) and d), and also that the maximum loads are significantly reduced, even if they are not included in the merit function. Including them in the merit function for cases c) and d) makes little difference, but increasing the loads weighting in case e) does reduce the loads a little, at the expense of a significant error in the curtailment level. The results are detailed in Table 6-1. Case d) should be better than c) because all setpoints are being optimised, but it is actually slightly worse, indicating firstly that this optimisation (which is numerically much more demanding) may not have quite fully converged, but also the setpoints required – 12.25 in case b), defined as in Table 4-4 – are already close to the maximum value of 13, leaving little scope for further adjustment.

Table 6-1: Optimisation results for at 9 m/s: uncurtailed case, and curtailment to 25 MW

Case	Base case	a)	b)	c)	d)	e)
Power, MW	30.01	30.76	25.00	24.98	24.84	22.84
Max blade root DEL	100%	80.71%	41.32%	41.29%	42.47%	39.85%
Max tower base DEL	100%	83.05%	51.89%	51.88%	52.15%	49.13%

Repeating with a curtailment level of 30MW, the setpoint is further from the maximum – 9.4 in case b), leaving more scope for adjusting the optimisation to include loads, and also to optimise setpoints individually as for case d), which now brings a small improvement. These results are shown in Figure 6-2 and Table 6-2.


Figure 6-2: Optimisation results for at 9 m/s: uncurtailed case, and curtailment to 30 MW
Table 6-2: Optimisation results for at 9 m/s: uncurtailed case, and curtailment to 30 MW

Case	Base case	a)	b)	c)	d)
Power, MW	30.01	30.76	30.00	29.47	29.90
Max blade root DEL	100%	80.71%	50.35%	46.62%	46.47%
Max tower base DEL	100%	83.05%	59.20%	57.50%	57.48%

Since case b) is simple and effective, also in terms of loading, this scheme has been chosen to take forward for further illustration. The setpoints are first calculated for the same range of wind conditions as used in Section **Error! Reference source not found.**, and then dynamic simulations

with the same wind conditions are performed. A curtailment level of 20 MW has been chosen, as the wind conditions are mostly well below 9 m/s, and simulations are carried out with and without the curtailment, and the power and loads are compared. The simulation setup is as described in Section **Error! Reference source not found.**, except that for the curtailed case, no setpoint smoothing was applied as this might be distorted when the setpoint reaches the maximum allowed limit. A final simulation was therefore carried out with this modification together with a reduction in proportional gain, and the results, shown in Figure 6-5 to Figure 6-8, demonstrate that the desired result has been achieved: the power tracks the desired level well whenever possible, with the reduced gain having cured the oscillatory behaviour, and the maximum loads now remain low throughout.

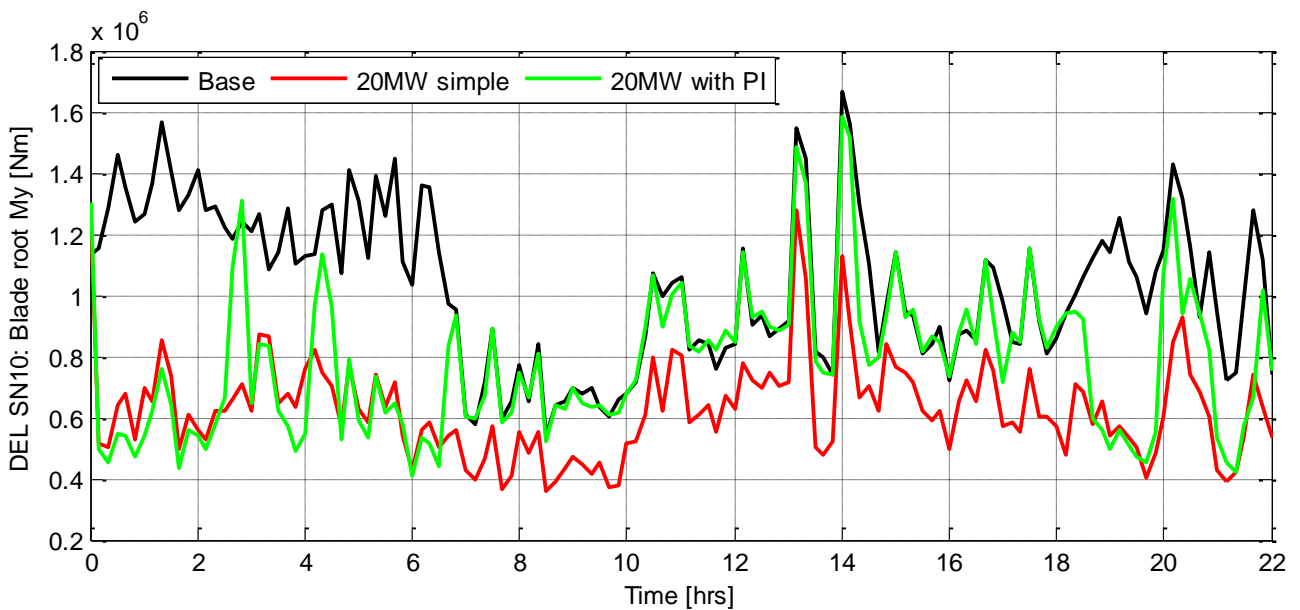


FIGURE 6-3: Maximum blade root fatigue with and without a PI controller

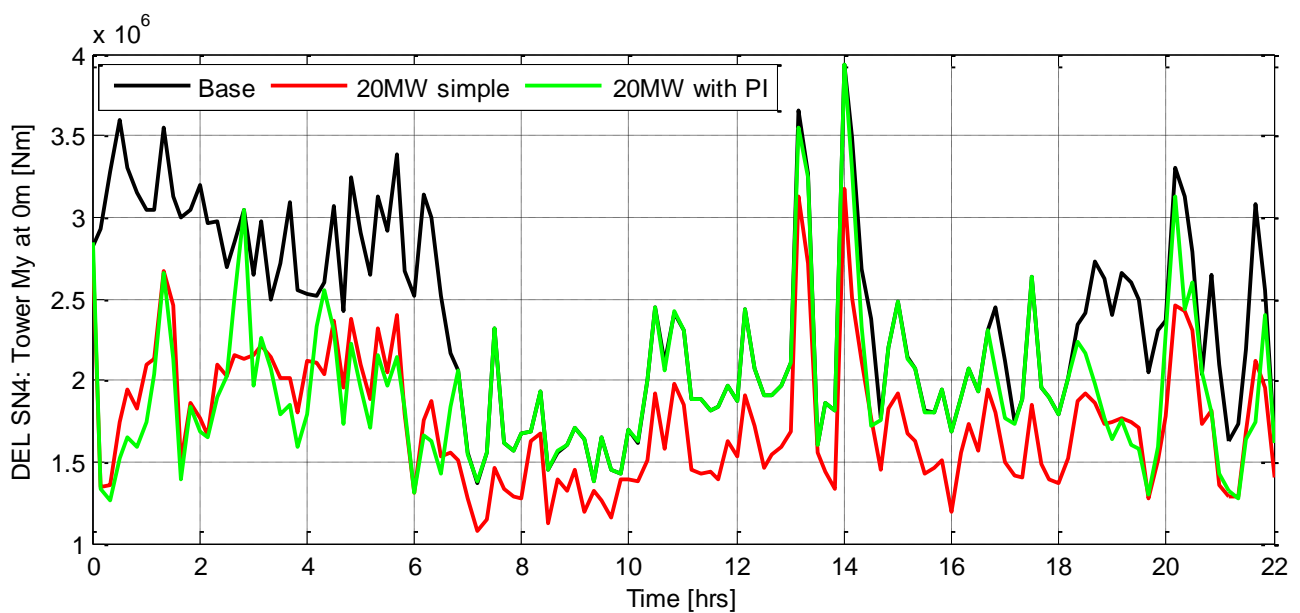


FIGURE 6-4: Maximum tower base fatigue with and without a PI controller

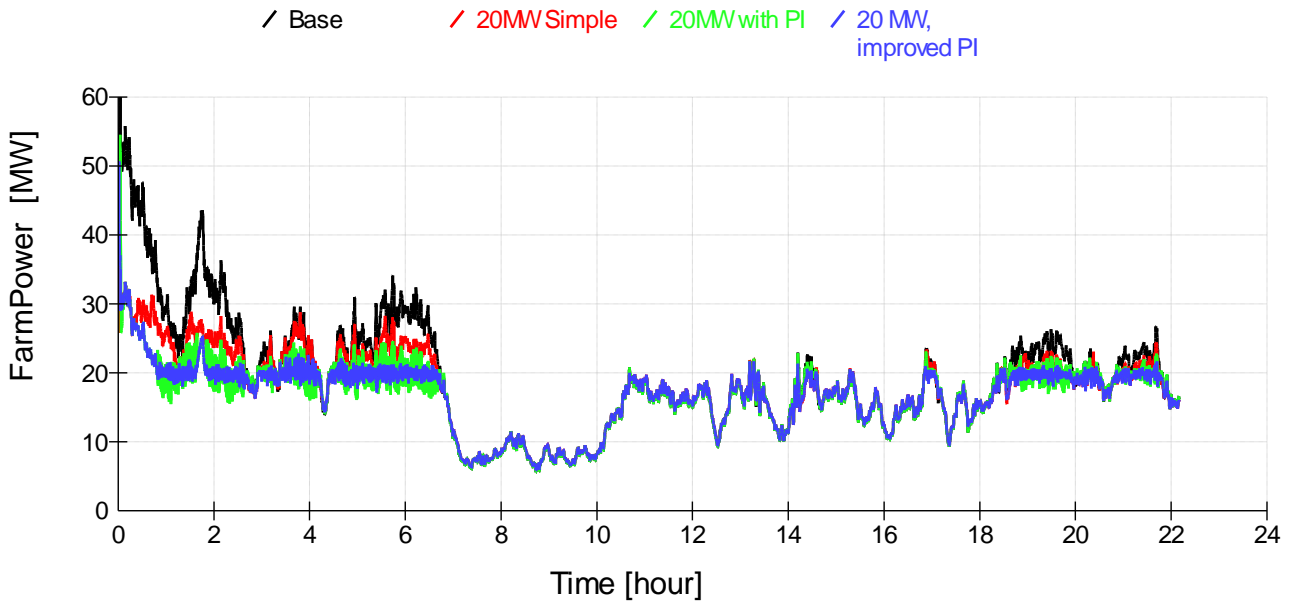


FIGURE 6-5: Improved PI controller: power regulation

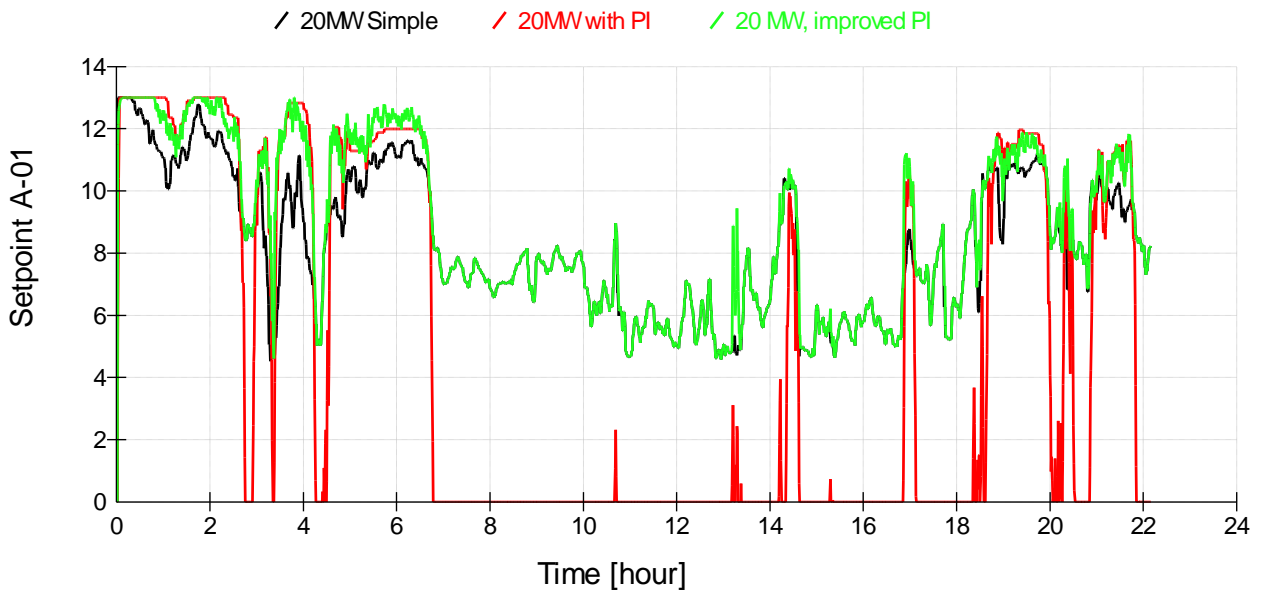


FIGURE 6-6: Improved PI controller: setpoints

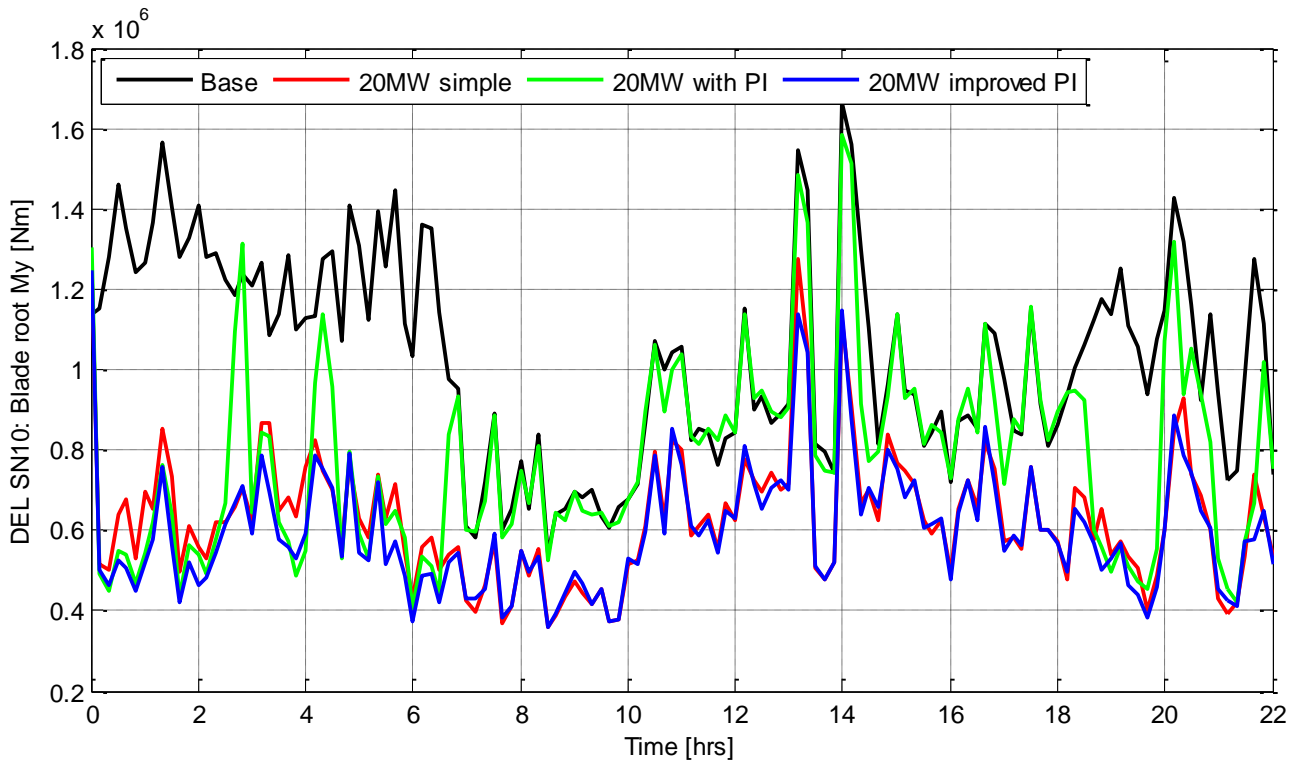


FIGURE 6-7: Improved PI controller: maximum blade root fatigue

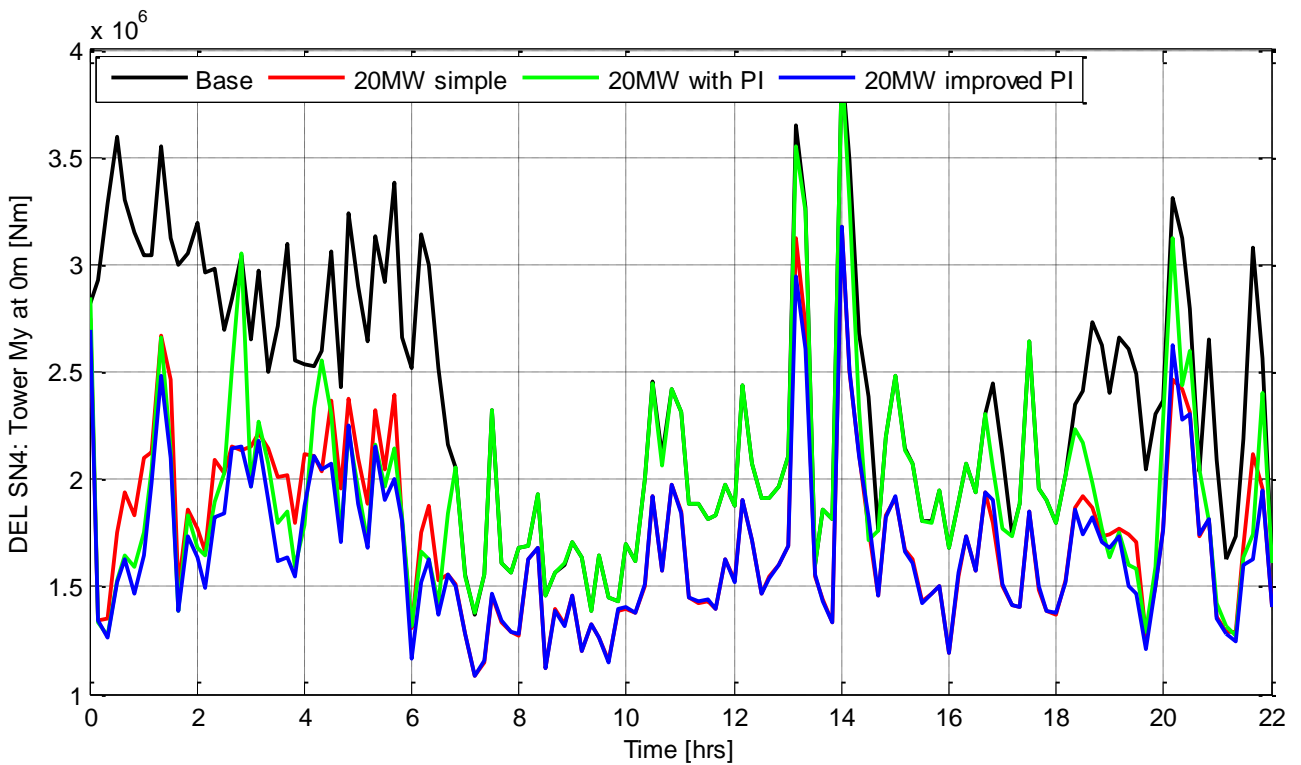


FIGURE 6-8: Improved PI controller: maximum tower base fatigue

This represents an open-loop curtailment control, and any inaccuracies in the modelling or wind condition estimations will mean that the actual power production may not be exactly what is demanded. This can be compensated by an outer feedback loop, for which a simple PI controller is probably adequate, which compares the actual and desired power and adds a uniform adjustment to all the turbine setpoints, causing the actual power to track the desired power in closed loop fashion.

6.2 DELTA CONTROL

Delta control refers to the possibility to operate a wind farm at a reduced power level in order to provide a margin ΔP of reserve capacity which the grid can call upon at short notice. Below rated, this means generating a varying amount of power which is always ΔP less than whatever power the wind farm could have been producing in the wind conditions pertaining at that time.

The thrust reduction settings defined in Section **Error! Reference source not found.** can be used for this, because they also result in a power reduction. A lookup table can be constructed which allows the appropriate thrust setting to be calculated for the desired power reduction ΔP at any given wind condition. However, this will not give the correct power margin because the wake losses will also change. There are various possible ways to achieve the correct margin, for example:

- Estimate the wind condition as for wind farm control (see Section **Error! Reference source not found.**), and use this to calculate the expected wind farm power (including wake losses) from a pre-calculated set of wind direction dependent wind farm power curves
- Calculate the curtailed power level which would give the desired ΔP at that moment in time
- Use the curtailment setpoint tables calculated as in Section 6.1 to get the appropriate turbine setpoints for that power level in that wind condition.

An outer PI loop can also be used, as in the case of curtailment, to maintain closed loop tracking of the desired ΔP margin.

7. APPLICATION OF MULTIDIMENSIONAL SET POINT CONTROL TO THE DTU 10 MW TURBINE IN THE REFERENCE WIND FARM (EQUINOR)

The application of wake control in offshore wind farms has an interesting potential to increase power production. The two mainstream approaches are wake deflection through yawed operation and induction control by means of de-rating of turbines, the latter was investigated here. The aero-elastic code HAWC2 with the integrated DWM model was applied in the investigations with the generic DTU 10MW wind turbine. A set of parameter studies covering turbine distance, wind speed and turbulence intensity with different controller setups was carried out. In the development of the DWM model, the focus was to create a high-fidelity engineering wake model where the parameters affecting power production and loads of a turbine in wake operation are modelled in a physically consistent manner. To achieve that, observations as well as physical and numerical experiments were included in the design of the DWM model. The wake deficit evolution, the increased turbulence level in the wake and the large-scale meandering have been identified as the most important processes for wake evolution. A fundamental assumption of the DWM model is the split in scales which results in the decoupling of the wake deficit evolution from the wake meandering.

Reference is made to the publications (Madsen, 2010), (Larsen, 2013) and (Larsen, 2015).

In the activities, configurations with two turbines was examined. A two-turbine setup is the most basic approach, but it is regarded as suitable to explore the main challenges to increase the common energy production of an upstream turbine and a downstream turbine its wake. Any larger-scale application depends on the solution for the two-turbine problem.

To vary turbine setpoints/induction, controller setups for power- and thrust reduction were developed. The power derating was applied in a broader range from 5 to 13 m/s, three levels (70%, 80% and 90% of original power production) were applied. Thrust reduction setups were realized in a more small-banded wind speed range from 9 to 12 m/s around rated wind speed for two thrust reduction levels (70% and 80%). Furthermore, a thrust reduction with optimized power production was investigated.

7.1 THE DTU 10 MW TURBINE

The growth trend for offshore wind turbines is strong, in 2020/2021 three turbine designs with rotors equal or larger than 220 m will enter the market. Technical data from these large designs are not publicly available. However, the DTU 10 MW reference turbine has dimensions and specifications in the same range as the largest turbines, data are publicly available, and this turbine design is chosen for this study.

Data can be found at (<https://www.hawc2.dk/Download/HAWC2-Model/DTU-10-MW-Reference-Wind-Turbine>, u.d.)

1.1 Turbine data

The DTU 10 MW reference turbine was ready developed in 2013 at DTU in the Section for Aeroelastic Design and Section for Structures, (Bak, 2008). The turbine is an available large generic design and regarded as representative for a large wind turbine. Equinor has applied the design in internal studies for evaluation of next-generation turbines.

Main data for the DTU 10 MW turbine are given in **Table 7.3**.

Table 7.3: Technical data DTU 10 MW turbine.

Turbine power	10 MW
Rotor orientation configuration	Upwind, 3 blades
Control	Variable speed, collective pitch
Drivetrain	Medium speed, multiple stage gearbox
Rotor, Hub diameter	178.3 m, 5.6 m
Cut-in, Rated, Cut-out wind speed	4 m/s, 11.4 m/s, 25 m/s
Cut-in, rated rotor speed	6 rpm, 9.6 rpm
Rotor mass	229000 kg
Nacelle mass	446000 kg
Tower mass	605000 kg

A challenging (and time-consuming) activity is the detailed aero-elastic modeling of a large turbine design. For the current project activity, the available model for the Hawc2 code from DTU was used.

7.2 INDUCTION CONTROL

Induction control is one of several means to control the wake flow in an offshore wind farm. The power production can be distributed more even throughout the park and a slight production increase seems possible. The induction control is regarded as load neutral. Wake control through yawed turbine operation was found to increase structural loads especially for large yaw angles.

The optimization of a complete operational park flow is a large task beyond the scope of this investigation. For the initial parameter studies carried out in this activity an array of two turbines was chosen. This seems to be quite basic however this approach enables very effective analysis of parameter variations for large number of cases.

The main parameters that impact the wake on the downstream turbine are the distance and the turbulence intensity. The inter-turbine distance affects the strength of the wake and the wind speed at the downwind turbine. The turbulence impact is complex, here power and loads are affected. Furthermore, wake recovery depends on turbulence intensity. Unstable atmospheric conditions generate more turbulence from convection effects and shear gradients. It increases wake mixing and results in increased park production. In this study, three typical turbulence intensities (5%, 10% and 15%) were applied.

Three approaches for induction control are evaluated. The standard power reduction, an approach based on thrust load reduction (thrust cutting/peak shaving) and a thrust reduction with optimized

power production are checked. Power reductions were designed to work in a broader range from 5 to 13 m/s. The reductions in thrust/ are established in a smaller wind speed range around the around rated wind speed. The modifications of single power and single thrust curves are shown in Figure 7-1, setpoints for the thrust reduction with optimized C_p are shown in Table 7.2.

Table 7.10.

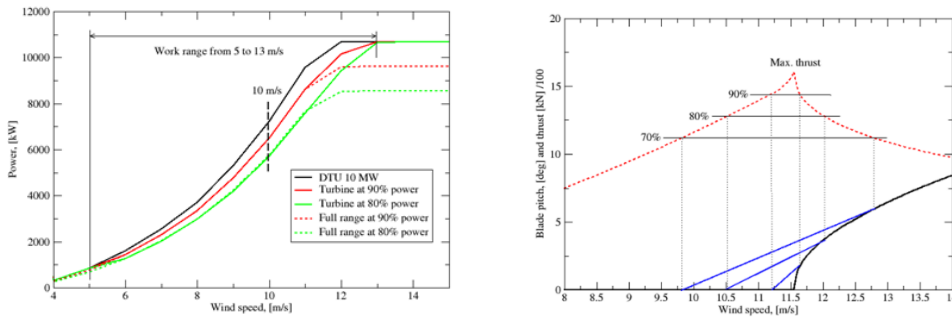


Figure 7-1: Targets for modified controller schemes, power reduction (left) and thrust cut (right).

7.3 SETPOINT MODIFICATION BASED ON POWER REDUCTION

The setpoint is influenced by several operational factors and the blade pitch has a strong effect in particular. The option to comprise pitch actuation for the control of power, thrust and induction/wake effects is further applied.

In first tests, different power curves were developed. The derivation of setpoints was carried out with simulation data, here fixed pitch angles were used in the Hawc2 simulations to generate power and thrust data for the wind speed range from 4 to 15 m/s.

Results are given in **Figure 7-2**. This data set was used to estimate a 90% and 80% power production in the wind speed range from 5 to 13 m/s.

Note that to achieve smooth transition, the 80% and 90% power production is applied in the wind speed range from 6 to 13 m/s. To avoid increased start/stop situations at low wind speeds (4 m/s to 6 m/s) no power reductions schemes were applied for this range.

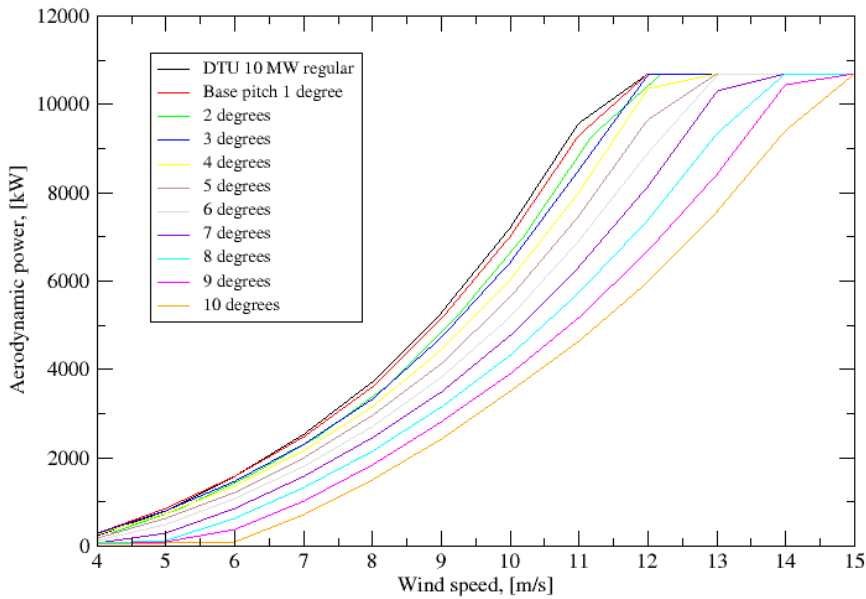


Figure 7-2: Aerodynamic power production as function of start pitch and wind speed, results are from HAWC2 simulations with deterministic wind from 4 to 15 m/s.

To estimate the power setpoints, simulation series with initial prescribed blade pitch were carried out. New setpoints are derived from the simulations for turbine power reductions in the range from 5 to 13 m/s. The turbine behaviour at very low wind speeds and wind speeds above rated was not modified.

Data for the controller input are given in Table 7.6 below.

Table 7.6: Setpoints from prescribed blade pitch for power level reductions.

Wind speed, [m/s]	Datum pitch, [deg.]	90% power, pitch, [deg.]	80% power, pitch, [deg.]
4	2.681	2.680706	2.68
5	1.896	1.896	1.896
6	0.863	2.99	4.3
7	0.000078	2.90	4.7
8	0.000048	2.88	4.8
9	0.000048	2.75	4.8
10	0.000048	2.76	4.8
11	0.000048	2.77	4.8
12	0.000048	5.07	5.3
13	0.000048	7.96	6.25
14	0.000048	0.000048	0.000048
50	0.000048	0.000048	0.000048

The setpoint variations impact the power generation in the medium wind speed range in particular. As designed, for low wind speeds and for wind speeds above rated there is no change.

Main turbine parameters as function of the wind speed with the different controller setups are given in **Figure 7-3** and **Figure 7-4** below.

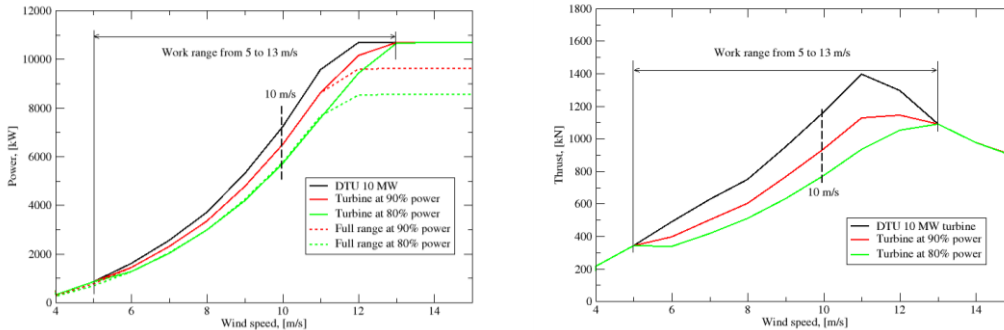


Figure 7-3: Power curves (left) and thrust curves (right) of the DTU 10 MW turbine with different power setpoints.

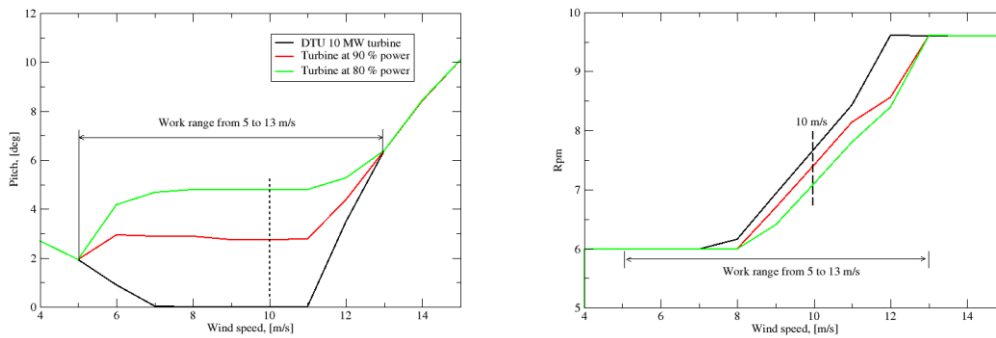


Figure 7-4: Pitch (left) and RPM (right) development of the DTU 10 MW turbine with different power setpoints.

A basic two-turbine park using the DTU 10MW turbine is further investigated with the developed controller settings. Simulations with operational parameter variations were carried out on three levels:

1. First, the behaviour of the turbine (with different controller setpoints) is evaluated at a single wind speed. Here the typical wind conditions of 10 m/s with a turbulence intensity of 10% are applied. The inter-turbine distance was chosen to be 8 rotor diameters.
2. The second step consisted of simulations throughout a wind speed range. The different controllers and their impact on power development are tested in a wind speed range from 5 to 15 m/s at 10% turbulence intensity. The inter-turbine distance is again 8 rotor diameters.
3. Finally, 3D-data are derived as function of turbine distance and wind speed. A wind speed range of 5 to 15 m/s and a distance range from 6 to 15 rotor diameters are computed to compare the different controller setups and their impact on overall power and thrust generation.

The studies are limited to a two-turbine park setup and aimed at the identification of main trends/impacts. The simple setup allows large numbers of simulations to analyse multi-parameter effects.

7.3.1 SINGLE OPERATIONAL POINT ANALYSIS

A single, typical operational point and set-up was chosen for the start of the simulations. Here, a windspeed of 10 m/s (close to the annual mean wind speed in the North Sea) at 10% turbulence intensity for a turbine distance of 8 diameters is taken as start point.

The following steps were carried out:

- Simulation of a single DTU 10 MW turbine with original controller setup
- Simulation of single DTU 10 MW turbines with modified controller, estimation of averaged values for pitch and rpm
- Application of the DWM model for a two-turbine setup. The first turbine uses the estimated averaged pitch- and rpm values, the second turbine operates with the original controller.

Data from the initial simulations are given in Figure 7-19, Figure 7-20, and Figure 7-21. Averaged simulation results are shown in **Table 7.7** and **Table 7.8**.

Table 7.7: Averaged power production [kW] for T1 and T2 at 8 rotor diameters distance, wind conditions 10 m/s with 10% turbulence intensity.

	Standard controller	Power at 90%, P90	Power at 80%, P80
T1 power	6651	6005	5298
T1 power loss	0	-646	-1353
T2 power	4194	4427	4691
T2 power gain	0	+233	+497
Net power	10845	10432 (-3.8%)	9989 (-8%)

Table 7.8: Averaged thrust from DWM simulations for T1 and T2. The T2 turbine is operated with the standard controller. Wind conditions 10 m/s and 10% turbulence intensity at turbine T1.

Averaged data	Datum	Power at 90%, P90	Power at 80%, P80
T1 thrust	1096	884	731
T2 thrust	798	829.4	862.1

It is now interesting to compare the power trends for the two turbines. The upstream turbine is downrated by 10% (P90 controller) and 20% (P80 controller) in this scenario. The power production of the downwind turbine catches somewhat up, but losses are not fully compensated. The downrating for the 10 m/s wind speed regime causes a loss of 646 kW and 1353 kW for the reduced power production on turbine 1. Turbine 2 gains respectively 233 kW and 497 kW. Overall, net losses of 413 kW (-3.8%) and 845 kW (-8%) are seen.

The thrust development shown in **Table 7.8** demonstrates a levelling of the thrust loads to a more even load distribution between the two turbines.

To get a better overview regarding the targeted net power increase, investigations are in 7.3.2 extended over a wind speed range.

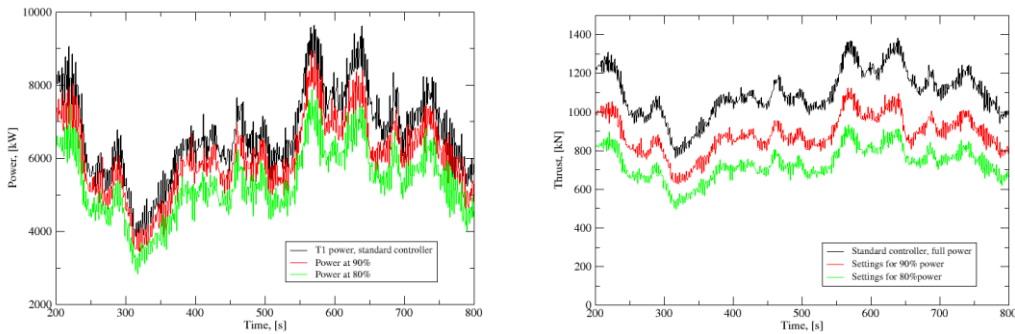


Figure 7-5: Power (left) and thrust data (right) for upstream turbine T1 with three different controller settings.

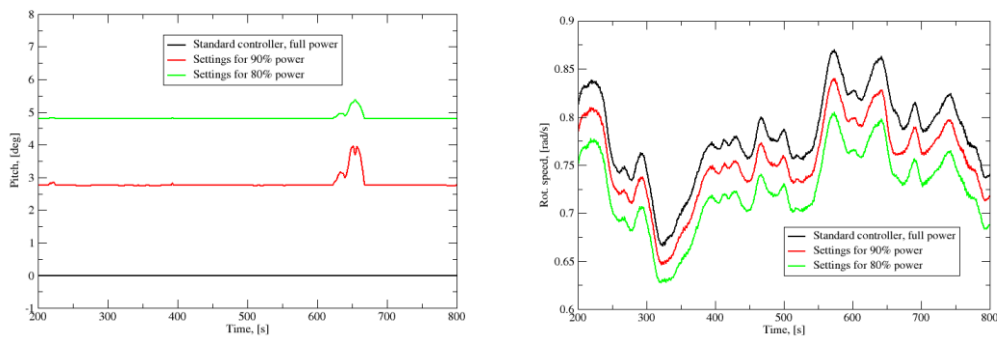


Figure 7-6: Blade pitch (left) and rotor speed data (right) for upstream turbine T1.

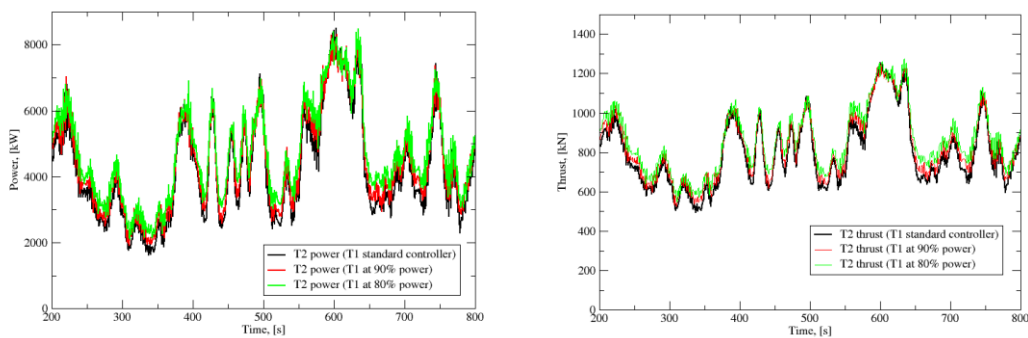


Figure 7-7: Power (left) and thrust data (right) for downstream turbine T2 in the wake of upstream turbine T1. The turbine T1 was operated with three different controller settings.

7.3.2 WIND SPEED RANGE TESTS

In a second step the 2-turbine park has been analysed for a wider operational range. The aero-elastic simulations have been carried out for turbulent wind conditions (from 5 m/s to 15 m/s), where typical turbulence intensities (5%, 10% and 15%) and a turbine spacing of 8 diameters have been investigated. To run these large numbers of cases, a MATLAB code was developed and the HAWC₂/DWM models were run in parallel on a 12-core machine. The data was then aggregated into large matrices where the statistical properties of relevant time series were stored.

The results for 8 rotor diameters spacing are presented in the three figures below for typical turbulence intensity values (5%, 10% and 15%).

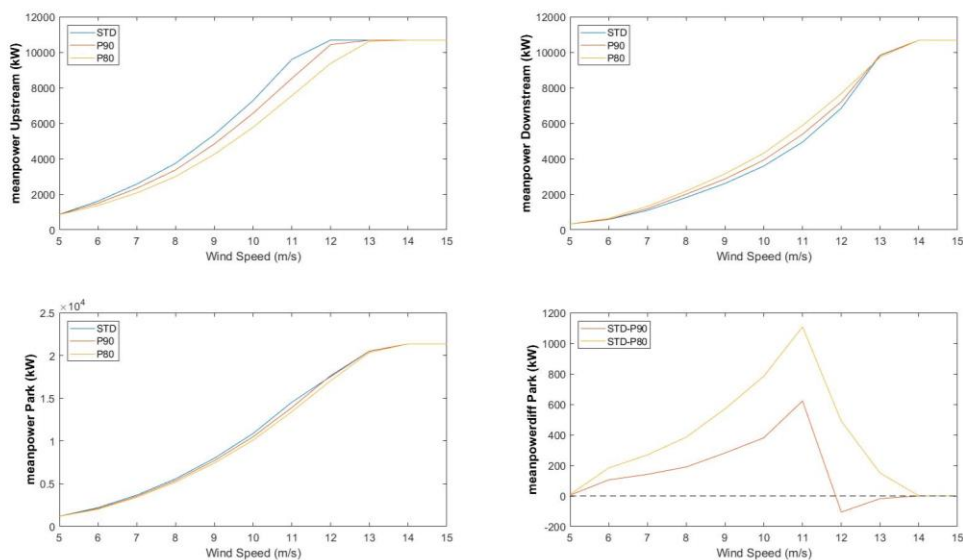


Figure 7-8: Power production for the upstream turbine (upper left), the downstream turbine (upper right) total park power production (lower left) and power production differences (lower right), with TI=5% and turbine spacing = 8 RD.

Power production data are given in **Figure 7-8**. The blue curve (or STD) is showing data where the upstream turbine is using a controller that maximizes power production (standard controller DTU 10MW). The orange curve (or P90) represents data where the upstream turbine is de-rated at 90% power. Last the yellow curve (or P80) shows data for cases where the upstream turbine is de-rated 80% at power. In all three different setups, the downstream turbine is using a controller that maximizes power production. Controller data are given in Table 7.6.

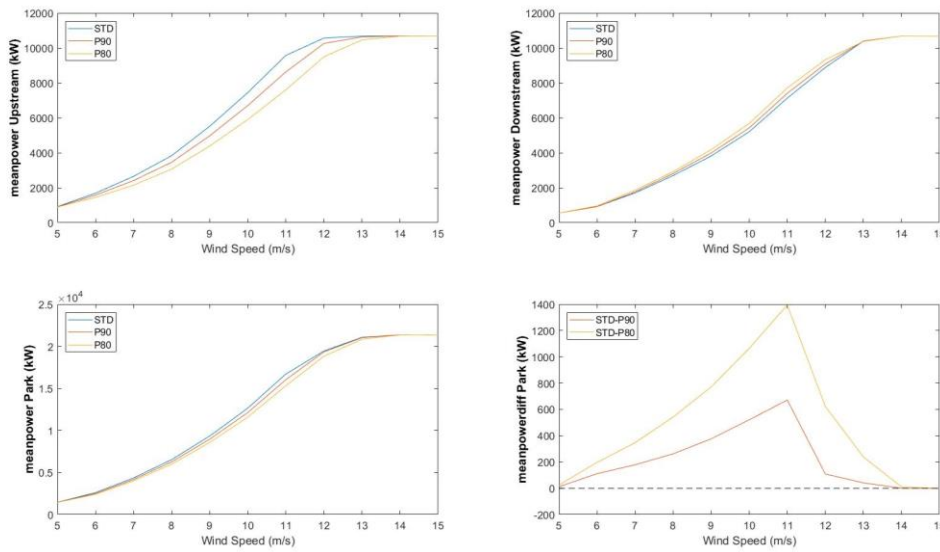


Figure 7-9: Power production for the upstream turbine (upper left), the downstream turbine (upper right) total power production (lower left) and power production differences (lower right), TI=10% and turbine spacing = 8 RD.

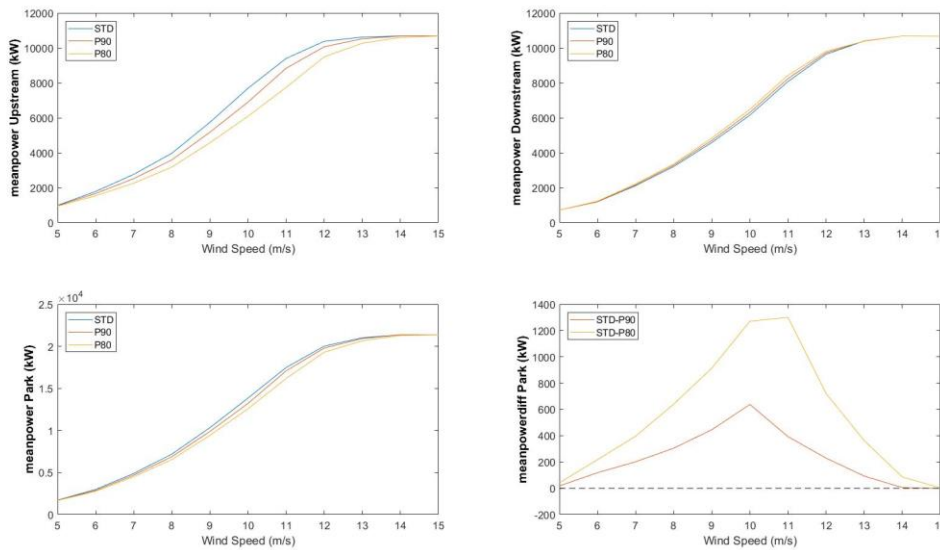


Figure 7-10: Power production for the upstream turbine (upper left), the downstream turbine (upper right) total power production (lower left) and power production differences (lower right), TI=15% and turbine spacing = 8 RD.

The impact of the application of the different controllers on the upstream turbine on the power production of the downstream turbine is as expected – a larger power production upstream reduces the power production downstream. The total energy production of the two turbines is not increased for nearly all wind speeds and controllers for this setup with 8 rotor diameters distance.

But there is an exception: At 12 m/s with 5% turbulence intensity there is a slight production increase if the first turbine is operated with the P90 controller setup. Here a production increase in the range of from 0.5-1% takes place, see **Figure 7-8**.

The same effect was found in another setup for low turbulence (5% ti); here the turbine distance of 5 rotor diameters was investigated for the same wind speed range from 5 to 15 m/s. Results are given below in **Figure 7-11**. Again, power production gains are observed around 12 m/s. The setup with the P90 controller produces here around 250 kW more than the standard setup and overall production is increased. The turbine distance of 5 rotor diameters is not feasible for an offshore park, however the increase of the power production by induction control is shown.

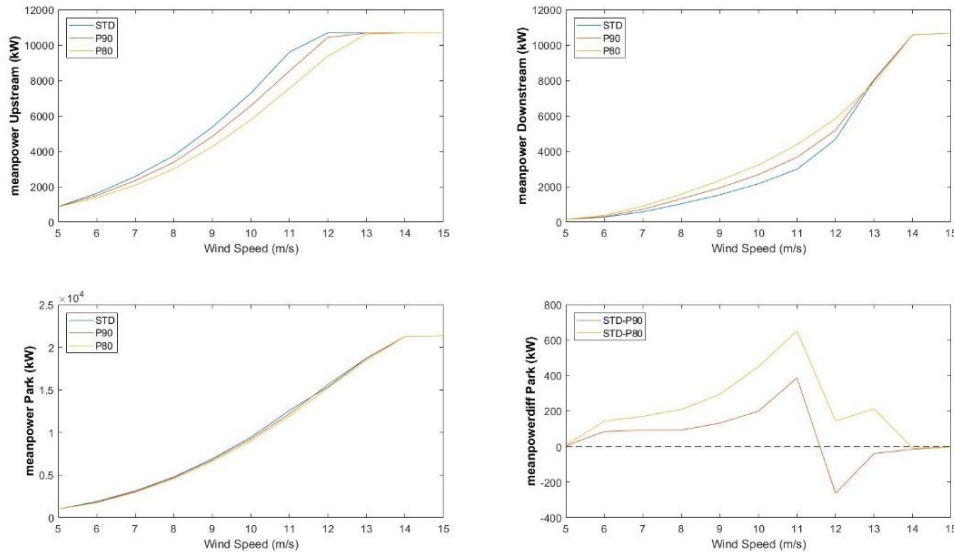


Figure 7-11: Power production for the upstream turbine (upper left), the downstream turbine (upper right) total power production (lower left) and power production differences (lower right), TI=5% and turbine spacing = 5 RD.

Last not least the overall thrust development has to be shown. As expected, the thrust of the upstream turbine (both maximum and averaged values) is reduced in simulations using induction control (P90 and P80) whereas average thrust values for the downstream turbine tends to be higher for de-rated cases compared to the standard setup.

It should be noted the maximum value for thrust experienced by the downstream turbine is identical in all three cases, see Figure 7-12. However, for the typical operational range around 10 m/s trust loads are more even distributed for the P90 and P80 controller setups.

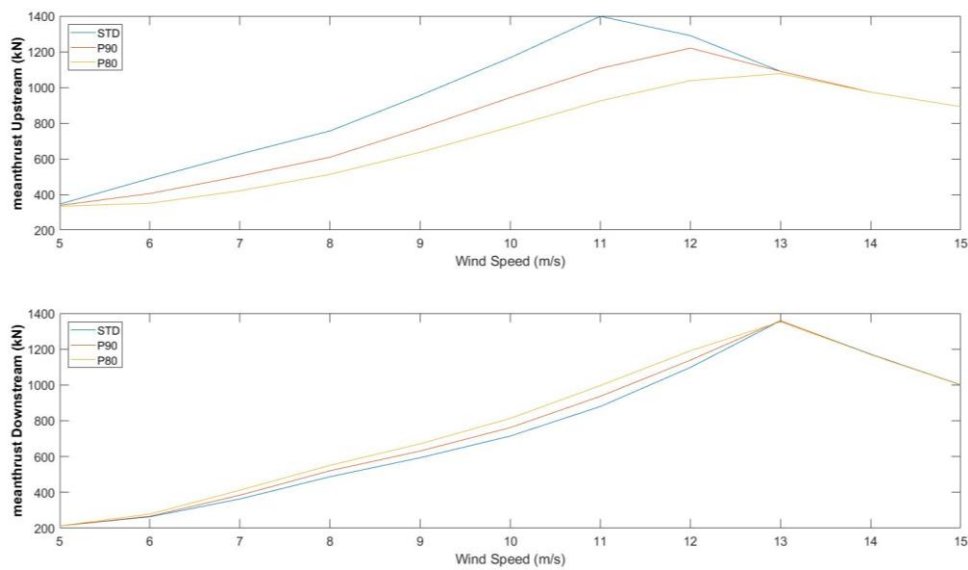


Figure 7-12: Mean thrust of the upstream turbine (up) and downstream turbine (down) in wind with 10% turbulence intensity.

7.3.3 WIND SPEED RANGE AND TURBINE DISTANCE RANGE SIMULATIONS

The investigations presented in 7.3.1 and 7.3.2 showed for induction control complex dependencies on several parameters. As main parameters regarded are wind speed, turbine distance, turbulence intensity and controller setup. Some production gains were identified around 12 m/s for the 5 rotor diameter case and the 8 rotor diameter case in winds with low turbulence (5% ti).

To get a better overview, parameter variations for wind speed and turbine distance were carried out for the different turbine configurations. Shown in **Figure 7-13** is the total mean power production for the turbulence intensity of 5%. The simulation setup was repeated for 10% turbulence intensity and 15% turbulence intensity, see **Figure 7-14** and **Figure 7-15**.

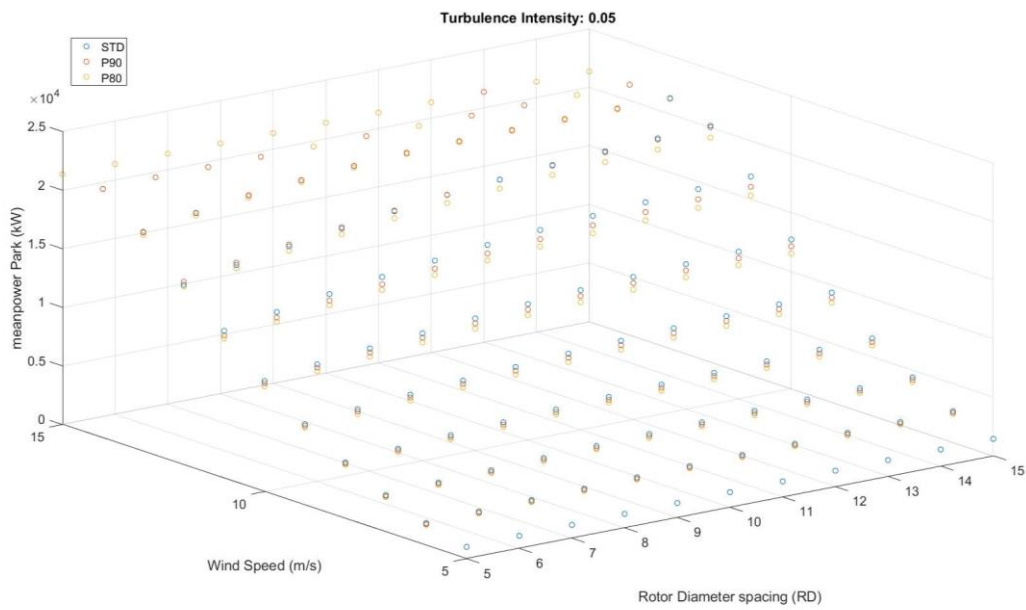


Figure 7-13: Mean power production of a 2-turbines park as function of turbine spacing for turbulent wind boxes ranging from 5m/s to 15m/s with turbulence intensity of 5%

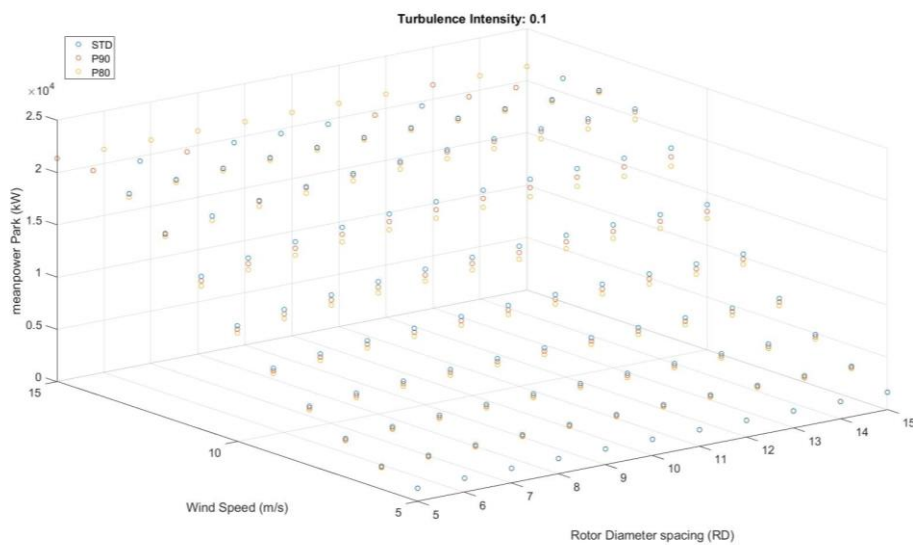


Figure 7-14: Mean power production of a 2-turbines park as function of turbine spacing for turbulent wind boxes ranging from 5 m/s to 15 m/s with turbulence intensity of 10%.

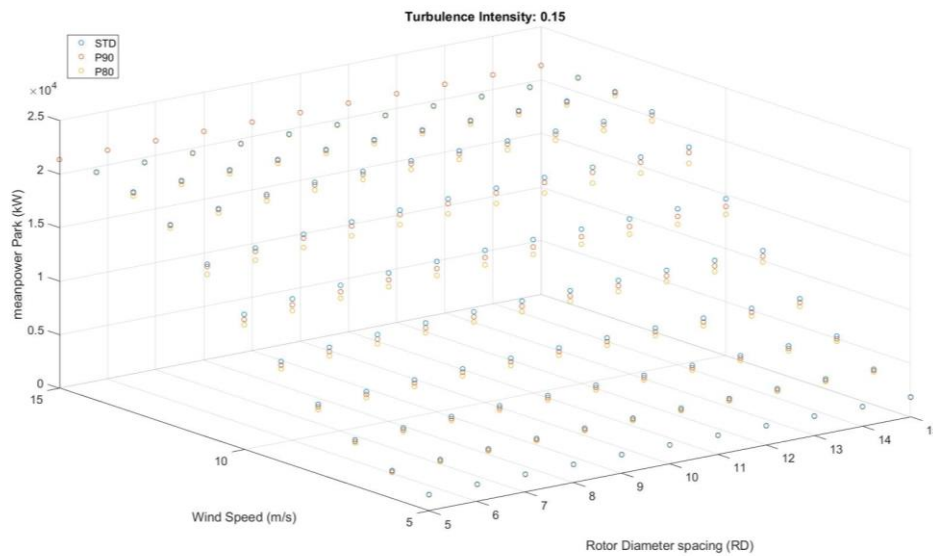


Figure 7-15: Mean power production of a 2-turbines park as function of turbine spacing for turbulent wind boxes ranging from 5 m/s to 15 m/s with turbulence intensity of 15%.

The 3D diagrams are showing that for higher turbine spacing, the scenario where both turbines maximize individually their power production (STD), is always better than a scenario where the upstream turbine works at reduced induction (P90 & P80). In fact, as the spacing between the turbines gets larger, scenarios with a de-rated upstream turbine get worst compared to the standard case.

The same trend is found for the variation of the turbulence intensity. One sees here for a turbulence increase (which generates better wake mixing) a non-optimal performance for the de-rating of the turbine.

The results show that application of controller settings to reduce power/induction in order to increase park production has a limited application for the modelled scenario.

The simulations show that derating makes sense where the turbine spacing is small and the incoming turbulent wind has low turbulence intensity. Gains were only observed in a small wind speed band slightly above rated.

Indeed, shoulder effects on power curves in turbulent wind imply that for a given wind increase, the production gains are higher when the turbine is below rated than around rated. It can be seen that by pitching the upstream turbine early the production losses are small, yet the downstream turbine will see a smaller wind deficit and will therefore experience a larger power production increase.

7.4 SETPOINT MODIFICATIONS BASED ON THRUST CLIPPING

Thrust clipping is typically applied for large turbine designs to avoid large thrust loads around rated wind speed. A small amount of power is sacrificed to obtain the effect. For the DTU 10 MW

turbine, three thrust reduction levels were designed (90%, 80% and 70% of maximum thrust) and they are further tested for their additional impact on the wake behaviour.

In **Figure 7-16**, thrust and pitch data are shown. The developed pitch data for the controller of the 10 MW turbine is given in **Table 7.9**.

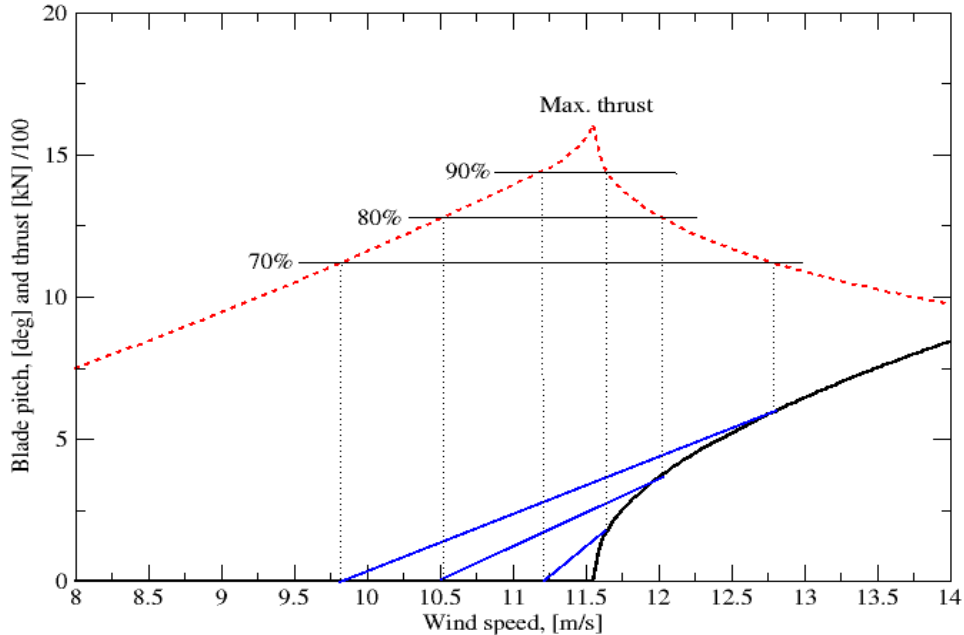


Figure 7-16: Designed thrust reduction levels and respective pitch ranges for the DTU 10 MW turbine.

Table 7.9: Setpoint realisations for three thrust level reductions.

DTU 10 MW		Thrust cut to 90%		Thrust cut to 80%		Thrust cut to 70%	
Wind speed	Datum setup	Wind speed	90% thrust	Wind speed	80% thrust	Wind speed	70% thrust
4	2.681	4	2.68	4	2.68	4	2.68
5	1.896	5	1.896	5	1.896	5	1.896
6	0.863	6	0.862669	6	0.862669	6	0.862669
7	0.000078	7	0.000078	7	0.000078	7	0.000078
8	0.000048	8	0.000048	8	0.000048	8	0.000048
50	0.000048	11.2	0.0	10.5	0.0	9.84	0.0
		11.5	1.13	11.0	1.164	10.0	0.313
		11.64	1.76	11.5	2.424	10.5	2.424
		50	0.000048	12.0	3.741	12.0	3.741
				50	0.000048	50	0.000048

The overall functionality and development of main turbine parameters are given in Figure 7-17 and Figure 7-18 below. Data were estimated in HAWC2 simulations.

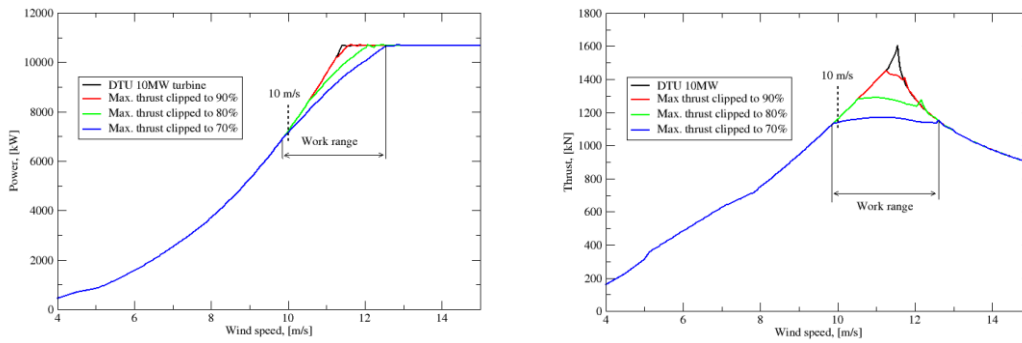


Figure 7-17: Power curves (left) and thrust curves (right) of the DTU 10 MW turbine with different thrust cut setups, HawC2 simulations with deterministic wind.

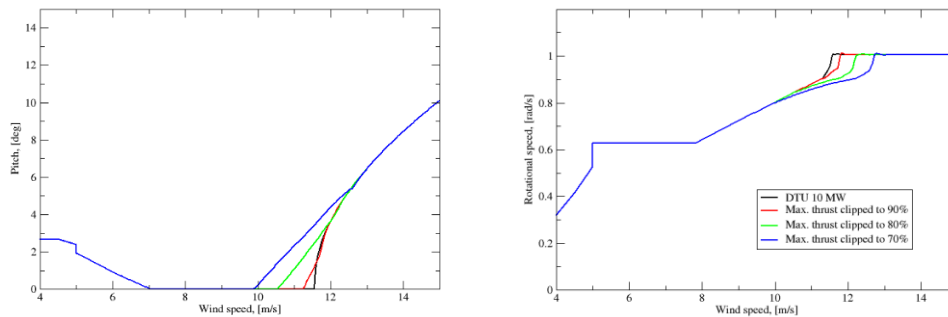


Figure 7-18: Pitch (left) and RPM (right) of the DTU 10 MW turbine with different thrust cut setups.

1.2 Single point evaluation for thrust reduction

A single operational point test was used as starting point. Thrust cutting was conducted around rated wind speed, here chosen was a wind speed of 11 m/s.

The investigation consisted of two steps:

1. Simulation of a single DTU 10 MW turbine with original controller setup followed by simulations with designed controller-setups, estimation of respective averaged data for pitch and rpm.
2. Application of the DWM model for a two-turbine setup. The first turbine uses then the averaged pitch- and rpm values. The second turbine operates with the original controller.

Data from the initial simulations with the upstream turbine T1 and the downstream turbine T2 are given in Figure 7-19, Figure 7-20 and Figure 7-21. Averaged data are shown in Table 7.10 and Table 7.11.

Again, the power development for the two turbines is compared. The upstream turbine is downrated by 133 kW, 447 kW and 801 kW in this situation. The power production of the downwind turbine catches somewhat up, but losses are not fully compensated. The approach to apply peak-shave or thrust-cut controllers to avoid wake losses is obviously not working in the investigated scenario. Losses are however very small.

Thrust loads are reduced as planned on the first turbine T₁; the impact of the TC controllers on the loads on the downwind turbine T₂ is positive. Thrust loads are distributed slightly more even in the array, see Table 7.11.

Table 7.10: Averaged power production [kW] for T₁ and T₂ at 8 rotor diameters distance, wind conditions 11 m/s with 10% turbulence intensity.

Averaged, [kW]	Datum	TC to 90%	TC to 80%	TC to 70%
T ₁ power	8624	8491	8177	7823
T ₁ power loss	0	-133	-447	-801
T ₂ power	5229	5278	5386	5536
T ₂ power gain	0	+49	+157	+307
Net power	13853	13769 (-0.5%)	13563 (-2.1%)	13359 (-3.5%)

Table 7.11: Averaged thrust from DWM simulations for T₁ and T₂. The T₂ turbine is operated with the standard controller. Wind conditions 11 m/s and 10% turbulence intensity at turbine T₁.

Averaged, [kN]	Datum	TC to 90%	TC to 80%	TC to 70%
T ₁ thrust	1304	1254	1171	1075
T ₂ thrust	913.8	919.9	933.4	951.9

Wind speed range tests are necessary to get a better overview, see next section for results.

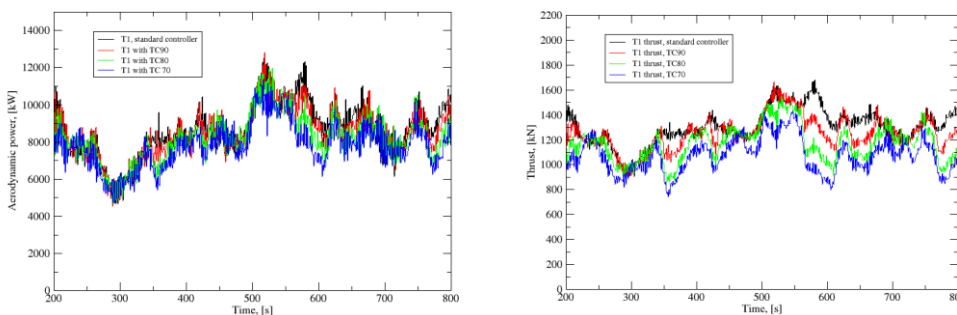


Figure 7-19: Power (left) and thrust data (right) for upstream turbine T₁ with four different controllers.

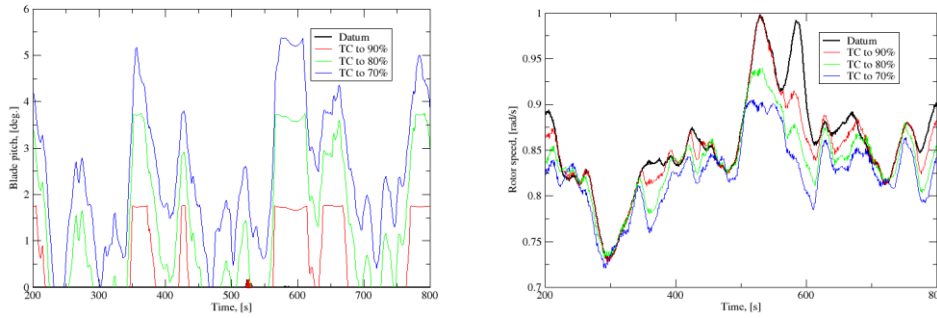


Figure 7-20: Blade pitch (left) and rotor speed data (right) for upstream turbine T1.

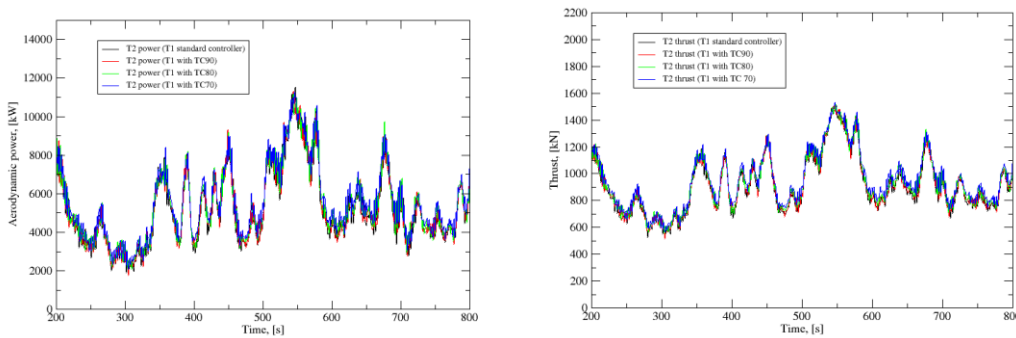


Figure 7-21: Power (left) and thrust data (right) for downstream turbine T2 in the wake of upstream turbine T1. T1 was operated with four different controllers.

7.4.1 WIND SPEED RANGE TESTS FOR THRUST REDUCTION

The wind speed range from 5 to 15 m/s was used for the power performance assessment of the controller setting for a maximal thrust reduction to 70% (TC70). This setting seems to have a slightly better potential to modify the wake behaviour than the two other controller settings TC80 and TC90.

Results from the TC70 simulations were compared with the standard controller (STD) and the P90 setup. Results are shown in Figure 7-22 (5-15 m/s, 5% ti), Figure 7-23 (5-15m/s, 10% ti) and Figure 7-24 (5-15m/s, 15% ti).

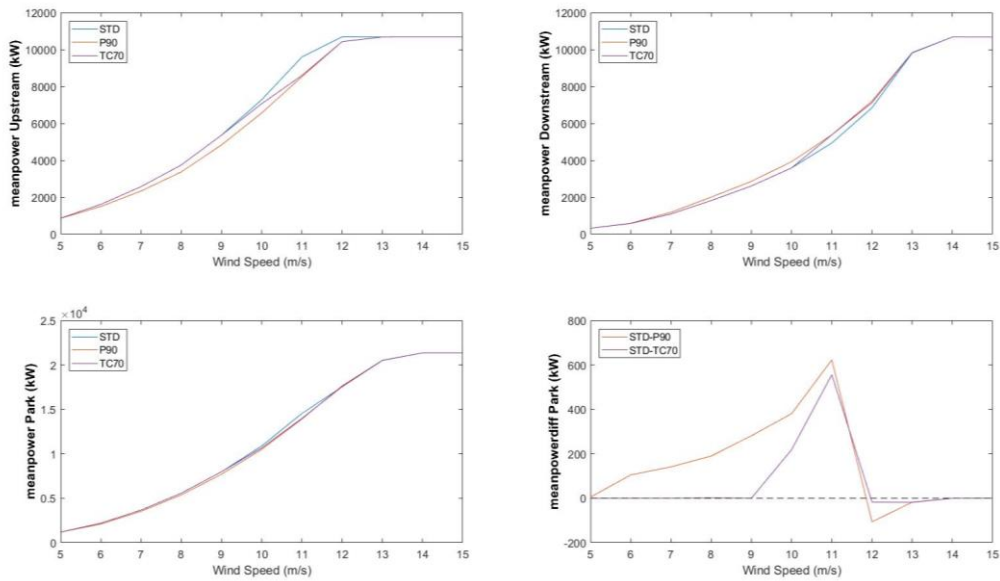


Figure 7-22: Power production for the upstream turbine (upper left), the downstream turbine (upper right) total power production (lower left) and power production differences (lower right), TI=5% and turbine spacing = 8 RD.

The blue curve (or STD) is showing data where the upstream turbine is using a controller that maximizes power production. The orange curve (or P90) represents data where the upstream turbine is derated at 90% power. Last the purple curve (or TC70) shows data for cases where the upstream turbine uses a peak shaving controller set to 70% of thrust. In all three different setups, the downstream turbine is using a controller that maximize power production. Controller setups are from Table 7.6 and Table 7.9.

The results for the total power production (lower diagrams in **Figure 7-22**, **Figure 7-23** and **Figure 7-24**) show again only a very little potential for the investigated configurations. As discussed previously, only at 5% ti, the P90 controller setting is able to create a small power production increase.

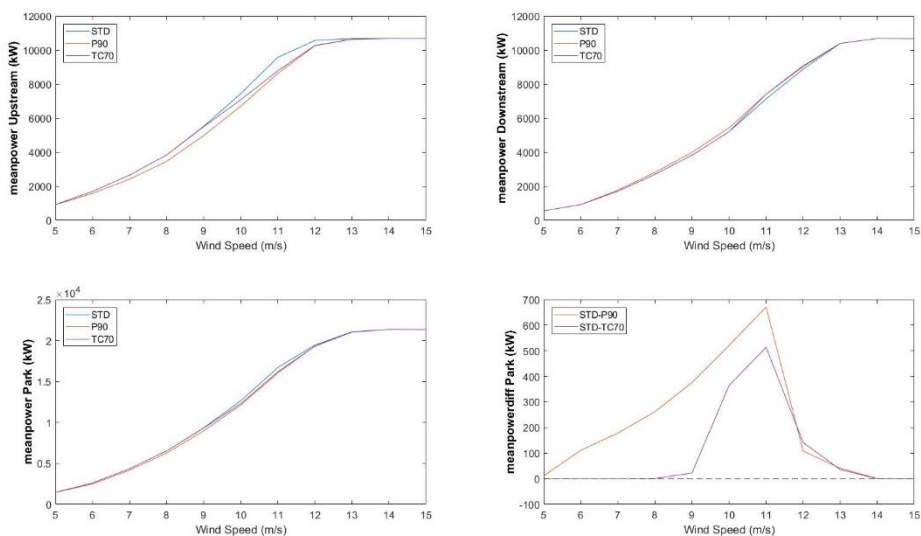


Figure 7-23: Power production for the upstream turbine (upper left), the downstream turbine (upper right) total power production (lower left) and power production differences (lower right), TI=10% and turbine spacing = 8 RD.

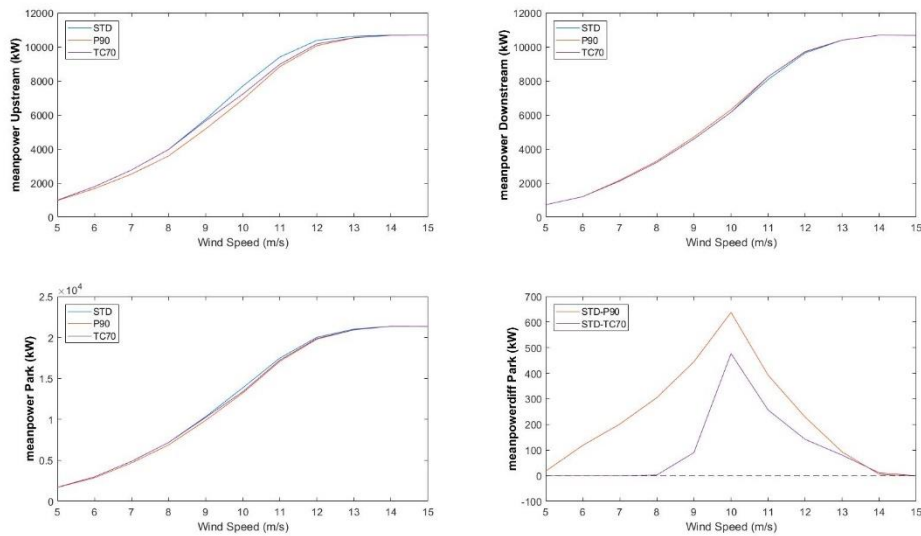


Figure 7-24: Power production for the upstream turbine (upper left), the downstream turbine (upper right) total power production (lower left) and power production differences (lower right), TI=15% and turbine spacing = 8 RD.

7.4.2 WIND SPEED RANGE AND TURBINE DISTANCE RANGE SIMULATIONS

Finally, for $ti=5\%$ simulations were conducted for a range of wind speeds and turbine spacings. The total park power production is shown in **Figure 7-25** below.

On the 3D plot the power production of the following scenarios can be found:

- two turbines working with the standard controller (STD, blue)
- Turbine 1 working with the P90 controller, turbine 2 with the standard controller. Shown as (P90, orange)
- Turbine 1 working with the TC70 controller, turbine 2 with the standard controller. Shown as (TC70, magenta)

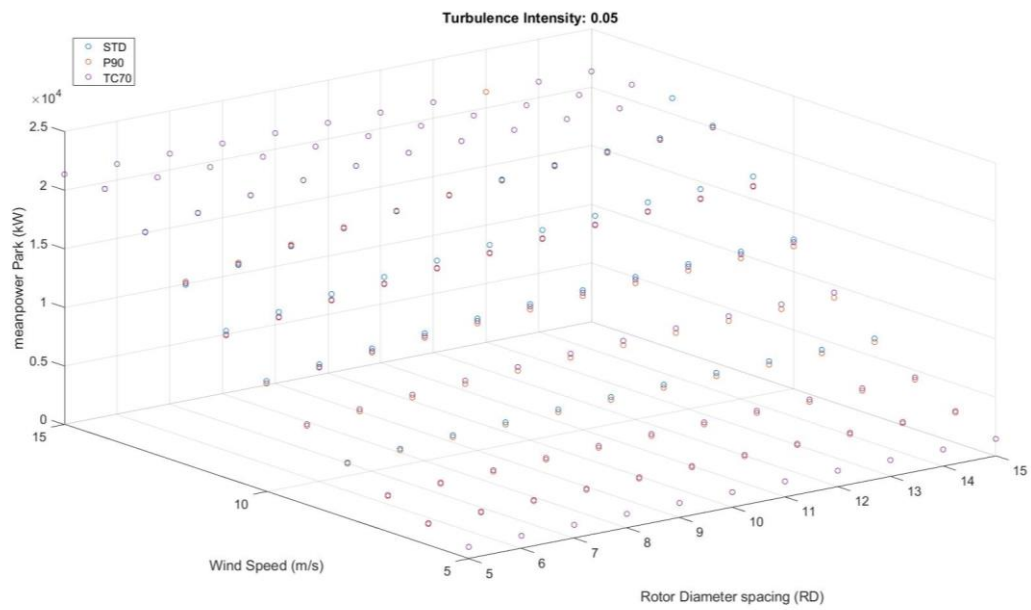


Figure 7-25: Mean power production of a 2-turbines park as function of turbine spacing for turbulent wind boxes ranging from 5m/s to 15m/s with turbulence intensity of 5%.

The plot above shows that it might be possible to design a controller setup for the turbines in a tandem array that would outperform the standard controller application for both turbines. But throughout most of the investigated operational range a standard controller setup performs better. Margins for induction control are with this approach really small and yet a setup would only work in some specific conditions like low turbulence intensity and small spacing between turbines.

7.5 SETPOINT TESTS WITH THRUST REDUCTIONS WITH IMPROVED C_p/C_t RATIO.

In the previous tests the operational behaviour of the first turbine was modified just by reducing power or reducing/limiting thrust to influence the wake behaviour. Simulation results from the two-turbine test case showed only a slight decrease of wake losses in a small operational range.

A more advanced approach was investigated by (J.A. Vitulli, 2021). The investigated open loop wind farm control relies on the optimization of collective pitch α and the tip speed ratio λ ; one target here was the identification of the lowest thrust coefficient for a given power coefficient. An example of pitch/TSR data for a SWT-2.3-93 turbine is given in Figure 7-26. For the operation of the DTU 10 MW turbine, an operational point at $C_p=0.42$ was chosen and in a multi-parameter investigation with the Qblade tool minimized C_t values and respective operational speeds and pitch angles were estimated. The new optimized operational points are given in Table 7.10.

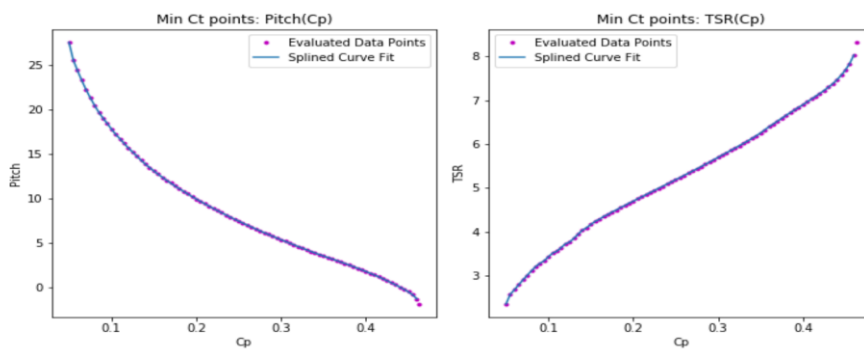


Figure 7-26: Pitch- and tip speed values to estimate lowest thrust for given C_p , SGS/SWT-2.3-93 turbine (J.A. Vitulli, 2021).

Table for the

Wind, [m/s]	C_p , [-]	C_t , [-]	Pitch, [deg.]	RPM
5	0.42	0.6	4.2	3.8
6	0.42	0.6	4.2	4.4
7	0.42	0.6	4.2	5.2
8	0.42	0.6	4.2	6
9	0.42	0.6	4.2	6.8
10	0.42	0.6	4.2	7.6
11	0.42	0.59	4.2	7.8
12	0.4	0.58	4.2	7.8

7.10: Optimised setpoints DTU 10MW turbine with increased C_p/C_t ratio.

7.5.1 SINGLE POINT INVESTIGATION FOR C_p/C_t OPTIMISED THRUST REDUCTION

The single point test was carried out at 10 m/s wind speed with 10% turbulence intensity. The results for the upstream turbine with original controller and with the Cp/Ct optimised controller are given in **Table 7.13** and **Table 7.14**.

Table 7.13: Averaged power data for T1 and T2 with CT 60 configuration. Wind speed 10 m/s with 10% ti.

Average, [kW]	Datum turbine, original controller	Turbine with CT60 (Cp/Ct opt. controller)
T1 power	6651	5565
T1 power loss	0	-1086
T2 power	4194	4610
T2 power gain	0	+416
Net power	10845	10175 (-6.2%)

Observed is a power increase for turbine T2 when the upstream turbine operates with reduced thrust (CT60 controller, maintaining a high Cp/Ct ratio). The power production is then increased. However, a net power gain is not obtained. The measure does not lead to a net power gain for the two-turbine setup under this operating conditions. Time series for power, thrust and operational data are given in **Figure 7-27** - **Figure 7-29**. A positive development is seen for the thrust development, the CT60 controller on the first turbine generates a more even distribution of thrust loads.

Table 7.14: Averaged thrust development for turbines T1 and T2. Wind 10 m/s and 10% ti.

Average, [kN]	T1 and T2 original controller	T1 with Cp/Ct opt controller, T2 with original controller
T1 thrust	1096	786
T2 thrust	798.8	851.6

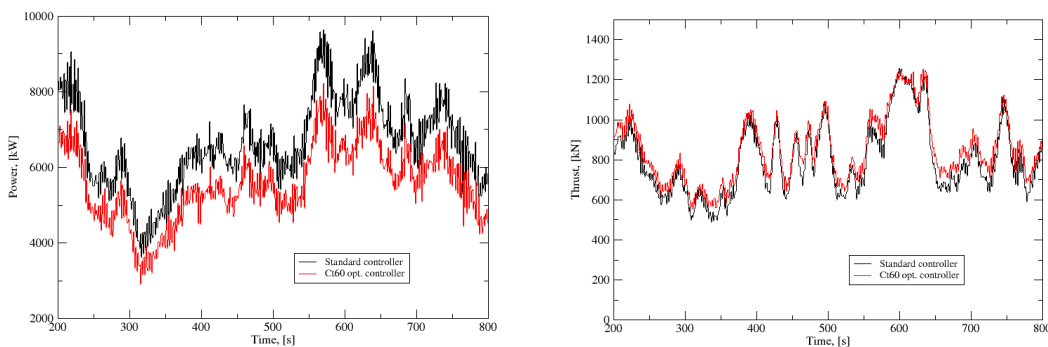


Figure 7-27: Power and thrust comparison for turbine 1.

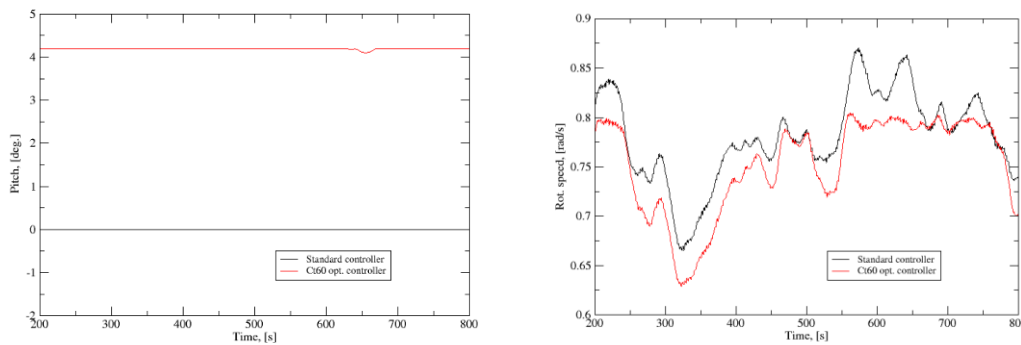


Figure 7-28: Pitch and Rpm development for turbine 1.

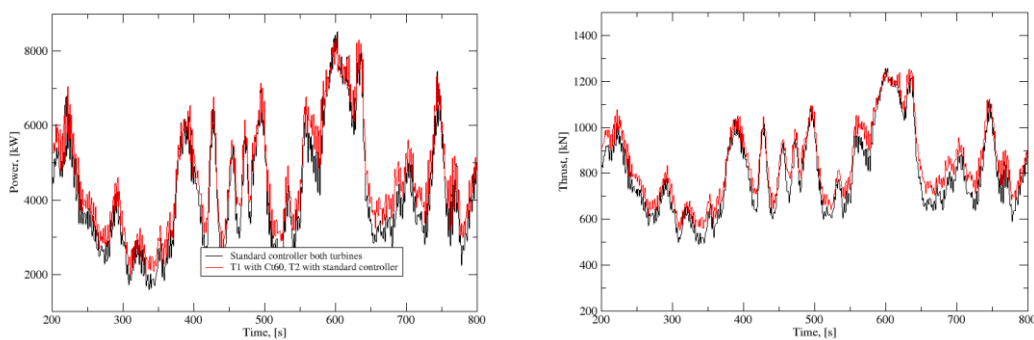


Figure 7-29: Power and thrust comparison for turbine 2.

7.5.2 WIND SPEED RANGE TESTS

With the two-turbine setup wind range tests were carried out. In **Figure 7-30** and **Figure 7-31** results for 5% turbulence intensity (turbine distance 5 rotor diameters) and 10% turbulence intensity (turbine distance 9 rotor diameters) are shown for:

- Operation with standard controller (STD) operating on both turbines
- P90 controller (see section 7.3, Table 7.6) on the 1st turbine, standard controller on the 2nd turbine.
- CT60 controller on the 1st turbine, standard controller on the 2nd turbine

The **Figure 7-30** shows only slight production gains for the low-turbulence scenario, where production is increased up to 250kW around 12 m/s (with the P90 controller) or up to 400 kW in the wind speed range from 11.5 m/s to 15 m/s (with the CT60 controller).

Results for operation of the turbines at higher turbulence intensity of 10% (9 rotor diameters turbine distance) are given in **Figure 7-31**. Under these operational conditions, no production gains are observed.

For this new controller approach, no large-scale improvements could be identified. However, production gains reached in small areas up to 5%.

7.5.3 WIND SPEED RANGE AND TURBINE DISTANCE RANGE SIMULATIONS

Simulations for the wind speed range from 5 m/s to 15 m/s with a turbine distance variation from 5 to 15 rotor diameters were carried out for 5% and 10% turbulence intensity, results are given in **Figure 7-32** and **Figure 7-33**.

The general trend seems to be a slight overall power increase for wind speeds around 12 to 13 m/s in a low-turbulent environment with 5% turbulence intensity. For higher turbulence intensities, these production gains disappear.

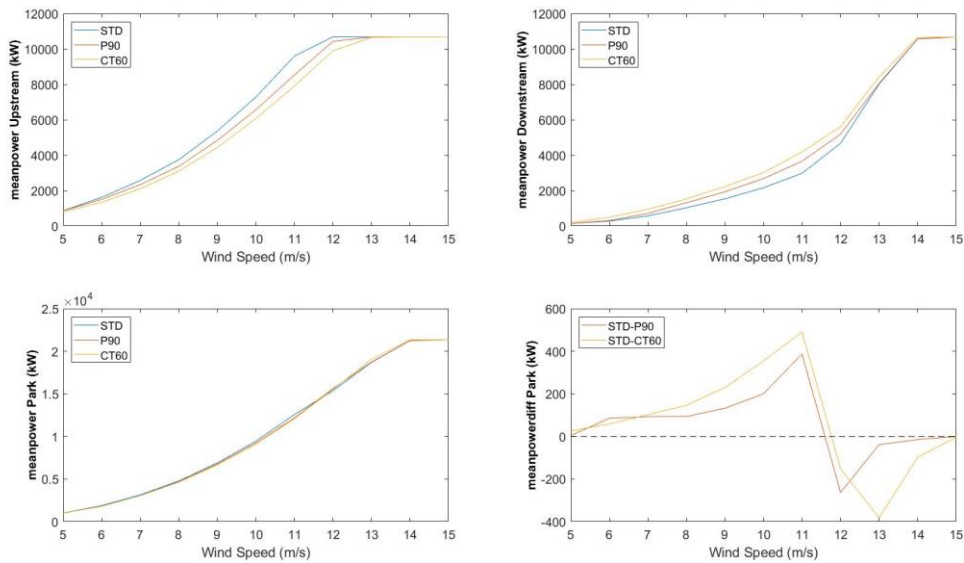


Figure 7-30: Power development vs wind speed for 5 rotor diameters distance and 5% ti.

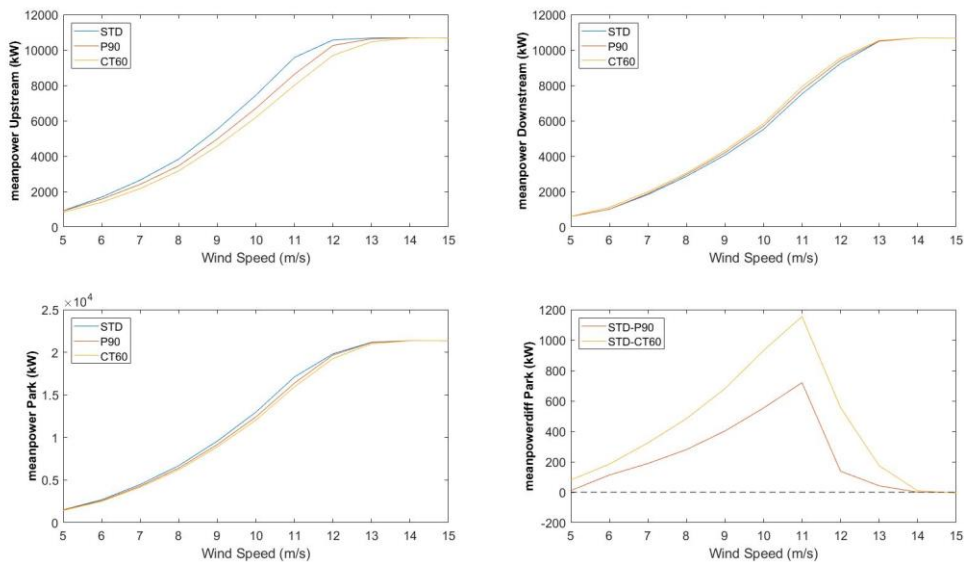


Figure 7-31: Power development for 9 rotor diameter distance and 10% ti.

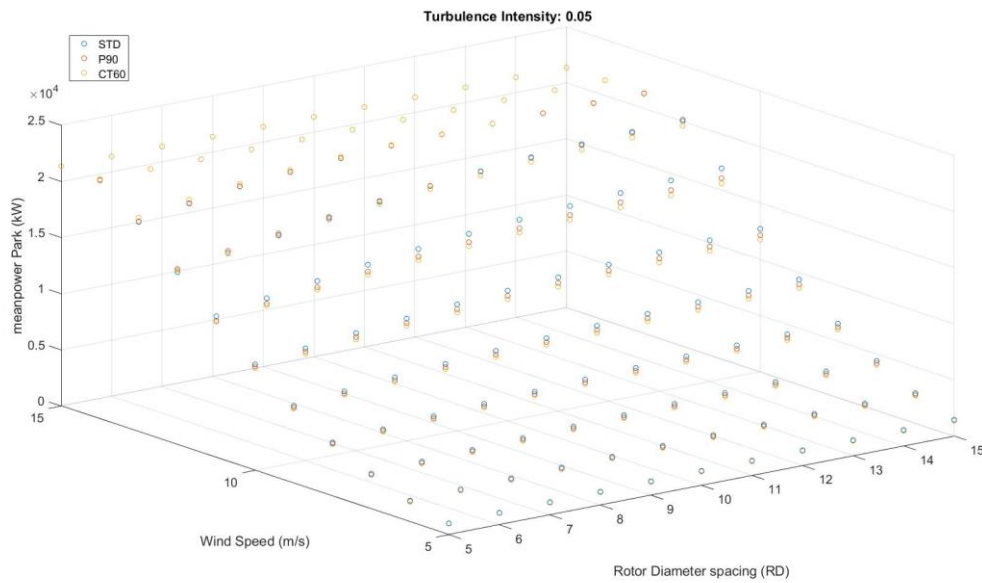


Figure 7-32: Mean power production of a 2-turbines park as function of turbine spacing for turbulent wind boxes ranging from 5m/s to 15m/s with turbulence intensity of 5%.

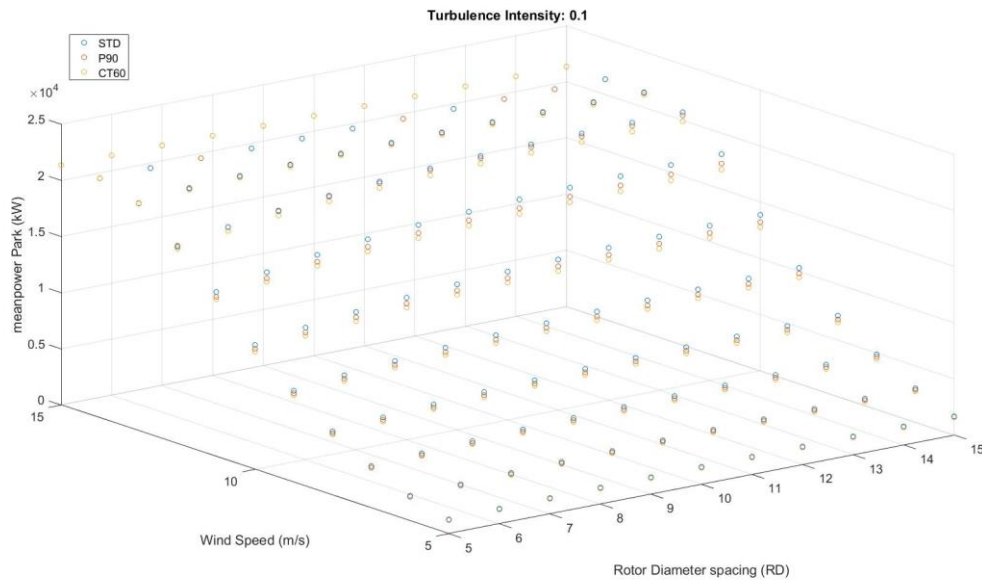


Figure 7-33: Mean power production of a 2-turbines park as function of turbine spacing for turbulent wind boxes ranging from 5m/s to 15m/s with turbulence intensity of 10%.

7.6 SUMMARY

The aero-elastic code HawC2 was applied in the investigations with the generic DTU 10MW wind turbine model. A set of parameter studies covering turbine distance, wind speed and turbulence intensity with different controller setups was carried out.

In the activities, configurations with only two turbines was examined. The two-turbine setup is the most basic approach, but it seemed suitable to explore the main challenge to increase the common

energy production of an upstream turbine and a downstream turbine in its wake. Any larger-scale application depends on the solution for the two-turbine problem.

To vary turbine setpoints/induction, controller setups for power- and thrust reduction were developed. The power derating was applied in a broader range from 5 to 13 m/s, three levels (reduced to 70%, 80% and 90% of original power production) were applied. Thrust reduction setups were realized in a more small-banded wind speed range from 9 to 12 m/s around rated wind speed for two thrust reduction levels (70% and 80%). Furthermore, a C_p/C_t optimised thrust reduction was tested.

Comprised for the estimation of the wake impact on the downstream turbine was the DWM model integrated in HawC2. Standard parameters for the generation of the turbulent components (free wind, rotor microscale, rotor meandering) were applied.

The investigations of the six controllers and the original controller were carried on three levels:

- Single point power performance at one wind speed
- Power performance in a wind speed range from 5 to 15 m/s
- Power performance as function of wind speed (5-15 m/s), turbine distance (6 – 12 rotor diameters) and turbulence intensity (5%, 10% and 15% ti)

The results from the large number of simulations identified trends. First, they showed clearly the complexity and difficulty to increase the power performance especially for this basic scenario. The observed power production gains were indeed in the range of up to 5% - but only in some areas. For a connected, large operational area a strong positive effect was not observed. Controller designs based on thrust reductions comprising an optimized power coefficient worked most effective. Simple de-rating and thrust clipping measures proved less efficient.

Production increases were observed for:

- Thrust reductions (to $C_t=0.6$) with maximized C_p
- Power reductions to 90%
- Low turbulence intensity
- Medium wind speeds around 12 m/s

In the full working range, the applied controller schemes could not increase overall power production for the investigated configuration. However, the application of two different setpoint schemes lead in some wind regime areas to production gains.

But for the two-turbine array, the establishment of a power production increase in the complete wind regime from 5 to 12 m/s could turned out to be difficult. The investigations revealed that the small 2-turbine array is challenging for wake control: cascade effects influence flow behaviour in large turbine array substantially – they are absent in the smallest array. This effect seems to reduce the potential for induction control with just two turbines. It seems that a larger number of downwind turbines have a better potential to establish wake control for net production gains.

The applied controller concepts and 1D, 2D and 3D parameter investigations have proven to be useful to get both detailed data and a good overview regarding power- and load generation.

Generally, the potential to increase power production by induction control was shown. Production gains were not large, but the investigated case two-turbine case is different from actual offshore wind farm arrays where possibilities for wake control are believed to have a better potential.

8. CONCLUSIONS

The application of wake control in offshore wind farms has an interesting potential to increase power production. Two primary approaches of wake reduction through yawed operation and induction control by means of de-rating of turbines were investigated here. Both types of wind farm control were implemented on the Lillgrund wind farm using optimization schemes to maximize power with loads constraints or to maximize power and minimize loads. The investigations were conducted with three types of fast (low-fidelity) wake models. The results showed that induction control can provide a net wind farm power increase from 1% to 3% and also reduce the peak blade root moment or peak tower base moment. The wake steering approach can provide much greater increase in power from 7% to more than 20% under some situations. However wake steering generally results in increased peak loading on the blades and tower and also increased fatigue loading. This increase in loads can be minimized by considering a strict constraint on the loads during optimization. A large difference in power increase due to wake steering was observed between the LongSim and the GWM models, which may be attributed to differences in the free stream turbulence and wake turbulence.

LongSim was also used under conditions of grid specified power curtailment, wherein it was shown that the individual wind turbine power could be set to a desired level without any oscillatory behaviour, and with the maximum wind turbine component loads maintained at a low acceptable level.

Induction control was also implemented using the medium fidelity DWM model on Lillgrund. Lifetime-equivalent load reduction in the order of 3 - 4% was observed for selective derating strategies aimed at pure power maximization. This led to an overall increase in AEP of the wind farm of about 1%. The reduction in fatigue damage could lead to 10-40% increase in the fatigue lifetime depending on the component. However a significant uncertainty in the power prediction was determined using the DWM model. Therefore, it could be beneficial to supplement wind farm surrogate models with power predictions based on PyWake simulations and use the DWM results for load predictions.

Three approaches for induction control for the DTU 10 MW wind turbine considering a two turbine small wind farm were evaluated using DWM by Equinor. The standard power reduction, an approach based on thrust load reduction (thrust cutting/peak shaving) and a thrust reduction with optimized power production were evaluated. The investigations revealed that due to the absence of cascade effects in this small 2-turbine array, the potential for induction control with just two turbines is reduced. It seems that a larger number of downwind turbines have a better potential to establish wake control for net production gains.

9. BIBLIOGRAPHY

- Allaerts, D. and Meyers, J., "Large eddy simulation of a large wind-turbine array in a conventionally neutral atmospheric boundary layer," *Phys. Fluids*, vol. 27, no. 6, 2015, doi: 10.1063/1.4922339.
- Allaerts, D. and Meyers, J. "Sensitivity and feedback of wind-farm-induced gravity waves," *J. Fluid Mech.*, vol. 862, pp. 990–1028, 2019, doi: 10.1017/jfm.2018.969
- Anderson, S.J., Meyers, J., Sood, I. and Troldborg, N. "TotalControl D 1.04 Flow Database for reference wind farms." 2020
- Bak, C. e. (2008). *The DTU 10-MW Reference Wind Turbine*. DTU Wind Energy - Risø Campus.
- Bastankhah M and Porté-Agel F. (2014) A new analytical model for wind-turbine wakes. *Journal of Renewable Energy*, 70:116-23
- Bastankhah, M. and Porté-Agel, F. "Experimental and theoretical study of wind turbine wakes in yawed conditions," *J. Fluid Mech.*, vol. 806, pp. 506–541, 2016, doi: 10.1017/jfm.2016.595.
- Bossanyi, E. (2018). Combining induction control and wake steering for wind farm energy and fatigue loads optimisation. *Journal of Physics: Conference Series*, Vol. 1037.
- Bossanyi, E. and Ruisi, R. (2021), Axial induction controller field test at Sedini wind farm, *Wind Energ. Sci.*, 6, 1–20, 2021 <https://doi.org/10.5194/wes-6-1-2021>
- Bossanyi, E. (2019), Optimising yaw control at wind farm level, Proc. WindEurope Conference, April 2019, Bilbao: *Journal of Physics: Conf. Series* 1222 (2019) 012023 IOP Publishing doi:10.1088/1742-6596/1222/1/012023.
- Bossanyi, E., D'Arco, S., Lu L., Madariaga, A., de Boer, W. and Schoot, W (2020), Control Algorithms for primary frequency and voltage support, TotalControl Deliverable no. D4.1, 2020.
- Burton, T., Jenkins, N., Sharpe, D. and Bossanyi, E. (2011), *Wind Energy Handbook*, Second Edition, Print ISBN:9780470699751, Online ISBN:9781119992714, DOI:10.1002/9781119992714, John Wiley & Sons, Ltd, 2011.
- Dimitrov, N. (2019) Surrogate models for parameterized representation of wake-induced loads in wind farms. *Wind Energy* 22: 1371- 1389
- Dimitrov, N., and Natarajan, A. (2021) Wind farm set point optimization with surrogate models for load and power output targets. Under review for the *Journal of Physics: Conference Series*, EERA DeepWind2021 conference
- Dimitrov, N., Kelly, M. C., Vignaroli, A., and Berg, J. (2018), From wind to loads: wind turbine site-specific load estimation with surrogate models trained on high-fidelity load databases, *Wind Energ. Sci.*, 3, 767–790, <https://doi.org/10.5194/wes-3-767-2018>, 2018.
- Goit, J.P. and Meyers, J. "Optimal control of energy extraction in wind-farm boundary layers," *J. Fluid Mech.*, vol. 768, pp. 5–50, 2015, doi: 10.1017/jfm.2015.70.
- H. P., "Cubature formulas for the unit disk," 2011. <http://www.holoborodko.com/pavel/numerical-methods/numerical-integration/cubature-formulas-for-the-unit-disk/>.
<https://www.hawc2.dk/download/general-information>. (u.d.). Downloaded from www.hawc2.dk.
<https://www.hawc2.dk/Download/HAWC2-Model/DTU-10-MW-Reference-Wind-Turbine>. (u.d.).
 Downloaded from www.hawc2.dk.
- Jimenez, A. C. (2009). Application of a LES technique to characterize the wake deflection of a wind turbine in yaw. *Wind energy*.
- Lanzilao, L. and Meyers, J., "A new wake-merging method for wind-farm power prediction in

- presence of heterogeneous background velocity fields," *arXiv*, pp. 1–19, 2020.
- Larsen, G. C., Ott, S., Liew, J., van der Laan, M. P., Simon, E., R.Thorsen, G. and Jacobs, P. (2020): Yaw induced wake deflection - a full scale validation study. *Journal of Physics - Conference Series*. 1618, 12 p., 062047.
- Larsen T J and Hansen A M 2014. How 2 HAWC2, the user's manual, Risø-R-1597(ver.4-5)(EN). Risø National Laboratory, Technical University of Denmark.
- Larsen G C, Madsen H A, Thomsen, K. and Larsen T J (2008). Wake meandering - a pragmatic approach. *Wind Energy* 11, pp. 377–395.
- Larsen, T. J. (2008). HAWC2Aero, the user's manual , Risø-R-1631(ver.1-0).
- Larsen, T. et.al. (2013). Validation of the Dynamic Wake Meander Model for Loads and Power Production in the Egmond aan Zee. *Wind Energy*, pp. 605-624.
- Larsen, T. et.al. (2015). Wake effects above rated wind speed. An overlooked contributor to high loads in wind farms. *EWEA 2015 Conference*.
- Pedersen, M.M., van der Laan,P., Friis-Møller, M., Rinker, J. and Réthoré, P.E., (2019, February 12). DTUWindEnergy/PyWake: PyWake (Version v1.0.10). Zenodo.
<http://doi.org/10.5281/zenodo.2562662>
- Madsen, H. et.al. (2003). A new method for prediction of detailed wake loads. *Proceedings of the IEA Joint Action of Wind Turbines 16th Symposium*.
- Madsen, H. et.al (2010). Calibration and Validation of the Dynamic Wake Meandering Model for Implementation in an Aeroelastic code. *Journal of Solar Energy Engineering*.
- Madsen, H. Aa., Mikkelsen, R., Sørensen, N.N., Hansen, M.L.O., Øye, S. and Johansen, J. (2007): Influence of wind shear on rotor aerodynamics, power and loads. Research in Aeroelasticity EFP-2006, Risø-R-1611(EN).
- Munters, W. and Meyers, J. "Dynamic strategies for yaw and induction control of wind farms based on large-eddy simulation and optimization," *Energies*, vol. 11, no. 1, 2018, doi: 10.3390/en11010177.
- Munters, W., Meneveau, C. and Meyers, J. "Turbulent Inflow Precursor Method with Time-Varying Direction for Large-Eddy Simulations and Applications to Wind Farms," *Boundary-Layer Meteorol.*, vol. 159, no. 2, pp. 305–328, 2016, doi: 10.1007/s10546-016-0127-z.
- Munters, W. &. (2018). Optimal dynamic induction and yaw control of wind farms: effects of turbine spacing and layout. *Journal of Physics: Conference Series*, Vol. 1037.
- Murcia Leon, J. P., Réthoré, P-E., Dimitrov, N. K., Natarajan, A., Sørensen, J. D., Graf, P., & Kim, T. (2018). Uncertainty propagation through an aeroelastic wind turbine model using polynomial surrogates. *Renewable Energy*, 119, 910-922.
<https://doi.org/10.1016/j.renene.2017.07.070>
- Niayifar, A. and Porté-Agel, F., "Analytical modeling of wind farms: A new approach for power prediction," *Energies*, vol. 9, no. 9, pp. 1–13, 2016, doi: 10.3390/eng090741.
- Ott, S., Berg, J. and Nielsen, M.: Linearised CFD Models for Wakes (2011). Danmarks Tekniske Universitet, Risø Nationallaboratoriet for Bæredygtig Energi, Denmark, Forskningscenter Risø, Risø-R-1772(EN).
- Ott, S., Laan, P. van der and Larsen, G.C.: Upgrade of Fuga (2019). Deliverable no. D1.7, TotalControl.
- Pedersen, M. M. and Larsen, G. C. (2020): Integrated wind farm layout and control optimization, *Wind Energ. Sci.*, 5, 1–17, <https://doi.org/10.5194/wes-5-1-2020>.

- Réthoré, P.-E., Fuglsang, P., Larsen, G. C., Buhl, T., Larsen, T. J. and Madsen, H. Aa. (2013): TOPFARM: Multi-fidelity optimization of wind farms. *Wind Energy*, vol. **17**, pp. 1797–1816.
- Ruisi, R. and Bossanyi, E. (2019), Engineering models for turbine wake velocity deficit and wake deflection. A new proposed approach for onshore and offshore applications, *J. Phys.: Conf. Ser.*, 1222, 012004, TS18, 2019, IOP Publishing, doi:10.1088/1742-6596/1222/1/012004.
- Schoot, W., de Boer, W. & Bossanyi, E. (2020), Grid Frequency Stability with Wind Power: Irish Case Study Using a New Closed Loop simulation Environment. *Proceedings of the 19th Wind Integration Workshop*, 2020
- Schottler, J. e. (2017). Comparative study on the wake deflection behind yawed wind turbine models. *Wind energy*.
- Sood, I., Meyers, I. and Lanzilao, L. "TotalControl D 1.8 Coupling of Gaussian wake merging to background ABL model." 2020.
- Vitsas, A. and Meyers, J. "Multiscale aeroelastic simulations of large wind farms in the atmospheric boundary layer," *J. Phys. Conf. Ser.*, vol. 753, no. 8, p. 082020, Sep. 2016, doi: 10.1088/1742-6596/753/8/082020.
- Vitulli, J. A., Larsen, G. C., Pedersen, M. M., Ott, S. and Friis-Møller, M. (2019): Optimal open loop wind farm control. *Journal of Physics - Conference Series*. 1256, 12 p., 012027.
- Vollmer, L. e. (2016). Estimating the wake deflection downstream of a wind turbine in different atmospheric stabilities: an LES study. *Wind energy*.